Coordination Chemistry Reviews, 50 (1983) 1–72
Elsevier Science Publishers B.V., Amsterdam – Printed in The Netherlands

DIOXYGEN ACTIVATION IN TRANSITION METAL COMPLEXES IN THE LIGHT OF MOLECULAR ORBITAL CALCULATIONS

ROMAN BOČA

Department of Inorganic Chemistry, Slovak Technical University, CS-812 37 Bratislava (Czechoslovakia)

(Received 10 March 1982)

CONTENTS

ABBREVIATIONS

acacen	*N*,*N*′-ethylenebis-(acetylacetoneiminato) dianion, $C_{12}H_{18}O_2N_2$
an	anthracene, $C_{14}H_{10}$
AO	atomic orbital
APS	adiabatic potential surface
ben	benzene, C_6H_6
bipy	2,2′-dipyridyl, $C_{10}H_8N_2$
bzacen	*N*,*N*′-ethylenebis-(benzoylacetoneiminato) dianion, $C_{22}H_{22}O_2N_2$
BzIm	1-benzylimidazole, $C_{10}H_{10}N_2$

0010-8545/83/$21.60

CI	configuration interaction method
CNDO	complete neglect of differential overlap method
dien	diethylenetriamine, $C_4H_{13}N_3$
dipic	dipicolinic acid anion, $C_7H_3O_4N$
DME	dimethoxyethane, $C_4H_{10}O_2$
DMF	dimethylformamide, C_3H_7ON
dppe	$Ph_2PCH_2CH_2PPh_2$
dppen	$Ph_2PCH:CHPPh_2$
dppm	$Ph_2PCH_2PPh_2$
EHT	extended Hückel theory
en	ethylenediamine, $C_2H_8N_2$
ESR	electron spin resonance
Et	ethyl, C_2H_5
F–H	Fenske–Hall method
F-salen	bis(3-fluorosalicylaldehyde)ethylenediimine dianion, $C_{16}H_{12}O_2N_2F_2$
3-F-saltmen	*N*,*N*′-(1,1,2,2-tetramethyl)ethylenebis(3-fluorosalicyliden-iminato) dianion, $C_{22}H_{20}O_2N_2F_2$
Hb	hemoglobin
H–L	Heitler–London method
HOMO	highest occupied MO
IEHT	iterative extended Hückel theory
Im	imidazole, $C_3H_4N_2$
INDO	intermediate neglect of differential overlap method
LCAO	linear combination of AO
Me	methyl, CH_3
MeIm	1-methylimidazole, $C_4H_6N_2$
2-MeIm	2-methylimidazole, $C_4H_6N_2$
MIL	mutual influence of ligands
MINDO	modified INDO
MO	molecular orbital
OEP	octaethylporphin, $C_{36}H_{44}N_4$
3-OMe-saltmen	*N*,*N*′-(1,1,2,2-tetramethylethylene)bis(3-methoxysalicyl-ideniminato) dianion $C_{22}H_{26}O_2N_2$
ophen	1,10-phenanthroline, $C_{12}H_8N_2$
pip	piperidine, $C_5H_{11}N$
Ph	phenyl, C_6H_5
ppm	PMe_2Ph
PPP	Pariser–Parr–Pople method
por	dianion of porphyrin
Py	pyridine, C_6H_5N
pydien	1,9-bis(2-pyridyl)-2,5,8-triazanonane, $C_{16}H_{23}N_5$

pydpt	1,11-bis(2-pyridyl)-2,6,10-triazaundecane, $C_{18}H_{27}N_5$
PyH	pyridinium cation, C_6H_6N
RHF	restricted Hartree–Fock method
salen	*N*,*N*′-ethylenebis(salicylideniminato) dianion, $C_{16}H_{14}O_2N_2$
salen · C_2H_4Py	α,α′-{2-(2′-pyridyl)ethyl}-ethylenebis(salicylideniminato) dianion, $C_{25}H_{21}O_2N_3$
saltmen	*N*,*N*′-(1,1,2,2-tetramethylethylene)bis(salicylideniminato) dianion, $C_{20}H_{22}O_2N_2$
salprtr	3,3′-diimino-di-n-propylamine-bis-salicylaldehyde dianion, $C_{20}H_{23}O_2N_3$
SCC-EH	self-consistent charge Extended Hückel method
SCCC	self-consistent charge and configuration method
SCF	self-consistent field method
t-Bsalten	*N*,*N*′-(1,1,2,2-tetramethyl)ethylenebis(3-t-butylsalicylideniminato) dianion, $C_{28}H_{38}O_2N_2$
t-Bu-salen	*N*,*N*′-ethylenebis(3-t-butylsalicylideniminato) dianion, $C_{24}H_{30}O_2N_2$
THF	tetrahydrofuran, C_4H_8O
tol	toluene, C_7H_8
TpivPP	meso-tetrakis(α,α,α,α-*o*-pivalamidophenyl)porphyrinato dianion, $C_{64}H_{64}N_8O_4$
TPP	*meso*-tetraphenylporphyrinato dianion, $C_{44}H_{28}N_4$
TTP	tetraparatolylporphyrinato dianion, $C_{48}H_{36}N_4$
UHF	unrestricted Hartree–Fock method

A. INTRODUCTION

Dioxygen complexes of transition metals have attracted attention for a number of decades because of their important role in biological processes and in catalysis. The literature available in this field has reached thousands of publications. This research has been the subject of several extensive reviews [1–29] where particular aspects of formation, structure, electronic structure, thermodynamics, kinetic, reactivity, catalytic and biological activity were summed up. However, in practice, it is impossible to summarize all these aspects in one article. Therefore, more specialized topics seem to be required such as those related to synthetic dioxygen carriers versus biological systems [29] or catalysis [26].

Unlike the earlier theoretical interpretations, based mainly on intuitive VB or MO theory, the prominent role of ESR and electronic spectroscopy, hand in hand with quantum chemical calculations, was utilized in contemporary research of the metal–dioxygen moiety so that the nature of dioxygen binding to transition metals becomes clearer. Nevertheless, some particular

problems require further experimental and/or theoretical investigation. Related aspects such as the assignment of oxidation states [30] or spin-pairing processes [31] are still questionable.

The scope of the present review covers:

(1) The mutual relationship between structure and electronic structure of metal–dioxygen complexes;

(2) The phenomenon of dioxygen activation in the light of recent quantitative molecular orbital calculations.

The latter means the oxygen–oxygen bond softening under coordination, so that the properties of superoxide anion, O_2^-, or peroxide dianion, O_2^{2-}, are simulated. In this way new reaction paths come into consideration so that the spin conservation rule or other selection rules can be evaded. However, the above mechanism represents only one way for dioxygen activation as discussed in more detail elsewhere [4].

Dioxygen activation is affected by several factors; among the most important of these are the central atom effect (the proton number, oxidation and spin state influence), the axial base (*trans*) influence and the equatorial–axial (integral *cis*) influence in square-bipyramidal complexes. The activation process can be considered a consequence of the mutual influence of ligands (MIL), realized via the central atom.

B. STRUCTURE AND BONDING OF DIOXYGEN COMPLEXES

(i) Experimental structure data

Many structures of metal–dioxygen complexes have been determined by X-ray structure analysis. There are also complexes stable in solution but not known in the form of a monocrystal so that X-ray studies are not possible. In this case the ESR technique is often used in order to predict the type of structure. However, this section is concerned only with X-ray structure determination.

There are a number of different structural types of dioxygen coordination. They can be classified by various criteria. The most frequently used classification corresponds:

(1) to the formal oxidation state of the coordinated dioxygen, namely the superoxo-like (O_2^-) or peroxo-like (O_2^{2-}) complexes;

(2) to the geometric arrangement of the metal–dioxygen moiety (Structures **I**–**XII**). A more detailed description of these structural types is shown in Table 1. The classification into the superoxo-like or the peroxo-like complexes is based mainly on the following criteria:

(1) the magnetic properties—the superoxo-like complexes are usually paramagnetic for an odd number of electrons and diamagnetic when this

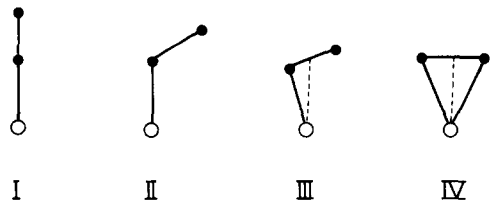

I II III IV

V VI

VII VIII

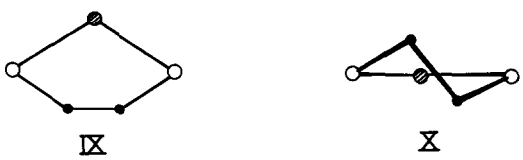

IX X

XI XII

number is even, unlike the majority of the peroxo-like complexes which are diamagnetic;

(2) the IR stretching wavenumber $\tilde{\nu}_{O-O}$ lies in the range 1075–1195 cm^{-1} for superoxo-like complexes instead of the range 742–932 cm^{-1} for peroxo-like complexes [26];

(3) the bond length R_{O-O} is considerably shorter in superoxo-like complexes than in peroxo-like complexes. Selected structural parameters for available structures are listed in Tables 2–6. Individual groups of structural types are discussed below.

Monomeric 1 : 1 superoxo-like complexes

These complexes were characterized by X-ray structure analysis for the central atoms Fe and Co only.

TABLE 1

Types of metal–dioxygen complex

Type	Description	$M:O_2$	Carrier	Example
(1) Monomeric complexes				
I	Linear end-on	1 : 1	Non-realized	Unknown
II	Bent end-on	1 : 1	Superoxo	$Co(bzacen)(Py)(O_2)$
III	Bent side-on	1 : 1	Superoxo	$(NEt_4)_3[Co(CN)_5(O_2)]\cdot 5H_2O$
			Peroxo	$[Co(dppen)_2(O_2)]BF_4$
IV	Symmetrical side-on	1 : 1	Peroxo	$Ti(OEP)(O_2)$
		1 : 2	Diperoxo	$Mo(TTP)(O_2)_2$
		1 : 3	Triperoxo	$Na_4[U(O)_2(O_2)_3]\cdot 9\,H_2O$
		1 : 4	Tetraperoxo	$K_3[Cr(O_2)_4]$
(2) Monobridging μ-O_2 dimeric complexes				
V	Linear	2 : 1	Non-realized	Unknown
VI	Planar end-on	2 : 1	Superoxo	$[(O_2)(Co(NH_3)_5)_2](NO_3)_5$
VII	Planar side-on	2 : 1	Non-realized	Unknown
VIII	Non-planar end-on	2 : 1	Peroxo	$[(O_2)(Co(NH_3)_5)_2](SO_4)_2\cdot 4\,H_2O$
		4 : 2	Peroxo	$[(H_2O)(F\text{-salen})Co(O_2)Co(F\text{-salen})]_2\cdot 2(CHCl_3)\cdot pip$
(3) Dibridging μ-O_2, μ'-NH_2 dimeric complexes				
IX	Planar end-on	2 : 1	Superoxo	$[(O_2)(NH_2)(Co(NH_3)_4)_2](NO_3)_4$
X	Non-planar end-on	2 : 1	Peroxo	$[(O_2)(NH_2)(Co(en)_2)_2](SCN)_3\cdot H_2O$
XI	Symmetrical side-on	2 : 1	Non-realized	Unknown
(4) Dibridging μ-O_2 dimeric complexes				
XII	Bent side-on and Bent end-on	2 : 2	Peroxo	$[(O_2)Rh(Ph_3P)_2Cl]_2$
(5) Bridging dimeric complexes				
XIII		2 : 4	Peroxo	$(NH_4)_4[O(VO(O_2)_2)_2]$
XIV		2 : 4	Peroxo	$(PyH)_2[(O_2H)_2(MoO(O_2)_2)_2]$
(6) Bridging polymeric complexes				
XV		2(+5) : 2	Peroxo	$K_6[Mo_7O_{22}(O_2)_2]\cdot 8\,H_2O$
XVI		4 : 2	Peroxo	$K_4[Mo_4O_{12}(O_2)_2]$

Three diamagnetic Fe^{II} complexes ("picket-fence" porphyrins) listed in Table 2 possess an O–O bond length ranging from 1.15 to 1.26 (all distances in units of 10^{-10} m) and an Fe–O–O bond angle of 129–137°. The structural data are not very reliable because of the disordered O_2 group, high thermal motion and consequently the high crystallographic *R*-factor [32–35]. On the other hand, the bent "end-on" mode of dioxygen coordination has unambiguously been proven. Except for the probably underestimated O–O bond length of 1.15–1.17 (as reported in ref. 34), the other determinations

TABLE 2

Structural parameters of monomeric 1 : 1 superoxo-like complexes [a]

No.	Compound	Temp. (K)	Distance (10^{-10} m)		Angle (deg)		R [b] (%)	Ref.
			O–O	M–O	M–O–O	β		
1	Fe(TpivPP)(MeIm)(O_2)		1.23 (8)	1.75 (2)	135 (4)			
			1.26 (8)		137 (4)		15	32, 33
2	[Fe(TpivPP)(MeIm)(O_2)]·$\frac{1}{2}$ben·$\frac{1}{2}$MeIm		1.15 (4)	1.75 (2)	133 (2)			
			1.17 (4)		129 (2)		11	34
3	[Fe(TpivPP)(2-MeIm)(O_2)]·EtOH		1.21 (2)	1.898 (7)	129 (1)			
			1.23 (2)		129 (2)		8	35
4	Co(acacen)(Py)(O_2)		NA	1.95 (5)	NA		19	36
5	Co(salen·C_2H_4Py)(O_2)		1.10 (10)	NA	136		10	37, 32
6	Co(bzacen)(Py)(O_2)		1.26 (4)	1.86	126 (2)		6	38
7	Co(t-Bu-salen)(Py)(O_2)		1.350 (11)	1.870 (6)	116.4 (5)	4	8	39
8	[Co(3-F-saltmen)(MeIm)(O_2)]·2 Me_2CO	102	1.302 (3)	1.881 (2)	117.4 (2)	4	6	40
9	[Co(saltmen)(BzIm)(O_2)]·THF		1.277 (3)	1.889 (2)	120.0 (2)	5	7	41
10	[Co(t-Bsalten)(BzIm)(O_2)]·$\frac{3}{2}Me_2CO$	121	1.273 (10)	1.873 (7)	117.5 (6)	3	8	42
		293	1.257 (10)	1.882 (6)	118.5 (5)	4	6	42
11	[Co(3-OMe-saltmen)(H_2O)(O_2)]·DME		1.282 (19)	1.885 (15)	117 (1)			
			1.223 (19)	1.868 (15)			10	43
12	$(NEt_4)_3$[Co($CN)_5$(O_2)]·5 H_2O		1.240 (17)	1.906 (14)	153.4 (21)	6	7	(44), 45

[a] References in parentheses = not reliable or later re-investigated structures; NA = no available data; cen = centrosymmetric; acen = noncentrosymmetric.

[b] The crystallographic R-factor.

TABLE 3

Structural parameters of monomeric 1 : 1 peroxo-like complexes [a]

No.	Compound	Distance (10^{-10} m)			R (%)	Ref.
		O–O	M–O	M–O		
1	$Ti(OEP)(O_2)$	1.458 (9)	1.822 (8)	1.829 (8)	11	46
2	$[Ti(dipic)(H_2O)_2(O_2)]\cdot 2\ H_2O$	1.464 (2)	1.834 (2)	1.858 (2)	3	47
3	$K_2[Ti(dipic)F_2(O_2)]\cdot 2\ H_2O$	1.463 (5)	1.846 (4)	1.861 (4)	5	47
4	$K_2[O(Ti(dipic)(O_2))_2]\cdot 5\ H_2O$	1.45 (1)	1.872 (7)	1.905 (7)	11	48
5	$NH_4[VO(dipic)(H_2O)(O_2)]\cdot x\ H_2O$ ($x \approx 1.3$)	1.441 (2)	1.870 (2)	1.872 (2)	3	49
6	$Na_2[NbF_5(O_2)]\cdot H_2O$	1.476 (7)	1.928 (4)	1.928 (4)	4	50
7	$Na_2[NbF_5(O_2)]\cdot 2\ H_2O$	1.46	1.933	1.962		51
8	$Na_3[HF_2][NbF_5(O_2)]$	1.481 (4)	1.924	1.940		51
9	$(C_9H_8NO)_2[NbF_5(O_2)]\cdot 3\ H_2O$	1.17 (9)	1.91 (4)	1.95 (7)	9	(51), 52
10	$K_2[MoOF_4(O_2)]\cdot H_2O$	1.440 (32)	1.935 (25)	1.949 (20)	14	53
11	$(NH_4)_3F[MoOF_4(O_2)]$	1.36 (3)	1.91 (3)	1.91 (2)	13	54
12	$(C_9H_8NO)_2[WOF_4(O_2)]\cdot 3\ H_2O$	1.20 (8)	1.92 (4)	2.03 (9)	7	52

13	$[Co(dppen)_2(O_2)]BF_4$	1.420 (10)	1.871 (7)	1.902 (7)	7	55
14	$[(CN)_2(ppm)_3Co(CN)Co(ppm)_2(CN)(O_2)]\cdot\frac{1}{2}$ben	1.441 (11)	1.888 (9)	1.910 (9)	6	56
15	$[Rh(dppe)_2(O_2)]PF_6$	1.418 (11)	2.025 (9)	2.026 (8)	5	57
16	$[Rh(PMe_2Ph)_4(O_2)]BPh_4$	1.429 (14)	2.033 (8)	2.038 (8)	8	58, (59)
17	$[Rh(AsMe_2Ph)_4(O_2)]ClO_4$	1.46 (2)	2.031 (10)	2.034 (9)	6	60, (59)
18	$[Ir(PMe_2Ph)_4(O_2)]BPh_4$	1.49	2.04	2.05	5	59
19	$[Ir(dppm)_2(O_2)]ClO_4$	1.49	2.05	2.06	5	59
20	$[Ir(dppm)_2(O_2)]PF_6$	1.45	2.00	2.01	6	59
21	$[Ir(dppe)_2(O_2)]PF_6$	1.52 (1)	2.052 (7)	2.062 (7)	4	61, (59)
		1.625 (23)	1.961 (18)	1.990 (16)	7	57, (62)
22	$Ir(Ph_2EtP)_2(CO)Cl(O_2)$	1.461 (14)	2.036 (9)	2.084 (9)	5	63
23	$Ir(Ph_3P)_2(CO)Cl(O_2)$	1.30 (3)	2.04 (3)	2.09 (3)	7	64, (65)
24	$Ir(Ph_3P)_2(CO)Br(O_2)$	1.36	2.00	2.00		66
25	$[Ir(Ph_3P)_2(CO)I(O_2)]\cdot CH_2Cl_2$	1.509 (26)	2.035 (20)	2.082 (22)	6	67, (68)
26	$[Pt(Ph_3P)_2(O_2)]\cdot 2\ CHCl_3$	1.505 (16)	2.006 (7)	2.006 (7)	7	69
27	$[Pt(Ph_3P)_2(O_2)]\cdot\frac{3}{2}$ben	1.45 (4)	2.01 (2)	2.01 (3)	10	70
28	$[Pt(Ph_3P)_2(O_2)]\cdot$tol	1.26 (5)	1.90 (5)	1.99 (5)	12	71

[a] For footnotes see Table 2.

TABLE 4

Structural parameters of monobridging dimeric 2 : 1 superoxo-like and peroxo-like complexes [a]

No.	Compound	Distance (10^{-10} m)		Angle (deg)			R (%)	Ref.
		O–O	M–O	M–O–O	β	ϕ		
1	$K_5[O_2(Co(CN)_5)_2]\cdot H_2O$,cen	1.289 (20)	1.919 (9)	120.7 (10)	3	180		
	acen	1.243 (13)	1.934 (9)	121.8 (7)	7	165.9		
			1.954 (9)	120.6 (6)	4		6	72
2	$[O_2(Co(NH_3)_5)_2]SO_4(HSO_4)_3$	1.312	1.894	117.8	4	180		
			1.894	117.5	2		8	(73), 74
3	$[O_2(Co(NH_3)_5)_2](NO_3)_5$	1.317	1.895	117.3	5	180	5	(75), 76
4	$K_8[O_2(Co(CN)_5)_2](NO_3)_2\cdot 4\ H_2O$	1.447 (4)	1.985 (3)	118.8	8	180	4	77
5	$[O_2(Co(NH_3)_5)_2](SO_4)_2\cdot 4\ H_2O$	1.473 (10)	1.876 (7)	113.2	4	145.5		
			1.889 (7)	112.3	3		7	78
6	$[O_2(Co(NH_3)_5)_2](SCN)_4$	1.469 (6)	1.879 (3)	110.8		180	4	(79), 80
7	$[O_2(Co(en)(dien))_2](ClO_4)_4$	1.488 (6)	1.896 (4)	110.0 (3)		180	5	81
8	$[O_2(Co(en)_2(NO_2))_2](NO_3)_2\cdot 4\ H_2O$	1.529 (9)	1.887 (6)	110.0 (6)		180	11	82
9	$[(H_2O)(F\text{-salen})Co(O_2)Co(F\text{-salen})]_2\cdot 2(CHCl_3)\cdot pip$	1.308 (28)	2.000	118		122		
			1.931	117			15	83
10	$[O_2(Co(salen)(DMF))_2]$	1.339 (6)	1.910 (6)	120.3 (2)		110.1	8	(84), 85
11	$[O_2(Co(salen)(pip))_2]\cdot \frac{2}{3}Me_2CO\cdot \frac{1}{3}pip$	1.383 (7)	1.909 (5)	120.5 (4)		121.9		
			1.914 (5)	119.6 (4)			7	86
12	$[O_2(Co(salprtr))_2]\cdot tol$	1.45 (2)	1.93	118.5 (7)		149.3	12	87
13	$[O_2(Co(pydpt))_2]I_4\cdot 3\ H_2O$	1.456 (9)	1.888 (6)	115.4 (5)		162		
			1.894 (6)	114.3 (4)			7	88
14	$[O_2(Co(pydien))_2]I_4$	1.489 (8)	1.876 (4)	112.5 (4)			5	89

[a] For footnotes see Table 2.

TABLE 5

Structural parameters of dibridging 2:1 and 2:2 complexes [a]

No.	Compound	Distance (10^{-10} m)		Angle (deg)		R (%)	Ref.
		O–O	M–O	M–O–O	φ		
1	$[(O_2)(NH_2)(Co(NH_3)_4)_2](NO_3)_4$	1.320 (5)	1.865 (4)	120.4 (3)	0		
			1.869 (4)	121.3 (3)		5	90
2	$[(O_2)(NH_2)(Co(en)_2)_2](NO_3)_4 \cdot H_2O$	1.353	1.878	119.2	23.4		(91), 92
3	$[(O_2)(NH_2)(Co(en)_2)_2](NO_3)_3 \cdot \frac{15}{8}(AgNO_3) \cdot H_2O$	1.43 (3)	1.88 (1)	110.9 (4)	61	11	129
4	$[(O_2)(NH_2)(Co(en)_2)_2](SCN)_3 \cdot H_2O$	1.458	1.870	109.0	62.5		
			1.873	110.3		8	93
5	$[(O_2)Rh(Ph_3P)_2Cl]_2$	1.44 (2)	1.98 (1)				
			2.19 (1)				
			2.07 (1)	102.5 (3)		5	94
6	$[(O_2H)(NH_2)(Co(en)_2)_2](NO_3)_4 \cdot 2\ H_2O$	1.42	1.92	115			91

[a] For footnotes see Table 2.

TABLE 6

Structural parameters of 1:2, 1:3 and 1:4 peroxo-like complexes [a]

No.	Compound	Distance (10^{-10} m)			R (%)	Ref.
		O–O	M–O	M–O		
1	$NH_4[VO(NH_3)(O_2)_2]$	1.472 (4)	1.882 (3)	1.883 (3)	3	95
2	$(NH_4)_4[O(VO(O_2)_2)_2]$	1.449 (26)	1.851 (19)	1.870 (18)		
		1.447 (24)	1.875 (18)	1.915 (15)		
		1.442 (24)	1.851 (18)	1.857 (18)		
		1.436 (24)	1.839 (18)	1.876 (18)	11	96
3	$(NH_4)_3[Nb(C_2O_4)_2(O_2)_2]\cdot H_2O$	1.480 (6)	1.981 (4)	1.961 (4)		
		1.485 (6)	1.969 (4)	1.982 (4)	4	97
4	$K[Nb(ophen)(O_2)_3]\cdot 3\ H_2O$	1.470 (10)	1.981 (7)	1.988 (7)		
		1.496 (11)	1.980 (7)	1.981 (7)		
		1.500 (8)	1.979 (7)	2.014 (7)	5	98
5	$K[Nb(ophen)(O_2)_3]\cdot 3\ H_2O\cdot H_2O_2$	1.499 (6)	1.966 (6)	1.994 (5)		
		1.503 (6)	1.982 (6)	2.005 (6)		
		1.524 (5)	1.979 (6)	1.986 (5)	5	98
6	$KMg[Nb(O_2)_4]\cdot 7\ H_2O$	1.495 (4)	2.015 (2)	2.063 (2)		
		1.500 (3)	1.993 (4)	2.066 (3)		
		1.502 (3)	2.014 (2)	2.038 (2)		
		1.504 (6)	2.004 (3)	2.011 (2)	4	99
7	$CrO(ophen)(O_2)_2$	1.40 (2)	1.80 (1)	1.87 (1)		100
8	$CrO(bipy)(O_2)_2$	1.40 (2)	1.78 (1)	1.92 (1)	12	101
9	$CrO(Py)(O_2)_2$	1.45	1.80	1.80		102–
		1.42	1.78	1.81	13	104
10	$Cr(NH_3)_3(O_2)_2$	1.28	1.88	2.02		
		1.31	1.87	1.89		
		1.31	2.02	2.04		
		1.33	1.86	1.93	22	105

11	$K_3[Cr(O_2)_4]$	1.489 (22)	1.895 (15)	1.944 (15)	13	106
		1.472 (25)	1.874 (19)	1.972 (18)	9	107
12	$Mo(TTP)(O_2)_2$	1.399 (6)	1.958 (4)	1.958 (4)	4	108
13	$[MoO(PO(NMe_2)_3)(H_2O)(O_2)_2]$	1.494 (8)	1.929 (5)	1.952 (5)		
		1.498 (8)	1.935 (5)	1.952 (5)	3	109
14	$[MoO(PO(NMe_2)_3)(Py)(O_2)_2]$	1.439 (15)	1.918 (11)	1.938 (12)		
		1.442 (15)	1.905 (12)	1.943 (11)	5	109
15	$K_2[MoO(C_2O_4)(O_2)_2]$	1.474 (22)	1.949 (16)	1.933 (15)		
		1.439 (24)	1.963 (18)	1.935 (14)	11	110
16	$K_6[Mo_7O_{22}(O_2)_2]\cdot 8\ H_2O$	1.38 (6)	1.86 (5)	1.96 (4)	10	(111), 112
17	$K_4[Mo_4O_{12}(O_2)_2]$	1.48	2.22, 2.21			
			2.30, 2.25		10	111
18	$[Zn(NH_3)_4][Mo(O_2)_4]$	1.55 (5)	1.93 (3)	2.00 (2)	8	113
19	$(PyH)_2[O(MoO(H_2O)(O_2)_2)_2]$	1.480 (11)	1.961 (7)	1.977 (8)		
		1.488 (11)	1.955 (7)	1.961 (8)	4	(114), 115
20	$(PyH)_2[(OOH)_2(MoO(O_2)_2)_2]$	1.466 (10)	1.920 (6)	1.954 (6)		
		1.473 (10)	1.925 (6)	1.948 (6)	3	(114), 115
21	$K_2[O(MoO(H_2O)(O_2)_2)_2]\cdot 2\ H_2O$	1.525 (16)	1.974 (10)	1.980 (9)		
		1.455 (16)	1.953 (12)	1.959 (10)		
		1.498 (17)	1.966 (12)	1.938 (15)		
		1.453 (19)	1.972 (9)	1.976 (10)	10	116
22	$K_2[O(WO(H_2O)(O_2)_2)_2]$	1.46	1.81	1.84		
		1.50	1.96	1.93		
		1.50	1.96	1.96		
		1.54	1.96	2.00	16	117
23	$Na_4[U(O)_2(O_2)_3]\cdot 9\ H_2O$	1.439 (56)	2.201 (47)	2.292 (36)		
		1.485 (64)	2.273 (48)	2.332 (44)		
		1.602 (62)	2.289 (35)	2.322 (47)	12	(118), 119

[a] For footnotes see Table 2.

indicate values ranging around the distance found in the free dioxygen molecule (1.21). Significant structural changes occur upon oxygenation [35]. Within the series of Fe(TTP)(2-MeIm), Fe(TpivPP)(2-MeIm), Fe(TpivPP)(2-MeIm)(O_2) and Fe(TpivPP)(MeIm)(O_2) the central atom displacement from the equatorial plane (measured towards the dioxygen ligand) increases as follows: -0.42, -0.399, -0.086 and $+0.03$.

Three sub-groups of Co-containing complexes can be distinguished. The first sub-group is represented by complexes of acacen, salen and bzacen with the pyridine in the role of an axial base. These earlier reported structure determinations are rather rough (nos. 4–6 in Table 2). However, the bent "end-on" mode of dioxygen coordination is unequivocal.

The next group covers derivatives of the salen-type Schiff base (nos. 7–11 in Table 2) [38–43]. Except for no. 11 (the crystallographic R-factor of which is 10%), they exhibit an unambiguous correlation between the Co–O bond length, r_2, and the Co–O–O bond angle, α, as shown in Fig. 1. The lower the angle α, the shorter the distance r_2 and simultaneously the larger the O–O

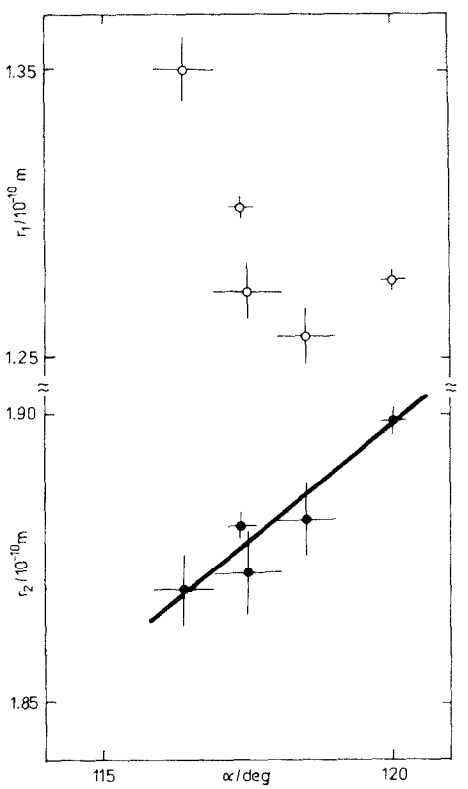

Fig. 1. Plot of the O–O distance r_1 and Co–O distance r_2 vs. the Co–O–O angle α in 1 : 1 superoxo-like complexes.

bond length r_1. This indicates that dioxygen activation (expressed through an O–O bond lengthening) is accompanied by shortening of the Co–O distance. Considering the next degree of freedom, the angle β (i.e. deviation of the Co–O linkage from the normal of the equatorial plane) the structural changes discussed above can be expressed as in Fig. 2.

Since the single representative of the last sub-group follows these trends, this compound (no. 12 in Table 2) differs from the others mainly in the type of the ligand sphere. Here five cyanide ligands tend to stabilize the higher oxidation state of the central atom, so that the activation process is rather inhibited. The highest Co–O–O angle of the cobalt 1 : 1 superoxo-like complexes ($\alpha = 153°$) was originally explained in terms of the interaction of negative charge on the terminal oxygen with four adjacent cyanide anions in the equatorial plane [45]. This leads to the observation that the mutual influence of ligands manifests itself in the degree of dioxygen activation; the *cis* influence of four equatorial CN^- ligands makes the activation process less efficient. The significant value of the angle $\beta \approx 6°$ also permits the unsymmetrical, bent "side-on" classification (Structure **III**).

Monomeric 1 : 1 peroxo-like complexes

X-ray structures of this type were reported with complexes of Ti, V, Nb, Mo, W, Co, Rh, Ir and Pt [46–71]. Some of the central atoms are characterized by the formal d^2 electronic configuration prior to oxygenation (Ti^{II}, V^{III}, Nb^{III}, Mo^{IV}, W^{IV}) and, after oxygenation the d^0 configuration is obtained so that the following assignment of oxidation states is possible: Ti^{IV}–$(O_2)^{-II}$, V^{V}–$(O_2)^{-II}$, Nb^{V}–$(O_2)^{-II}$, Mo^{VI}–$(O_2)^{-II}$ and W^{VI}–$(O_2)^{-II}$. The second sub-group of $M^I = Co^I$, Rh^I and Ir^I complexes undergoes the following re-formulation after oxygenation: M^{III}–$(O_2)^{-II}$, i.e. d^8 to d^6 charge transfer takes place. For the last sub-group the assignment of Pt^{II}–$(O_2)^{-II}$ is valid after oxygenation (d^{10} to d^8 charge transfer). The typical interval for the O–O bond lengths is 1.40–1.50 (with some exceptions).

The symmetrical "side-on" mode of dioxygen coordination (Structure **IV**) rarely occurs; the majority of the peroxo-like complexes belong to the

Fig. 2. Schematic drawing of structural changes in 1 : 1 superoxo-like Co^{II} complexes.

category of unsymmetrical, bent "side-on" type (Structure **III**). This leads to a loss in symmetry, so that the group-theoretical analysis (as discussed in the next section) must be applied carefully.

The most frequently cited series of $Ir(Ph_3P)(CO)X(O_2)$ (X = Cl, Br, I) exhibit O–O bond lengths of 1.30, 1.36 and 1.51, respectively. While the first corresponds to the superoxo-type, the last distance is typical of the peroxo-type. The less electronegative more polarizable iodide ligand appears to have raised the metal valence orbitals to higher energy. Consequently, the three-center bonding molecular orbital, formed from metal orbitals and dioxygen π antibonding (π^*) orbitals, becomes mostly dioxygen in character. Therefore, there will be little dioxygen to metal σ bonding. The π back bonding (metal to dioxygen charge transfer) increases and the strength of the O–O bond decreases [11]. Similarly, by substituting the Ph_3P ligand with L = Ph_2EtP, a more weakly back-bonding ligand, the O–O bond length increases from the value of 1.30 to 1.46 in $Ir(L)_2(CO)Cl(O_2)$ complexes. Thus, the mutual influence of ligands again affects the degree of dioxygen bond lengthening.

The complex $[Pt(Ph_3P)_2(O_2)]\cdot$sol (sol = 3 $CHCl_3$, 3/2 ben and tol) adopts a square-planar arrangement of the PtP_2O_2 chromophore for various solvent molecules. The structural data for the last complex (no. 28 in Table 3) are not very reliable (probably underestimated O–O bond length of 1.26, crystallographic *R*-factor = 12%). The chloroform molecules exhibit hydrogen bonds to both oxygen atoms with a linear Pt–O–H linkage and an O–H distance of 2.04. For this reason the O–O bond length (1.50) increases in comparison with the case of the benzene solvent (1.45) [69].

Monobridging dimeric 2 : 1 complexes

Crystal structures were reported only for the Co centres. They cover either the formally assigned superoxo-like complexes (paramagnetic) or peroxo-like complexes (diamagnetic). The former exhibit O–O bond lengths within the range 1.24–1.32 whereas the latter lie between 1.38–1.53. One peroxo-like complex (no. 9 in Table 4, *R*-factor = 15%) is out of this range but this compound may be formulated instead by a 4 : 2 metal to dioxygen ratio. In the superoxo-like complexes the value of $\phi = 180°$ for the dihedral angle Co–O–O–Co was postulated (Structure **VI**) unlike the peroxo-complexes, where ϕ often is less than 180° (Structure **VIII**).

Avdeef and Schaefer have reported [86] that, "of the structural parameters only the Co–O–O angles appear to correlate with the O–O bond distances". A revised plot of r_1 versus α is shown in Fig. 3 for the peroxo-like complexes. In addition, Fig. 4 serves not only to show a correlation for the superoxo-like complexes, but also that between the Co–O bond lengths and Co–O–O bond angles. Nearly the same conclusions can be drawn from Figs. 3 and 4

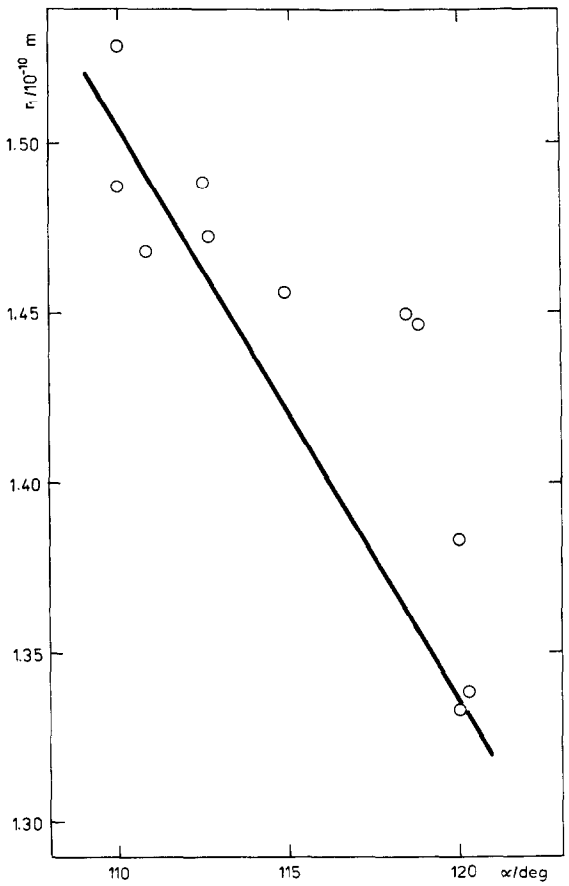

Fig. 3. Plot of the O–O distance r_1 vs. the Co–O–O angle α in 2:1 peroxo-like complexes.

as those previously discussed on the basis of Fig. 1: the larger the bond length r_1 (or the degree of dioxygen activation), the lower the bond angle α. Moreover, in the superoxo-like complexes the degree of dioxygen bond lengthening increases passing from the CN^- ligands to the NH_3 (the O–O bond length increases from 1.24–1.29 to 1.31–1.32). Similarly, for the peroxo-like complexes of the type $[L_5Co(O_2)CoL_5]^q$ the O–O bond length increases in the series $L_5 = 5\ CN^-$, $5\ NH_3$, (en)(dien) and 2(en)(NO_2) from 1.45, 1.47, 1.49 to 1.53. Evidently neutral ligands with a good donor ability tend to stabilize a lower oxidation state of the central atom, thus supporting the dioxygen activation. For this reason the MIL concept appears to be useful in explaining the degree of dioxygen bond extension.

A *trans* influence of the axial base is also visible. The O–O bond length

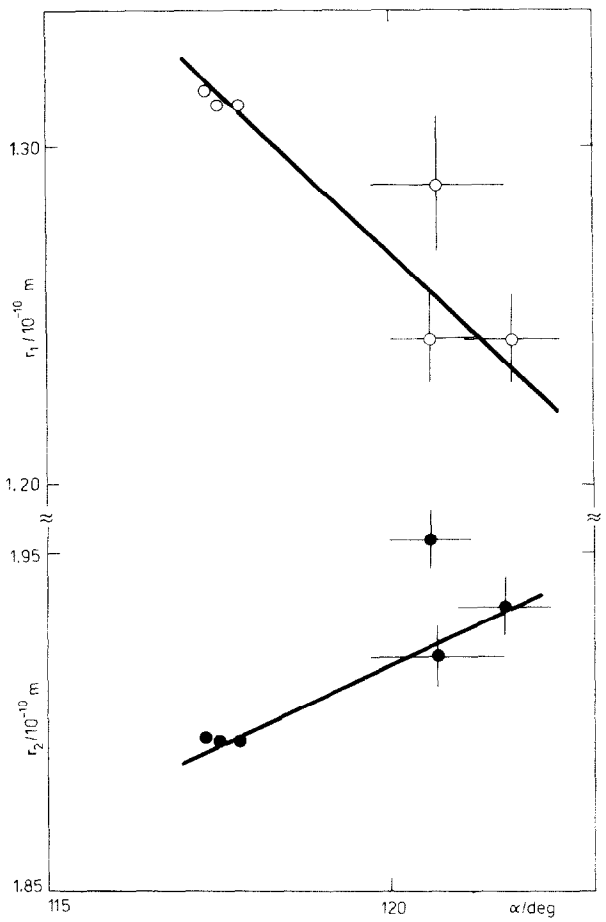

Fig. 4. Plot of the O–O distance r_1 and Co–O distance r_2 vs. the Co–O–O angle α in 2 : 1 superoxo-like complexes.

increases with substitution of the axial base B = DMF with B = pip in complexes of the type $[O_2(Co(salen)(B))_2]$ (nos. 10 and 11 in Table 4).

Dibridging dimeric 2 : 1 complexes

These Co-containing complexes exhibit one NH_2 bridge and one O_2 bridge. The superoxo-like complexes were expected to be planar (Structure **IX**) while the peroxo-like complexes appear to have a non-zero Co–O–O–Co dihedral angle ϕ (Structure **X**). The structural parameters (Table 5) follow the above trends: the lower the Co–O–O angle α, the longer the O–O bond length r_1. Consequently, the dihedral angle increases as $\phi = 0°$, 23°, 61° and 63°. By substitution of $L_4 = 4\ NH_3$ with $L_4 = 2$ en for complexes of the

$[L_4Co(O_2)(NH_2)CoL_4]^{4+}$ type, the O–O bond length increases in agreement with the better donor ability of the ethylenediamine ligands. Simultaneously, the dihedral angle ϕ increases, so that a situation intermediate between the limiting superoxo and peroxo cases is adopted.

Other complexes

Structures of multiperoxo complexes (1 : 2, 1 : 3 and 1 : 4) were reported only for the group V and VI elements (V, Nb, Cr, Mo, W and U). They display both the symmetrical "side-on" (Structure **IV**) and bent "side-on" (Structure **III**) modes of dioxygen coordination (Table 6). They also possess unusual coordination numbers such as $2 + 2(+2)$, $2 + 2(+3)$, $2 + 2(+4)$, $2 + 2 + 2(+2)$ and $2 + 2 + 2 + 2$, where values in parentheses correspond to the donor atom without the dioxygen ligands. These complexes are either monomeric, dimeric (with an oxo bridge or two hydroperoxo bridges) or polymeric. Despite the peroxo-like assignment these complexes are not necessarily diamagnetic; they are paramagnetic if the number of electrons is odd, e.g. in $K_3[Cr(O_2)_4]$.

An unusual situation was found in the 2 : 2 complex $[(O_2)Rh(Ph_3P)_2Cl]_2$, (no. 5 in Table 5), where two dioxygen bridges belong to the superoxo-like as well as to the peroxo-like classes (Structure **XII**). Here the coordination number of each rhodium centre is $2 + 1(+3)$.

Quite an unusual mode of dioxygen coordination also occurs in $K_4[Mo_4O_{12}(O_2)_2]$, (no. 17 in Table 6), where two dioxygens are coordinated to four molybdenum centres.

(ii) Quantum chemical calculations

A bonding model is to be constructed by a theoretical approach in terms of which the principal electronic properties of the adduct system $M(O_2)$ can satisfactorily be explained. Here, two different approaches can be distinguished, as discussed below.

Qualitative approach

The bonding model is postulated a priori for a given molecular geometry (level I). There are four general methods, namely: (1) intuitive VB or MO theory; (2) group-theoretical analysis; (3) electronic spectra analysis; and (4) ESR spectra analysis, as shown in Table 7.

Dioxygen coordination in hemoglobin was investigated by Pauling. Originally, he proposed a linear "end-on" mode of dioxygen coordination (Structure **I**) [120], then [121,122] a bent "end-on" mode (Structure **II**) with an Fe–O–O angle of 120° and formal valency of Fe^{II}. On the other hand, Weiss [123,124] deduced the Fe^{III}–$(O_2)^{-1}$ formulation as a charge transfer com-

TABLE 7

Various bonding models of coordinated dioxygen

No.	System	Approach [a]	Ref.
1	$Hb(O_2)$	1	120–124
2	$Hb(O_2)$	2	125
3	$M(O_2)$	1	11
4	$[L_4Co(O_2)(X)CoL_4]^q$ ($L = NH_3$)	2	127
5	$[L_5Co(O_2)CoL_5]^q$ ($L = NH_3$)	2	3, 127, 128
6	$M(O_2)M \rightarrow 2\ MO$	1	130
7	$Ti(por)(O_2)$	2	131
8	$Mo(por)(O_2)_2$	2	131, 132
9	$M(por)(O_2)$	2	133
10	$M(O_2)$	3	28
11	$CoL_n(O_2)$	3	134
12	$[CoL_5(O_2)]^{3-}$ ($L = CN^-$)	3, 4	135
13	$[L_5Co(O_2)CoL_5]^{5-}$ ($L = CN^-$)	3, 4	135
14	$M(por)(O_2)$ (M = Co, Fe)	3, 4	136
15	$CoL(O_2)$	4	137
16	$FeL(O_2)$	1	29, 30, 163
17	$ML(O_2)$ (M = Cr, Mn, Fe, Co)	1	31
18	$ML(O_2)$ (M = Mn, Fe, Co)	4	138
19	$Mn(TPP)(O_2)$	4	139

[a] Notation used: 1, intuitive VB or MO theory; 2, group theoretical analysis; 3, electronic spectra analysis; 4, ESR spectra analysis.

plex. Finally, Griffith [125] considered dioxygen in a "valence state" and proposed a symmetrical "side-on" coordination (Structure **IV**) similar to that of the Chatt–Duncanson model [126] for π complexes of olefins. Here donor–acceptor interactions appear to be relevant: electron density is transferred from the occupied $\pi(O_2)$ orbital to the vacant d_{z^2} orbital of the central atom (the σ bond) and simultaneously, back-donation from the metal d_π (e.g. d_{xz}) to the vacant $\pi^*(O_2)$ orbital (the π bond) appears.

Valentine [11] distinguished three cases dependent on the relative energy of dioxygen and central atom orbitals:

(1) the bonding molecular orbitals being predominantly of the $\pi(O_2)$ character, i.e. a weak σ bond is formed; at the same time the π electron density transfer should be significant so that a lengthening (or softening) of the O–O bond occurs;

(2) the case of a strong σ bond and weak π bond, so that O–O bond lengthening is not significant;

(3) the situation intermediate between above limiting cases. These relationships are illustrated in Fig. 5.

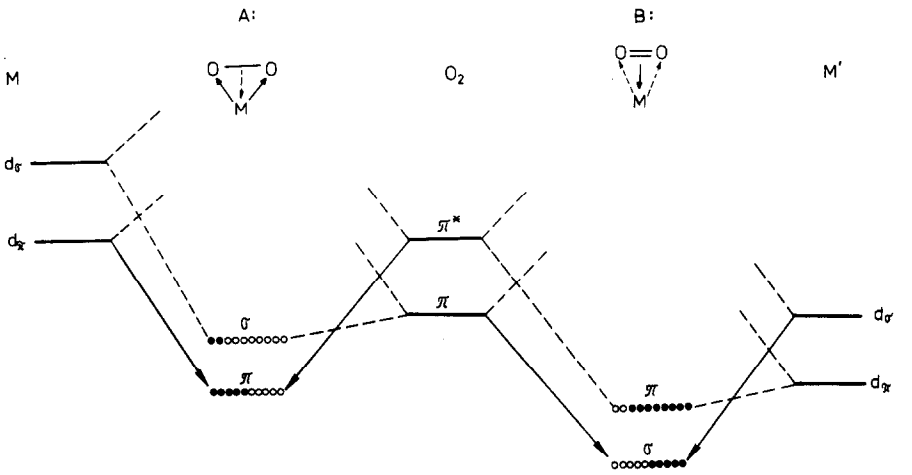

Fig. 5. Main features of metal–dioxygen interactions. A, weak dioxygen to metal σ bond, strong metal to dioxygen π bond; B, strong dioxygen to metal σ bond, weak metal to dioxygen π bond; ●, the *d*-character of MOs; ○, the dioxygen character of MOs (in 10 percent).

A bonding model in O_2-bridging dimeric Co-containing complexes was proposed by Vlček [127]. He considered formation of the four-center π type molecular orbital. An alternative model to Vlček's hypothesis can be found in the article of Bayer and Schretzman [3] which describes a bonding situation in real structures of O_2-bridging complexes.

Ochiai [130] explained the existence of irreversible products of the following reactions

$$\mathrm{M} + \mathrm{O_2} \underset{(a)}{\rightleftarrows} \mathrm{MO_2} \overset{\mathrm{M}}{\underset{(b)}{\rightleftarrows}} \mathrm{MO_2M} \underset{(c)}{\rightarrow} 2\,\mathrm{MO} \overset{\mathrm{M}}{\underset{(d)}{\rightarrow}} \mathrm{MOM} \qquad (1)$$

for complexes of V^{II}, Cr^{II}, Mn^{II} and Fe^{II} taking into account the fact that complexes of the CoOCo type were not experimentally known. He considered that the high energy barrier of O–O bond cleavage in step (c) can be compensated by stabilization of the $M^+(O)^-$ product. A simple MO model indicates that such stabilization is possible for d^1–d^5 electron configurations of M^+, i.e. for complexes of V^{II}, Cr^{II}, Mn^{II} and Fe^{II}. An antibonding orbital or higher levels are filled for $d^n (n \geqslant 6)$ configurations of M^+ (i.e. beginning with Co^{II}), and the irreversible product $M^+(O)^-$ is destabilized.

A group-theoretical analysis has been used [131,132] in order to predict the most stable conformer of the "side-on" type of oxygenated Ti-containing or Mo-containing porphyrins (dioxygen versus nitrogens of the pyrrole group conformations). It must be mentioned that the group-theoretical

analysis yields only a rough picture of the electronic properties of the system under study because the quality of isoelectronic central atoms (e.g. Fe^{II} and Co^{III}) as well as the quality of ligands (e.g. O_2, N_2^{2-} or L_4-porphin, tetraphenylporphin, octaethylporphin) are not distinguished. A recent paper of Bersuker and Stavrov [133] summarizes the vibronic effects in geometry and stereochemistry of metalloporphyrins and hemoproteins.

The interpretation of electronic spectra and ESR spectra also lead to a bonding model by means of an MO diagram. The work of Lever and Gray [28,134], McLendon et al. [135], Wayland et al. [136], Drago et al. [31,137], Tovrog et al. [138], Hoffman et al. [139], Jones et al. [29] and Summerville et al. [30] belong to this category. For the monomeric 1 : 1 superoxo-like complexes of Co^{II} (bent "end-on" mode of coordination, Structure **II**), both techniques can be used to deduce the MO interaction diagram [28,31,134,135,137,138] given in Fig. 6. A spin-pairing process occurs, one electron of the $Co^{II}(d^7)$ system being paired with one of the π^* electrons from the triplet dioxygen. The dioxygen character of the resulting σ type MO ψ_1 depends upon the relative energy levels of interacting orbitals $\pi_v^*(O_2)$ and $d_{z^2}(Co)$ which can be affected by ligand environment around the cobalt centre. The amount of charge transfer onto dioxygen is mediated by this interaction and experimental data indicate the interval of 0.1 to 0.8(e) [138]. An electron on the second orbital $\psi_2 \approx \pi_h^*(O_2)$ remains unpaired. For this

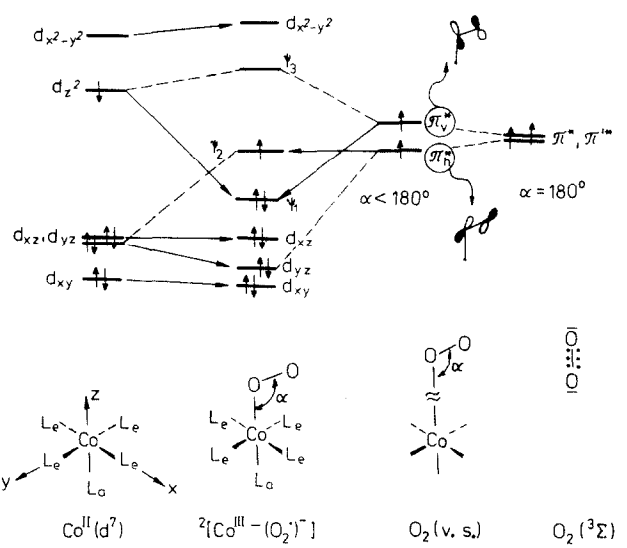

Fig. 6. Simplified MO diagram in cobalt–dioxygen complexes. → strong interactions; - - - - - -, weak interactions.

reason the formulation of $Co^{III}-(O_2^{\cdot})^{-1}$ was accepted regardless of the dioxygen effective charge.

Similar models of the spin-pairing processes were also proposed for dioxygen complexes of Cr^{II}, Mn^{II} and Fe^{II} [31,138,139] or alternative models for Fe^{II} like those found in [29,30]. However, it seems that general acceptance of these models requires further theoretical and experimental activity.

Quantitative calculations

The bonding model is obtained a posteriori and calculations cover the next three levels (Table 8), namely: II, calculations without a transition metal; III, calculations with very simplified or without the actual ligand sphere; IV, calculations where the transition metal as well as the actual ligand sphere are taken into account. Moreover, the mode of dioxygen coordination requires at least a limited geometry variation. Thus, the bonding model obtained is continuously dependent on the molecular geometry.

From the point of view of methodology, further classification is possible: (1) semiempirical methods based on an effective Hamiltonian, such as SCC, SCCC, EHT, IEHT; (2) semiempirical methods based on the zero-differential-overlap hypothesis, such as PPP, CNDO and INDO; (3) the non-empirical methods such as GVB, H–L, F–H and X–α; (4) ab initio calculations (usually in the minimum or valence split basis set). The reliability of these methods increases in the order given.

A simple $Fe(O_2)$ adduct was the subject of investigation using either the Heitler–London (H–L) type or generalized valence bond with configuration interaction (GVB + CI) methods [140–143]. Of more significance appear to be calculations where the low-spin $Fe(por)L(O_2)$ complexes were studied as models of oxyhemoglobin (the ligand L represents an axial base, such as L = none, H_2O, NH_3, Py, Im and MeIm) [144–157]. At least six problems require more detailed discussion: (1) the mode of dioxygen coordination, i.e. either "end-on" or "side-on" as suggested by Pauling [122] and Griffith [125], respectively; (2) the nature of the disordered structures of synthetic dioxygen carriers rationalized in terms of intramolecular motion (rotation about the iron–oxygen bond or inversion via a flipping of coordinated dioxygen); (3) the nature of the large quadrupole splitting observed in the Mössbauer resonance spectra; (4) the assignment of oxidation states such as $Fe^{II}-(O_2)$ or $Fe^{III}-(O_2)^{-1}$; (5) the possible stabilization of coordinated dioxygen through hydrogen bonding to the distal imidazole; (6) an axial base influence in stabilization of the $L-Fe-O_2$ bond.

The "end-on" mode of dioxygen coordination in iron(II) complexes is unequivocal. Both semiempirical [151] and ab initio [154,155] calculations favour the bent Fe–O–O moiety in comparison with alternative symmetrical "side-on" types, in full agreement with X-ray structure data (Table 2). A

TABLE 8

Quantum-chemical calculations of metal–dioxygen complexes

No.	System	Level [a]	Method	Ref.
Iron complexes				
1	$Fe(O_2)$	III	HL	140–142
2	$Fe(O_2)$	III+	GVB+CI	143
3	$Fe(por)(O_2)$	III	SCC	144, 145
4	$Fe(por)L(O_2)$ (L = H_2O, Py, MeIm)	IV	IEHT	146–148
5	$Fe(por)Im(O_2)$	III+	IEHT	149
6	$Fe(SCH_3)(O_2)$	III	IEHT	149
7	$Fe(por)Im(O_2)$	IV+	IEHT	150–152
8	$Fe(por)Im(O_2)$	IV	PPP+CI; $X-\alpha$	153
9	$Fe(por)L(O_2)$ (L = none, NH_3, Im)	IV+	Ab initio	154, 155
10	$[Fe(por)(NH_3)(O_2)\cdots NH_3]$	IV	Ab initio	154, 155
11	$Fe(por)Im(O_2)$	IV+	INDO+CI	156, 157
12	$[FeL_4L'(O_2)]^q$ (L = Cl^-, NH_3; L' = NH_3, Im, Py)	IV	CNDO	158
Cobalt complexes				
1	$Co(acacen)L(O_2)$ (L = none, NH_3; acacen ~ $(C_4H_5NO)_2$)	IV	INDO	159
2	$Co(acacen)L(O_2)$ (L = none, H_2O, CO, CN^-, Im; acacen ~ $(C_3H_4NO)_2$)	IV+	Ab initio	160–162
3	$Co(por)(O_2)$	III	SCC	145
4	$[XCo(O_2)CoX]$ (X = Cl^-, Br^-, I^-)	III	EHT	18, 164
5	$[L_5Co(O_2)CoL_5]^q$ (L = NH_3 or CN^-; q = +4, +5 or −6)	III	SCCC	165, 166
6	$[L_4Co(O_2)(X)CoL_4]^{4+}$ (L = NH_3; X = NH_2^-, OH^-)	IV	FH	167
7	$[Co(PH_3)_4(O_2)]^+$	IV+	FH	168
8	$[Co(CN)_5(O_2)]^{3-}$	IV+	FH	168
9	$[CoCl_4L(O_2)]^{2-}$ (L = none, NH_3, Im, Py)	IV+	CNDO	169, 171
10	$[CoX_4(O_2)\cdots tol]^{2-}$ (X = Cl^-, Br^-)	IV+	CNDO	183
Other complexes				
1	$M(O_2)M$ (M = Ti, V, Cr, Mn, Fe Co, Ni)	III	EHT	163, 164
2	$[M_mO_n]_x\cdots(O_2)$ (M = Fe, Co, Ni)	III	EHT	172
3	$Ti(por)(O_2)$	IV	Ab initio	174
4	$Mn(por)(O_2)$	IV+	Ab initio	175, 176
5	$Mn(por)(O_2)$	IV+	IEHT	177
6	$Pt(PH_3)_2(O_2)$	IV	$X-\alpha$ SW	173
7	$M(PH_3)_2(O_2)$ (M = Ni, Pd, Pt)	IV	CNDO	178
8	$M(PH_3)_2(CO)X(O_2)$ (M = Rh, Ir; X = Cl^-, I^-)	IV	CNDO	178
9	For M = Mn, Fe, Co, Ni, Cu and m = 1 or 2, 3 or 4			
	$^m[MCl_4(NH_3)(O_2)]^q$, q = −3, −2, −1	IV	CNDO	179

TABLE 8 (continued)

No.	System	Level [a]	Method	Ref.
	$^{m}[M(NH_3)_5(O_2)]^q$, $q = 0, 1, 2, 3$	IV	CNDO	180
	$^{m}[M(CN)_5(O_2)]^q$, $q = -4, -3, -2$	IV	CNDO	181
	$^{m}[M(H_2O)_5(O_2)]^q$, $q = 0, 1, 2, 3$	IV	CNDO	182
10	$[MCl_4(O_2)]^{2-}$ (M = Mn, Co, Cu)	IV+	INDO	184
11	Ni(an)(O_2)	II	CNDO	185
12	Ag(O_2)	III	EHT	186
13	$[CH_2CHR \cdots (O_2)]^q$ on Ag (R = H, CH_3)	II	MINDO/2	186
14	$[CH_2CHCH_3 \cdots (O_2)]^-$ on Ag	II	MINDO/2	187

[a] Notation used: II, calculations without a transition metal; III, calculations with simplified or without the actual ligand sphere; IV, calculations with the transition metal and its ligand sphere; + means the dioxygen geometry variation.

more detailed mapping of the adiabatic potential surface (the total energy function of internal coordinates) indicated that a non-symmetrical "side-on" mode (with a non-zero angle β, Structure **III**) is also relevant [151,152]. The values obtained for the stabilization energies are not very reliable because a refinement of calculations (such as full geometry optimization, the inclusion of configuration interaction, correction of the zero-point vibrations, etc.) can affect their values. Both rotation about the iron–oxygen bond and inversion via flipping, belong to possible intramolecular motions of coordinated dioxygen. The former possesses a low barrier to rotation (ca. 6 kcal mol^{-1} [154] according to ab initio calculations for Fe(por)(O_2) and 7 kcal mol^{-1} according to INDO calculations for Fe(por)Im(O_2) [156]). Such rotation also has an influence on the electric field gradient of the iron centre. The last quantity was studied by various methods [144,145,149,151–153,156]. The electric field gradient and related quantities such as the quadrupole splitting or asymmetry parameter are very sensitive to details of calculations (see, for instance ref. 156).

The assignment of oxidation states to the Fe(O_2) unit has a long history [29,30,122–124]. In terms of simple valence bond theory, two possibilities were proposed: (1) an even number of electrons about dioxygen is obtained by considering a resonance hybrid of two structures (Structures **XIII**, **XIV**) as suggested by Pauling; (2) an odd number of electrons localized on dioxygen is obtained by considering a resonance hybrid of two other structures (Structures **XV**, **XVI**). Here diamagnetism results from the opposite spin orientation of unpaired electrons $Fe^{III}(\uparrow)$–$(O_2)^{-I}(\downarrow)$, as suggested by Weiss [123,124].

XIII XIV

XV XVI

Another approach in assigning oxidation states is based on molecular orbital theory. One of the possibilities was derived from a qualitative MO diagram, considering the energy difference Δ (the separation of d_{xy} and $\pi^*(O_2)$ orbitals) versus the pairing energy [29,30]. Of more significance appear to be results of quantitative MO calculations. A corresponding MO diagram showing the main interactions in the low-spin $Fe(por)NH_3(O_2)$ complex (as follows from ab initio calculations [155]) is presented in Fig. 7. The diagram indicates the absence of any appreciable d_{z^2}–π_v^* interaction, unlike the d_{yz}–π_h^* which is apparent. The coordinated dioxygen is nearly neutral thus supporting the description Fe^{II}–$(O_2)^0$, the dioxygen being in the singlet spin state and with electron configuration $(d_{xz})^2(d_{yz})^2$-$(d_{xy})^2(\pi_v^*)^2(\pi_h^*)^0$. This is in agreement with the value of $\tilde{\nu}(O_2) = 1385\ cm^{-1}$ reported for synthetic iron-containing dioxygen carriers only 100 cm^{-1} below that of free singlet dioxygen [188]. Moreover, the Fe–O bond length of 1.75 is considerably shorter in comparison with 1.86 for the Co-containing complexes indicating possible back-bonding in the Fe^{II} complexes. On the other hand IEHT calculations support the Fe^{III}–$(O_2)^{-1}$ formalism following from the large negative charge localized on the coordinated dioxygen (Table 9). Such a description was also proposed on the basis of INDO calculations with empirical two-electron integrals. This method, giving excellent agreement between the calculated and the experimental electric field gradients, however, yields the electron population of $d^{6.1}$, a value in disagreement with the $Fe^{III}(d^5)$–$(O_2)^{-1}$ formulation.

Further, on the basis of ab initio calculations the following conclusions were drawn [155].

(1) Stabilization of the coordinated dioxygen through hydrogen bonding to distal imidazole in the hemoproteins was not supported by a model calculation of $[Fe(por)NH_3(O_2) \cdots NH_3]$, where the proximal and the distal imidazole were replaced by two ammonia molecules. The calculated interac-

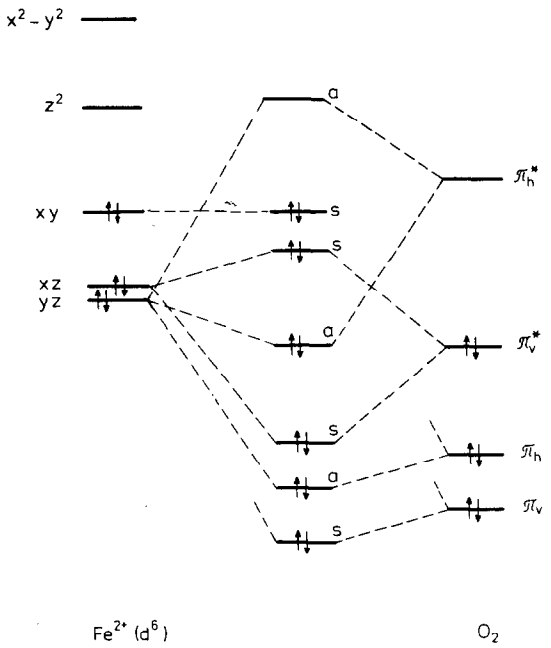

Fig. 7. Simplified MO diagram of the Fe(por)$NH_3(O_2)$ complex. s, orbitals symmetric with respect to the Fe–O–O plane; a, antisymmetric.

TABLE 9

Calculated charge distributions within the Fe(O_2) unit

System	Population		Charge (e)		Method [a]	Ref.
	$3d$	$4s$, $4p$	Q(Fe)	Q(O_2)		
Fe(por)$NH_3(O_2)$	6.33	0.45	1.22	0.02	Ab initio	155
Fe(por)Im(O_2)	6.32	0.44	1.23	0.03	Ab initio	155
	6.19	1.37	0.44	0.06	PPP	153
	7.54				$X-\alpha$	153
	6.37	0.84	0.80	−0.08	INDO-t	156
	6.07	0.53	1.41	−0.75	INDO-e	156
	7.03	0.71	0.26	−0.56	IEHT	149, 151, 152
Fe(SCH_3)(O_2)			0.20	−0.69	IEHT	149
$[FeCl_4Im(O_2)]^{2-}$	6.02	1.82	0.16	0.07	CNDO-t	158
$[Fe(H_2O)_5(O_2)]^{2+}$	6.14	1.66	0.20	0.27	CNDO-t	182
$[Fe(NH_3)_4Im(O_2)]^{2+}$	6.36	2.02	−0.38	0.25	CNDO-t	158
$[Fe(CN)_5(O_2)]^{3-}$	6.61	2.69	−1.30	0.03	CNDO-t	158

[a] t, theoretical two-electron integrals; e, empirical.

tion of NH_3 to the middle oxygen of the $Fe(O_2)$ unit is repulsive. This point probably requires further re-investigation.

(2) No significant changes were registered by replacing the axial base $L = NH_3$ with L = Im in $Fe(por)L(O_2)$ type complexes. Thus, the imidazole ligand seems to function as a pure σ donor without an additional π electron donor or acceptor ability.

(3) Inversion at the bound oxygen atom seems to be easier through the linear Fe–O–O transition state (an energy barrier of 14 kcal mol^{-1}) than through the "side-on" transition state (a barrier of 55 kcal mol^{-1}).

(4) The triplet spin state with the electron configuration of $(d_{xy})^2(d_{xz})^2(d_{yz})^1(\pi_v^*)^2(\pi_h^*)^1$ should be rather close in energy to the singlet ground state. The INDO + CI calculations for $Fe(por)Im(O_2)$ indicate an energy separation of 129 cm^{-1} [156].

A significant contribution to our understanding of the nature of $Co–O_2$ bonding was obtained on the basis of ab initio RHF calculations [160–162] for models of $Co(acacen)L(O_2)$. According to these calculations [162]: (1) the mode of dioxygen coordination is unequivocally the bent "end-on" type; (2) a charge-transfer configuration of $Co^{III}–(O_2^-)^{-1}$ represents the formal valency; however, the electron density transfer does not approach a complete electron charge; (3) the simplified MO diagram is similar to that deduced from the ESR spectra analysis (Fig. 6); the calculated ground-state electronic configuration is $(d_{xz})^2(d_{yz})^2(d_{x^2-y^2})^2(\pi_v^*)^2(\pi_h^*)^1(d_{z^2})^0$ and can be rationalized in terms of a spin pairing process; (4) the perpendicular, "side-on" geometry is destabilized by at least 50 kcal mol^{-1} over the bent geometry; the destabilization of the linear Co–O–O geometry is only ca. 10 kcal mol^{-1}; (5) the calculated enthalpies of oxygenation point to the stabilizing effect of the fifth ligand $L = H_2O$, CO, Im, CN^-; a relationship between the ease of oxygenation, the σ donor ability of the fifth ligand, and the ease of oxidation of Co^{II} to Co^{III} was found; (6) the π electron donor or acceptor ability of the imidazole ligand seems to be overemphasized.

These conclusions do not contradict the semiempirical INDO–UHF calculations of another model of $Co(acacen)L(O_2)$, L = none, NH_3 [159], or CNDO–UHF calculations of other model complexes [169–171]. The spin density is completely localized on the dioxygen moiety whereas the metal to dioxygen charge transfer is less than one-half of an electron charge. On the other hand, the earlier SCC calculations [145] of $Co(por)(O_2)$ yield the unacceptable spin-density distribution: 25% d_π, 20% O_2 and 55% N_π in character.

Fenske–Hall parameter-free MO calculations of $[Co(CN)_5(O_2)]^{3-}$ were used in order to localize the energy minimum as a function of the Co–O–O bending angle α [168]. The calculated value of $\alpha = 132°$ corresponds to the "end-on" mode of dioxygen coordination in agreement with the X-ray

structure analysis ($\alpha = 153°$). The O–O bond order $b = 1.59$ is not too far from the experimental estimate of 1.54. The calculated ground-state electron configuration of $d^6(\pi_v^*)^2(\pi_h^*)^1$, the dioxygen charge $Q(O_2) = -0.53$ (the terminal oxygen being more negative, $Q(O_b) = -0.44$), and the orbital character of 10% d_{yz} + 89% π_h^* for the unpaired electron agree well with the above conclusions. On the other hand, the $[Co(PH_3)_4(O_2)]^+$ complex, used as a model of $[Co(dppen)_2(O_2)]^+$, yields the energy minimum for the triangular geometry ("side-on" mode of dioxygen coordination, $\alpha = 69°$), a result which is again in agreement with X-ray structure data. Here the calculated electron configuration is $d^8(\pi_h^*)^2(\pi_v^*)^0$, the dioxygen charge is $Q(O_2) = -0.58$ and the O–O bond order is $b = 1.35$ (cf. an experimental estimate of 1.23).

The electronic properties of some binuclear dioxygen complexes at a fixed geometry were studied by EHT, SCCC and F–H methods [164–167].

The manganese porphyrin dioxygen carrier has been the subject of extensive discussions [175–177,189–191]. In toluene solutions (194 K) dioxygen binds reversibly to Mn(TTP)Py with replacement of pyridine to form a five coordinate complex. The resulting Mn(TTP)(O_2) complex exhibits the intermediate $S = 3/2$ spin state (with three unpaired electrons on the Mn-centre and little unpaired spin density on the O_2) as indicated by the ESR spectra analysis [189]. Optical spectra indicated an extensive Mn to O_2 charge transfer. Thus experimental data support a $^4(t_2)^3$ ground state and Mn^{IV}–$(O_2)^{-II}$ valency formalism with the dioxygen bound in the Griffith mode (symmetrical "side-on", or "edge-on", parallel to the porphyrin plane). Recent IEHT calculations [177] indicate that the Griffith geometry, with molecular orbital energies most consistent with the optical spectra, and which best fits the observed ^{55}Mn and ^{17}O hyperfine splitting, has a long Mn out-of-plane displacement toward the O_2 (ca. 0.5 in units of 10^{-10} m), a long "peroxo-type" O–O bond and the O–O linkage in staggered conformation with respect to the pyrrole nitrogens. On the contrary, earlier ab initio calculations [175] favour the Pauling (bent "end-on") mode of dioxygen coordination and Mn^{III}–$(O_2)^{-I}$ valency formalism. However, this prediction was based upon computations on eclipsed models with a small Mn out-of-plane displacement and short Mn–O distances which lead to extremely short oxygen to pyrrole nitrogen distances for the Griffith geometry. Nevertheless, the mode of dioxygen bonding to manganese complexes is still not unequivocal. Because of a large number of relevant electron configurations lying close to each other, the definite conclusion cannot be drawn without full geometry optimization and the inclusion of configuration interaction.

Some "side-on" type of dioxygen complexes of group VIII elements, $M(PH_3)_2(O_2)$ for $M = Ni^0$, Pd^0, Pt^0 and $M(PH_3)_2(CO)X(O_2)$ for $M = Rh^I$, Ir^I and $X = Cl^-$, I^-, were studied by the CNDO method [178]. The energy

partitioning and the configuration analysis permit us to conclude that the dioxygen π^* orbital mixes significantly with the metal d_π orbital (this was not obtained by the earlier $X\alpha$–SW calculations of $Pt(PH_3)_2(O_2)$ [173]). The π back-donation contributes to both the electron distribution, the metal–O_2 bond strength, and the O–O bond weakening. The large metal to dioxygen charge transfer (i.e. $Q(O_2)$ ranging from -0.6 to -1.0) is mainly contributed from the π back-donation through which about 0.9–1.4 electrons are transferred; about 0.3 electron is donated from the dioxygen π bonding and σ orbitals to the central atom. The geometry variation, namely the dioxygen ligand rotation about the coordinate bond, indicate that the chromophore PtP_2O_2 and the $IrICO_2$ fragment of the chromophore IrP_2ICO_2 are planar (in agreement with X-ray structure data). In these geometries the coordinated dioxygen has the greatest negative charge and the O–O interaction is weakest (it is measured through the bicentric part of the energy), so that dioxygen activation may be most efficient.

Finally, recent CNDO–UHF studies [169–171,179–184] of electronic factors supporting dioxygen activation in complexes of the type $^m[M(L_e)_4L_a(O_2)]^q$ will be reviewed in the next section.

C. DIOXYGEN ACTIVATION IN MONONUCLEAR COMPLEXES OF Mn, Fe, Co, Ni AND Cu

(i) Qualitative considerations

The properties of free dioxygen and related species such as O_2^+, O_2^- and O_2^{2-} have been reviewed elsewhere many times (see, for example [11,19]). Such data are not repeated here. Recalling only the spin-conservation rule, according to which the dioxygen in the triplet ground state ($^3\Sigma$) reacts with organic substrates (these are the spin-singlets $^1\Sigma$) predominantly as a one-electron oxidant

$$RH + O_2 \rightarrow R^{\cdot} + OOH^{\cdot} \tag{2}$$

because the two-electron process

$$RH_2 + O_2 \rightarrow R + H_2O_2 \tag{3}$$

and similar four-electron processes are spin forbidden. On the other hand, the formation of the $OOH^{\cdot}$ radical in aqueous solutions is an energetically unfavourable process: the corresponding redox potential is ≈ -0.13 V. As mentioned above, the addition of dioxygen to transition metal centres significantly changes its electronic configuration and related electronic properties. As a result of coordination, the dioxygen is activated: the electron density transfer to the π^* orbitals causes the molecular oxygen to be "softened".

The electronic structure of metal–dioxygen complexes can be influenced by several factors. The main factors affecting the dioxygen activation may be classified as geometric and electronic. The geometric factors cover: (1) the number of metal centres and the coordination number of each central atom; (2) the mode of dioxygen coordination; (3) the symmetry of the complex; (4) the out-of-plane, metal to dioxygen displacement; (5) the steric hindrance or fixation of a certain conformer. To the electronic factors belong: (1) the nature of the central atom (number of protons); (2) its oxidation state (or the number of valence electrons); (3) its spin state (or the number of unpaired electrons); (4) the composition of the ligand sphere (e.g. the *trans* and *cis* influence of ligands).

Other factors, such as the solvent effect or the environmental conditions (temperature, pressure) are not considered here. To study the effect of a particular factor on the dioxygen activation the other factors have to be constant. This can easily be secured by a quantum chemical study of model complexes. However, in order to start such a project, the following assumptions were made. Only complexes of the type $^{m}[M(L_e)_4L_a(O_2)]^q$ are under study (Fig. 8) where: (1) the central atom M is surrounded in the equatorial plane by four monodentate ligands L_e; (2) on the axial ordinate the ligand L_a is localized in the position *trans* to the dioxygen; (3) the dioxygen coordination varies from the linear, through bent, to the symmetrical "side-on" mode. Thus, the chromophore $MD_4D'O$ has either C_{4v} or C_s symmetry for the linear and bent geometry, respectively, and in the symmetric "side-on" geometry the chromophore $MD_4D'O_2$ has the symmetry C_{2v} (D and D′ are the donor atoms of L_e and L_a ligands, respectively). In these particular cases six internal degrees of freedom of coordinated dioxygen are reduced to only: (1) two distances, r_1 and r_2, for the linear geometry; (2) two distances, r_1 and r_2, and two angles, α and β. The staggered ($\phi = 45°$) or eclipsed ($\phi = 0°$)

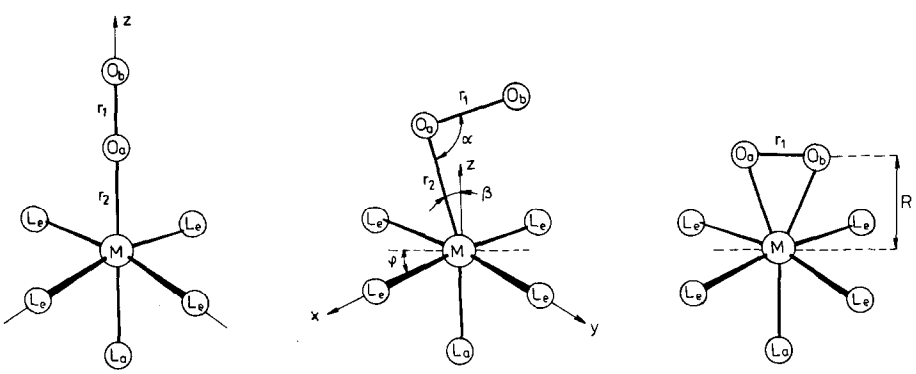

Fig. 8. Linear, bent and triangular geometry of $[M(L_e)_4L_a(O_2)]$ type complexes.

conformers will be considered for the bent geometry; (3) two distances, r_1 and R, (if $\phi = 0$ or 45°) for the triangular geometry.

According to the experimental data, some geometric factors are mutually conditioned by electronic factors: the bending of the M–O–O group is a function of the electron density, n, localized on the π^* orbitals of the O_2 (or, generally, of XY) molecule (Table 10). Simultaneously, the relative energies of the π^* orbitals of the XY system with respect to the central atom d-orbitals play an important role. Since the π^* orbital energies decrease and n generally increases along the series of XY = CO, NO, O_2, it is not surprising to find that carbonyls adopt only the linear geometry, whereas nitrosyls can exist in either a linear or a bent geometry and dioxygen complexes exhibit either a bent or a triangular structure [136,168].

The relative energies of π^* orbitals versus the d orbitals can also be affected by the number of protons on the central atom and its oxidation state. Further, the splitting of the metal d orbitals, Δ_M, depends on the ligand field strength of equatorial ligands L_e. The relative energy of the d_{z^2} orbital (Δ_z) can be affected by the basicity of an axial ligand L_a. Finally, the dioxygen π^* orbitals, which are degenerate in the free molecule, are split (Δ_O), dependent of the bending of the M–O–O group. If this splitting is greater than the pairing energy, the dioxygen molecule is considered to be in the singlet spin state.

These considerations are illustrated in Fig. 9 for the case of the d^7–$(\pi^*)^2$ interaction. Here, the energy levels are classified according to the individual irreducible representations of the molecular symmetry point group (Table 11). The dioxygen π^* orbitals are classified as symmetric, $\pi_v^* = S$, and antisymmetric, $\pi_h^* = A$, with respect to the M–O–O plane (Fig. 10).

TABLE 10

Mode of XY ligand coordination versus occupation of the π^* orbitals

Occupation $(\pi_v^*, \pi_h^*)^n$	Geometry [a]			Examples
	Linear	Bent	Triangular	
0	+	–	–	CN^-, CO, N_2, NO^+
1	–	+	–	NO
2	–	+	–	NO^-, O_2
3	–	+	–	O_2^-
4	–	–	+	O_2^{2-}

[a] +, Realized geometry; –, non-realized geometry.

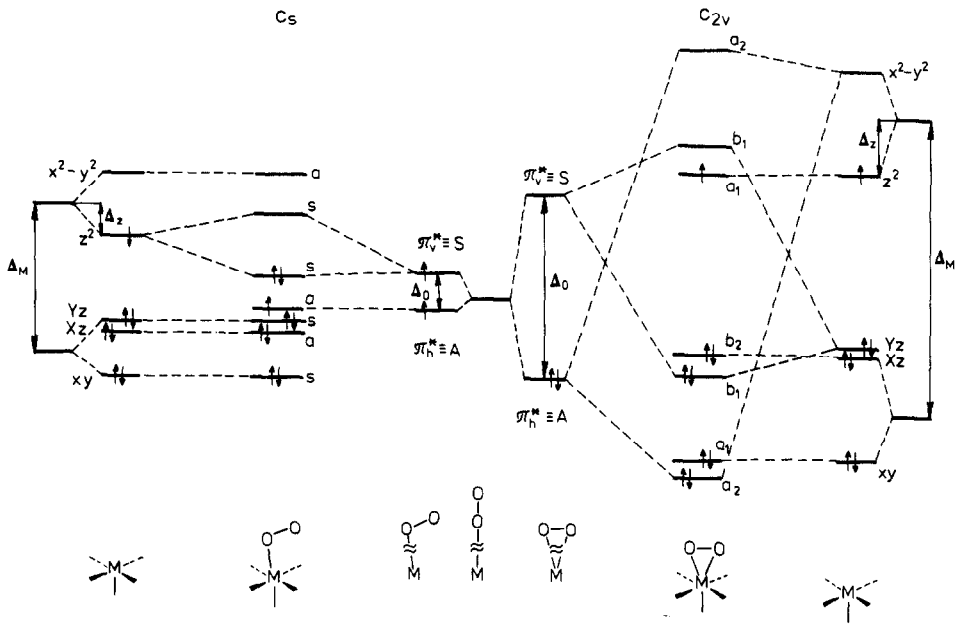

Fig. 9. Qualitative MO diagram of $[ML_5 \cdots (O_2)]$ interactions. C_s symmetry: the case of a weak ligand field, C_{2v} symmetry: the case of a strong ligand field. Occupations are valid for $M = Co^{II}$.

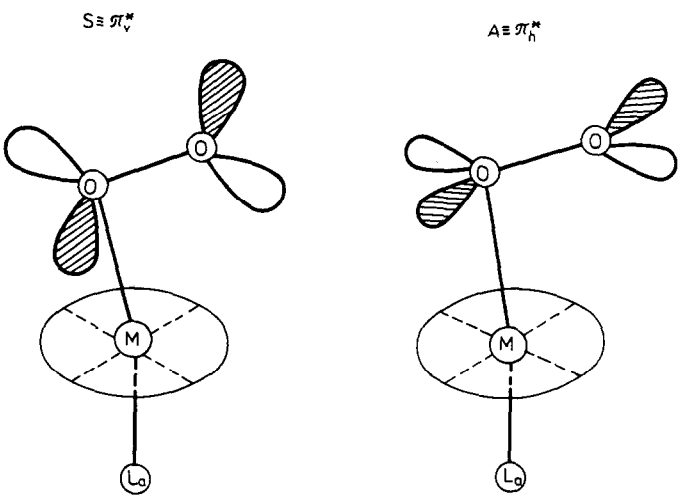

Fig. 10. Dioxygen π^* orbitals. S, symmetric with respect to the M–O–O plane; A, antisymmetric.

TABLE 11

Components of the irreducible representations for some point groups

Group		Components [a]	
C_s	C_{2v}	Central atom *d* orbitals	Dioxygen π^* orbitals
$a' = s$	a_1	z^2, xy	
	b_1	$Yz = (xz - yz)/\sqrt{2}$	$\pi_v^* = S$
$a'' = a$	a_2	$x^2 - y^2$	$\pi_h^* = A$
	b_2	$Xz = (xz + yz)/\sqrt{2}$	

[a] Valid for the axis choice according to Fig. 8.

(ii) Calculation methods

The quantum chemical study of metal–dioxygen complexes is accomplished in the following fashion. The first complication occurs in the self-consistent-field procedure. The solution of the Roothaan matrix equations for the MO–LCAO coefficients requires an initial approximation. If this is not the case, the SCF procedure can oscillate and convergence is not obtained. This complication occurs especially in transition metal complexes, where the possible bonding situations range over a large interval. Usually, either level-shifting or damping procedures are applied in order to obtain the stationary value of the energy. Unfortunately, the SCF level of approximation is not sufficient in several cases and applying the configuration interaction technique, the results can be changed not only quantitatively, but also qualitatively. The CI, in general, is a very tedious step. Usually, either double excitations must be taken into account in the framework of the variation approach, or third-order perturbation theory must be used. Thus, for a fixed geometry, only one point of the multi-dimensional adiabatic potential surface is obtained and in order to localize an equilibrium geometry the full geometry optimization has to be performed. Further, the correction to the zero-point vibrations requires vibrational analysis where knowledge of the full force-constant matrix is necessary. Finally, if a crossover of APSs is the case, the adiabatic approximation fails and the correct approach requires the non-adiabatic theory.

From the point of view of reliability, the ab initio methods are usually highly preferable to semiempirical methods. Unfortunately, the basis sets used (the minimum or valence split) give an energy value which is rather far from the Hartree–Fock limit. Some ab initio calculations are known where the net result of the SCF procedure does not agree with experiment. Recall, as an example, that Co(acacen) was reported as having the ground-state

electron configuration $d^6(d_{z^2})^1$ [162] in contrast to that of $d^6(d_{yz})^1$ as deduced from the single-crystal ESR experiments [192]. Moreover the triplet state of Fe(por)(O_2) was found to be lower in energy in comparison with the singlet spin state [155]. This, however, does not indicate a failure of the ab initio approach because CI can interchange these energy levels. On the other hand, such extensive calculations have not up to now been performed.

Some problematic results can also be found within the X–α calculations. For example the $3d$ electron population in Fe^{II}(por)Im(O_2) was reported [153] to be too high (> 7.5), and an absence of d_π(Pt)–π^*(O_2) mixing in Pt(PH_3)(O_2) was criticized in ref. 178.

The failure of semiempirical methods like IEHT, CNDO or INDO is well known in some particular cases. Thus a correct interpretation of those results requires a study of a series of compounds where the absolute values of molecular properties are usually meaningless, so that only their trends are to be controlled by experimental data. Such an approach was excellently illustrated in the CNDO study of some group VIII dioxygen complexes [178]. Here, although the atomic charges on the central atom Pt, in general, do not agree with experimental estimates, their trend is quite correct within a large interval. This "scaling" of the results obtained is important especially for transition metal complexes, mainly for the following reasons. In semiempirical methods like CNDO or INDO some integrals in the Fock operator matrix are substituted by parameters. Their values are kept constant despite the fact that a relaxation during oxidation or reduction is expected. The electron repulsion term only partially follows such a relaxation. This leads to a result that the calculated d-electron populations change only by a fraction of an electron during oxidation.

In order to finish these preliminary comments, consider a large series of metal–dioxygen complexes by means of MO–LCAO–SCF calculations. The central atom is varied through M = Mn, Fe, Co, Ni and Cu, in the oxidation states of M^0, M^I, M^{II} and M^{III}, where low-spin (spin multiplicity $m = 1, 2$), as well as high-spin ($m = 3, 4$) complexes are considered. The equatorial ligands were $L_e = H_2O$, NH_3, Cl^- and CN^- whereas an axial base was L_a = none, NH_3, Im and Py in some particular cases. This represents a typical area where the semiempirical methods can be successfully applied but an ab initio study is not available from the point of view of computing facilities.

Actually, the CNDO–UHF method [193,194] was used in calculations. Its basic features and parametrization are described elsewhere [195–197]. The valence basis set consists of $3d$, $4s$ and $4p$ atomic orbitals for transition metal elements and valence ns and np orbitals for other atoms. Slater AOs [198] were used with the Zerner–Gouterman exponents for transition metals [199] and the hydrogen exponent equal to 1.2. The convergence of the SCF

TABLE 12

Calculated equilibrium metal–ligand distances $R_{M-L}(10^{-10}\,m)$ in low-spin complexes $[M^{II}L_4]^q$

M	Ligand			
	H_2O	NH_3	Cl^-	CN^-
Mn	2.00	1.95	2.35	1.90
Fe	1.96	1.90	2.31	1.85
Co	1.87	1.83	2.24	1.80
Ni	1.80	1.80	2.18	1.75
Cu	1.80	1.77	2.164	1.75

procedure was secured using a variable damping approach [200], if needed. The sub-set of occupied MOs was selected as usual according to the lowest eigenvalues in each step of the SCF procedure. The total molecular energy, E_T, was decomposed into one-center and two-center, E_{AB}, terms according to the energy partitioning as found in ref. 201. The Wiberg (bond-strength) index, W_{AB}, was calculated as usual [202]. The electron density on the orbital $A = \pi_h^*$ was summed up by introducing the π-acceptor index, $X(\pi_A)$, defined elsewhere [203]. The spin-densities were projected according to the method of Amos and Hall [204] in the open-shell case. Also, the INDO–UHF method [205] was used in some particular cases and its parametrization is described elsewhere [195,206–209].

Experimental geometries of ligands L = NH_3, H_2O, CN^-, Im and Py were used [210]. The metal–ligand distances were optimized for low-spin square-planar complexes of the type $[M^{II}L_4]^q$ (Table 12) and the equilibrium values of R_{M-L} were used in model complexes $^m[M(L_e)_4L_a(O_2)]^q$ under study.

(iii) Dioxygen geometry optimization

Although full geometry optimization is preferable for a quantum chemical study, such a project can hardly be performed if more than one hundred metal–dioxygen complexes are to be studied. Therefore, only a limited geometry variation which covers the mode of dioxygen coordination is considered.

The calculated geometries of some simple model compounds are listed in Table 13. They are not too far from the experimental data, if available. The calculated O–O bond distance, r_1, is somewhat shorter in comparison with experimental data for the free dioxygen, superoxide or peroxide ion (Table 14). The calculated value of r_1 in model complexes best corresponds to the

TABLE 13

Equilibrium geometries of some 1 : 1 metal–dioxygen complexes

Complex	Type [a]	Method	Technique [b]	Geometric parameters [c]				
				R	r_1	r_2	α	β
$^4[MnCl_4(O_2)]^{2-}$	T	CNDO	S	2.086	1.196	(2.163)		
$^2[MnCl_4(O_2)]^{2-}$	T	CNDO	S	2.034	1.200	(2.125)		
$^2[CoCl_4(O_2)]^{2-}$	T	CNDO	S	1.94	1.17	(2.026)		
$^2[CuCl_4(O_2)]^{2-}$	T	INDO	A, S	1.875	1.169	(1.964)		
$^{2,4}[CoCl_4(O_2)]^{2-}$	L	CNDO	S		1.15	1.97		
$^2[CoCl_4(O_2)]^{2-}$	N	CNDO	S		1.19	1.875	95	10
$^2[CoCl_4NH_3(O_2)]^{2-}$	N	CNDO	S		1.19	1.875	95	5
O_2 carriers of Co^{II}	N	Exptl.	X-ray		1.1–1.35	1.86–1.95	117–136	≈ 5
$^2[Co(CN)_5(O_2)]^{3-}$	N	CNDO	S		fixed	fixed	120	fixed
	N	Exptl.	X-ray		1.24	1.906	153	6
$^2[CuCl_4(O_2)]^{2-}$	N	INDO	A		1.161	1.957	75	17
$^m[M(L_e)_4L_a(O_2)]^q$	N	CNDO	P		1.19	1.85	100	10

[a] Type: N, non-symmetrical side-on (or bent end-on); T, triangular; L, linear.

[b] Technique: S, stepwise geometry variation [193,194]; A, automatic geometry optimization [205]; P, postulated.

[c] Distances in units of 10^{-10} m, angles in degrees.

calculated value for the free superoxide ion. The Co–O–O bond angle α is somewhat lower in comparison with values found in real dioxygen carriers. The calculated Co–O distance falls within the range of experimental values. It is important to point out that the non-symmetrical "side-on" structure (**III**) is the most stable within the Co^{II} complexes. The nature of the $\beta > 0$ distortion follows from the dominant role of the highest occupied molecular orbital (HOMO). This is composed of the dioxygen π_v^* orbital and cobalt d_{z^2} orbital, so that for $\beta > 0$ the overlap of d_{z^2} with π_v^* increases. Simultaneously the "destabilizing" overlap of the d_{z^2} orbital with the dioxygen nonbonding orbital (n) decreases. Therefore, the bent structure with $\beta > 0$ is stabilized (Fig. 11).

The optimum geometry of the $^2[CoCl_4(O_2)]^{2-}$ complex has been obtained from the position of the minimum on the multi-dimensional adiabatic potential surface (APS). However, there are several equivalent minima on this APS which correspond to the different geometries; a saddle point must exist between these minima. The transition state is probably represented by the triangular π structure. The calculated energy separation between the optimum bent structure (C_s symmetry) and the optimized π structure (C_{2v} symmetry) is $\Delta E = 0.5$ eV (the linear structure in C_{4v} symmetry being ca. 3 eV higher in energy). This quantity is much lower than the stabilization energy of the $[CoCl_4(O_2)]^{2-}$ complex of ca. 7.6 eV (calculated with respect to the planar $CoCl_4^{2-}$ ion and free triplet dioxygen). Although both these quantities are probably overestimated, their ratio seems to be acceptable. Thus, a flipping of the coordinated dioxygen is indicated between various minima on the APS at higher temperature (Fig. 12). This is in qualitative agreement with the interpretation of the ESR spectrum of Co(bzacen)Py(O_2) in solution [211], where the oxygen atoms were found to be magnetically equivalent under the condition of measurement. Another type of motion of the coordinated dioxygen was also considered. This is the rotation between

TABLE 14

Oxygen–oxygen distance $r_1(10^{-10}$ m) in various systems

System	Method		
	CNDO	INDO	Exptl.
$^3(O_2)$	1.132	1.140	1.207
$^1(O_2)$	1.132	1.140	1.216
$^2(O_2)^-$	1.187	1.198	1.341
$^1(O_2)^{2-}$	1.272	1.288	1.49

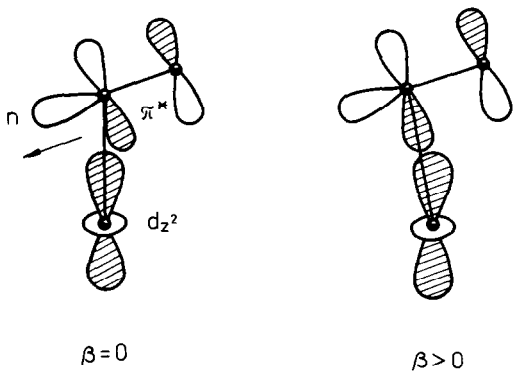

Fig. 11. Stabilization of a bent structure by $\beta > 0$.

various conformers of $[CoCl_4(O_2)]^{2-}$. The calculated barrier to rotation between staggered and eclipsed conformers is not too high: about 0.05 eV.

Table 13 also includes the geometrical parameters used in CNDO calculations of a series of $^m[M(L_e)_4L_a(O_2)]^q$ type complexes in a fixed geometry.

(iv) The axial base influence

The dioxygen coordinated to Co^{II} has electronic properties similar to those of free superoxide ion. The calculated spin densities in $^2[CoCl_4(O_2)]^{2-}$

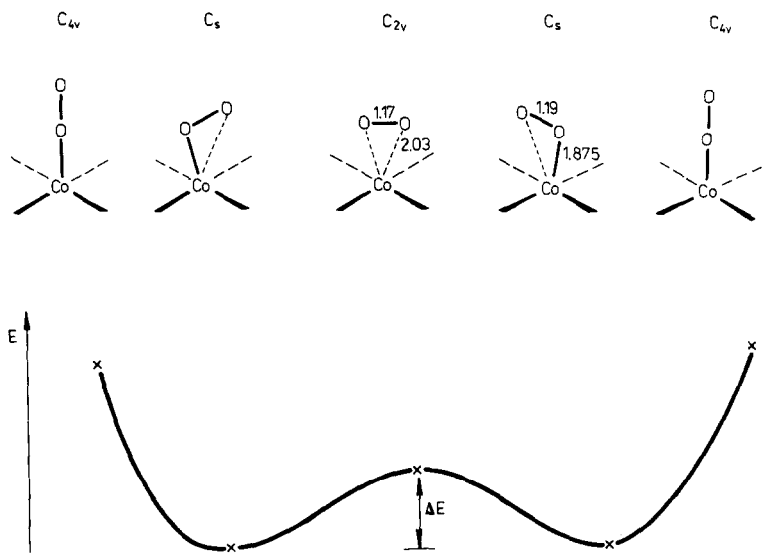

Fig. 12. Possible flipping of coordinated dioxygen.

are: $\rho(O_a) = 0.34$ and $\rho(O_b) = 0.66$. They are in good agreement with the experimental data for the frozen Co(bzacen)Py(O_2) [212] or values calculated for the Co(acacen)NH_3(O_2) by the INDO–UHF method [159]. The atomic charges, $Q(O_a) = -0.23$(e) and $Q(O_b) = -0.22$, however, are far from the formally assigned oxidation states Co^{III}–$(O_2)^{-I}$; they are in good agreement with the suggestions of Tovrog et al. [138]. The other O–O bond characteristics, such as the equilibrium distance, R_{O-O}, the harmonic force constant, k_{O-O}, the bicentric part of the total energy, E_{O-O}, and the Wiberg index, W_{O-O}, are similar to those calculated for the free superoxide ion (Table 15).

Further, an axial base L_a was added, being either ammonia, imidazole, or pyridine [171]. Both orientations of their rings were considered: a parallel orientation with respect to the Co–O_2 plane (Im, Py) or perpendicular to it (Im′, Py′). No significant changes in properties of the coordinated dioxygen were noted (Table 15). Thus it seems, the speculation about additional π-donor or π-acceptor properties of the imidazole ligand [3,213–215] is rather overemphasized. The π electron density on the pyridine or imidazole ring remains about 6.0. Only the orbital energies of the HOMOs are slightly influenced by the change of an axial ligand.

Similar calculations were performed for a series of low-spin iron(II) containing complexes [158]. The degree of dioxygen activation significantly decreases (it follows from E_{O-O}, W_{O-O} and $Q(O_2)$ values). The coordinated dioxygen behaves in these complexes similarly to the free singlet molecule. A negligible axial base influence was noted within the series $L_a = NH_3$, Im, Im′, Py and Py′. Of more significance appears to be the integral *cis* influence of the equatorial ligands (discussed below within the equ–ax description). Passing from $L_e = Cl^-$ to $L_e = NH_3$ the coordinated dioxygen is more deactivated: W_{O-O} increases, E_{O-O} decreases and $Q(O_2)$ increases. Simultaneously the d^x populations increase and the orbital energies ϵ(HOMO) significantly decrease. A more detailed analysis [158] shows that the cluster of 3*d* orbitals is better localized as the three highest occupied MOs are ca. 90% versus 70% in 3*d* character.

(v) The central atom effect

This term represents the influence of the atomic number, M, the oxidation state, q, and the spin multiplicity, m. Such an influence, $^mM^q$, is related here to the electronic structure and the properties of the M–O_2 linkage. The quantities evaluated covered the d^x electron populations, spin densities ρ(M) and $\rho(O_2)$, effective charges Q(M) and $Q(O_2)$, Wiberg indices W_{O-O} and W_{M-O}, as well as the bicentric portions of the total energy E_{O-O} and E_{M-O}. The electron density on the dioxygen orbital $\pi_h^* = A$, normal to the M–O_2 plane, was expressed through the π-acceptor index $X(\pi_A)$. In this way

TABLE 15

Calculated characteristics of free and coordinated dioxygen [a]

No.	L_a	R_{O-O} (10^{-10} m)	k_{O-O} (N cm^{-1})	$-E_{O-O}$ (eV)	W_{O-O}	$\rho(O_2)$	$Q(O_2)$ (e)	ϵ(HOMO) (eV)	d^x
Free particles									
1	O_2	1.13	55.8	46.4	1.50	2.00	0		
2	O_2^-	1.19	45.2	34.4	1.25	1.00	−1.00		
Complexes $^2[CoCl_4L_a(O_2)]^{2-}$									
3	none	1.19	44.1	34.6	1.18	1.00	−0.45	−1.23	6.57
4	NH_3	1.19	40.1	34.7	1.18	1.00	−0.44	−0.42	6.67
5	Im			34.6	1.17	1.00	−0.44	−0.33	6.65
6	Im′			34.6	1.17	1.00	−0.44	−0.32	6.66
7	Py			34.6	1.17	1.00	−0.44	−0.55	6.66
8	Py′			34.6	1.17	1.00	−0.44	−0.54	6.66
Complexes $^1[FeCl_4L_a(O_2)]^{2-}$									
9	NH_3			40.9	1.73		0.08	0.26	6.04
10	Im			40.8	1.72		0.07	0.39	6.02
11	Im′			40.9	1.73		0.07	0.29	6.03
12	Py			41.0	1.75		0.10	−0.03	6.03
13	Py′			41.1	1.75		0.10	−0.15	6.04
Complexes $^1[Fe(NH_3)_4L_a(O_2)]^{2-}$									
14	NH_3			42.8	1.92		0.27	−20.65	6.37
15	Im			42.8	1.91		0.25	−19.46	6.36
16	Py			42.8	1.91		0.25	−19.69	6.37

[a] Equilibrium distance, R_{O-O}; stretching harmonic force constant k_{O-O}; bicentric part of the total energy, E_{O-O}; Wiberg index, W_{O-O}; spin density, $\rho(O_2)$; effective charge, $Q(O_2)$; orbital energy, ϵ, of HOMO; electron population of metal $3d$ orbitals, d^x; axial base L_a fixed at the distance of $R_{Co-N} = R_{Fe-N} = 1.90$.

TABLE 16

Calculated properties of $^{m}[MCl_4NH_3(O_2)]^{q}$ complexes [a]

M	q	m	Electron density			Spin density		Charge		Assignment
			A^iS^j	$X(\pi_A)$	d^x	$\rho(M)$	$\rho(O_2)$	$Q(M)$	$Q(O_2)$	
Mn	−1	1	S^2A^0	0.02	4.60			0.81	0.24	$Mn^{III}(O_2)^0$
		3	S^2A^0	0.02	4.60	1.96	0.00	0.82	0.24	$^{\uparrow\uparrow}Mn^{III}(O_2)^0$
	−2	2	$S^2A^{\downarrow}$	0.97	4.59	1.94	−0.96	0.87	−0.47	$^{\uparrow\uparrow}Mn^{III\downarrow}(O_2)^{-1}$
		4	$A^{\uparrow}S^2$	1.05	4.58	1.95	1.02	0.87	−0.48	$^{\uparrow\uparrow}Mn^{III\uparrow}(O_2)^{-1}$
	−3	1	A^2S^2	1.91	4.79			0.58	−0.99	$Mn^{III}(O_2)^{-II}$
		3	$A^{\uparrow}S^2$	1.04	4.56	1.93	1.02	0.92	−0.55	$^{\uparrow\uparrow}Mn^{III\uparrow}(O_2)^{-I\downarrow}A^{-I}$
Fe	−1	2	S^2A^0	0.02	5.65	0.98	0.00	0.61	0.27	$^{\uparrow}Fe^{III}(O_2)^0$
		4	$A^{\uparrow}S^{\uparrow}$	1.02	5.64	1.00	1.92	0.62	0.24	$^{\uparrow}Fe^{III\uparrow\uparrow}(O_2)^0$
	−2	1	S^2A^0	0.25	6.04			0.12	0.08	$Fe^{II}(O_2)^0$
		3	$A^{\uparrow}S^2$	0.95	5.62	0.96	1.03	0.62	−0.45	$^{\uparrow}Fe^{III\uparrow}(O_2)^{-I}$
	−3	2	$A^{\uparrow}S^2$	1.01	6.18	0.00	1.00	−0.03	−0.55	$Fe^{II\uparrow}(O_2)^{-I}$
		4	$A^{\uparrow}S^2$	1.00	6.16	1.94	1.00	−0.02	−0.55	$^{\uparrow\uparrow}Fe^{II\uparrow}(O_2)^{-I}$

Co	−1	1	S^2A^0	0.02	6.71			0.43	0.28	$Co^{III}(O_2)^0$
		3	$A^{\uparrow}S^{\uparrow}$	1.02	6.71	−0.01	1.93	0.42	0.25	$Co^{III\uparrow\uparrow}(O_2)^0$
	−2	2	$A^{\uparrow}S^2$	0.96	6.66	0.00	1.00	0.53	−0.44	$Co^{III\uparrow}(O_2)^{-I}$
		4	$A^{\uparrow}S^2$	0.96	6.62	1.75	1.03	0.59	−0.42	$^{\uparrow\uparrow}Co^{III\uparrow}(O_2)^{-I}$
	−3	1	A^2S^2	2.07	7.02			0.07	−0.74	$Co^{III}(O_2)^{-II}$
		3	$S^2A^{\uparrow}$	1.00	7.16	0.95	0.99	−0.11	−0.55	$^{\uparrow}Co^{II\uparrow}(O_2)^{-I}$
Ni	−1	2	$A^{\uparrow}S^{\downarrow}$	1.04	7.77	0.98	0.50	0.26	−0.05	$^{\uparrow}Ni^{III\uparrow\downarrow}(O_2)^0$
		4	$A^{\uparrow}S^{\uparrow}$	1.03	7.81	0.35	1.94	0.21	0.26	$^{\uparrow}Ni^{III\uparrow\uparrow}(O_2)^0$
	−2	1	A^2S^0	2.05	7.92			0.09	−0.05	$Ni^{II}(O_2)^0$
		3	$A^{\uparrow}S^2$	0.97	7.65	0.75	1.01	0.46	−0.41	$^{\uparrow}Ni^{III\uparrow}(O_2)^{-I}$
	−3	2	$A^2S^{\uparrow}$	1.94	8.08	0.07	0.90	−0.09	−0.49	$^{\uparrow\downarrow}Ni^{II\uparrow}(O_2)^{-I}$
		4	$S^2A^{\uparrow}$	1.01	8.10	1.86	1.03	−0.10	−0.57	$^{\uparrow\uparrow}Ni^{II\uparrow}(O_2)^{-I}$
Cu	−1	1	A^2S^0	2.03	8.81			0.12	0.16	$Cu^{III}(O_2)^0$
		3	$S^{\uparrow}A^{\uparrow}$	1.03	8.84	−0.68	1.76	0.08	0.15	$^{\downarrow}Cu^{II\uparrow\uparrow}(O_2)^{0\uparrow}E^{-III}$
	−2	2	$A^{\uparrow}S^2$	1.02	8.61	0.00	1.00	0.43	−0.29	$Cu^{III\uparrow}(O_2)^{-I}$
		4	$S^{\uparrow}A^{\uparrow}$	1.03	8.86	1.11	1.64	0.09	−0.05	$^{\uparrow}Cu^{II\uparrow\uparrow}(O_2)^0$
	−3	1	A^2S^{2y}	1.96	9.13			−0.23	−0.56	$(CuO_2)^I$
		3	$A^{\uparrow}S^2$	0.97	9.06	0.92	1.03	−0.13	−0.57	$^{\uparrow}Cu^{II\uparrow}(O_2)^{-I}$

[a] Unpaired electrons: ↑ for α spin, ↓ for β spin; fractional occupations $2y \in \langle 0,2 \rangle$; oxidation numbers of axial, A, and equatorial, E, ligands: omitted in usual cases (0 for neutral and −I for anionic ligands), but given if otherwise.

performing a detailed analysis of the MO–LCAO matrices, the local electron configurations A^iS^j were assigned (i and j being 0, ↑ for the α spin, ↓ for the β spin and 2 for an electron pair). These quantities are collected in Table 16 for $^m[MCl_4NH_3(O_2)]^q$ complexes. The quantities mentioned vary over a large range. Thus, the central atom effect manifests itself in a great variability of local electron configurations of A^iS^j and related electronic properties. However, these 30 different complexes may be classified on the grounds of their common occupation of the dioxygen π^* orbitals. Three groups of dioxygen complexes can then be distinguished: (1) complexes with non-activated dioxygen ($i+j=2$) as in free dioxygen (triplet or singlet); here there are complexes with electron configurations of S^2A^0, A^2S^0, $A^{\uparrow}S^{\uparrow}$ or

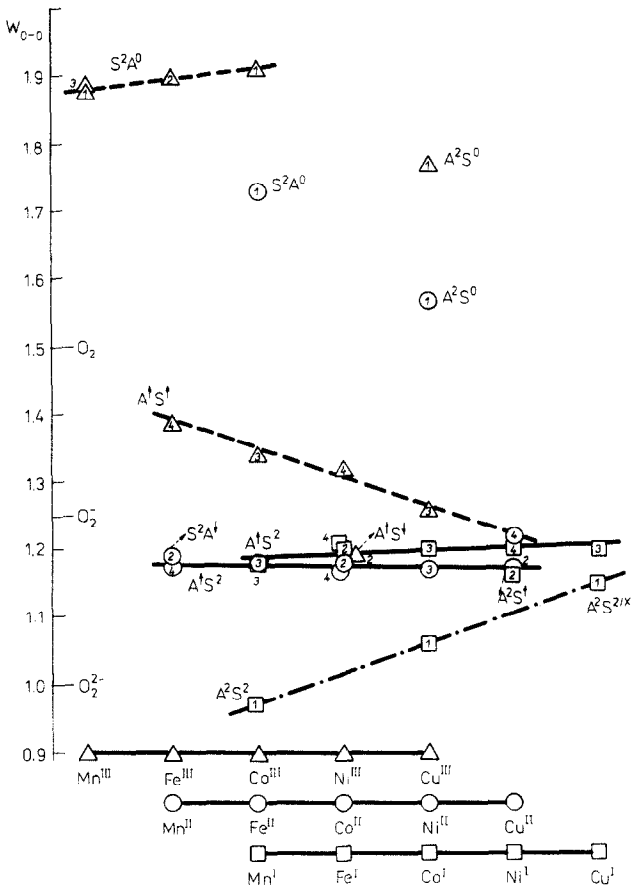

Fig. 13. Plot of the Wiberg index W_{O-O} vs. the number of valence electrons in $^m[MCl_4NH_3(O_2)]^q$ complexes of a given spin multiplicity m. ------, non-activated dioxygen; ———, one-electron activated dioxygen; ·–·–·, two-electron activated dioxygen.

$S^{\uparrow}A^{\uparrow}$, $A^{\uparrow}S^{\downarrow}$ and $A^{\uparrow}S^{2y}$; (2) complexes with one-electron activated dioxygen ($i+j=3$) as in the free superoxide, with electron configurations of $A^{\uparrow}S^2$ or $S^2A^{\uparrow}$, $A^2S^{\uparrow}$ or $S^{\uparrow}A^2$, $A^2S^{\downarrow}$ or $S^{\downarrow}A^2$, $S^2A^{\downarrow}$ or $A^{\downarrow}S^2$, S^2A^{2y} and A^2S^{2y}; (3) complexes with two-electron activated dioxygen ($i+j=4$) as in the free peroxide, having the electron configuration of A^2S^2. To the first group belong the complexes in higher oxidation states (M^{III} or M^{II}) and to the second group those of lower oxidation states (M^{II} or M^{I}). The last group contains only some low-spin low-oxidation state complexes. Let us mention that the complexes of M^{I} are considerably less stable in comparison with M^{II} or M^{III} complexes when considering values of the total energies. The dioxygen orbitals A and S, as well as the cluster of metal $3d$ orbitals are generally well localized. Only in some cases does significant mixing occur and it is expressed by the notations $A^{\uparrow}S^{2/x}$, $S^2A^{2/x}$ and $A^2S^{2/x}$, $x \in (1, \infty)$, or $A^{\uparrow}S^{2y}$, S^2A^{2y} and A^2S^{2y} where for fractional occupation $y \in (0, 1)$.

The Wiberg index is equal to 1.5 in free triplet dioxygen (2.0 in the singlet molecule), 1.25 in free superoxide and 1.0 in free peroxide anion. The bicentric part of the total energy has a negative value; its increase indicates a lowering of the O–O interaction energy and then weakening of the O–O

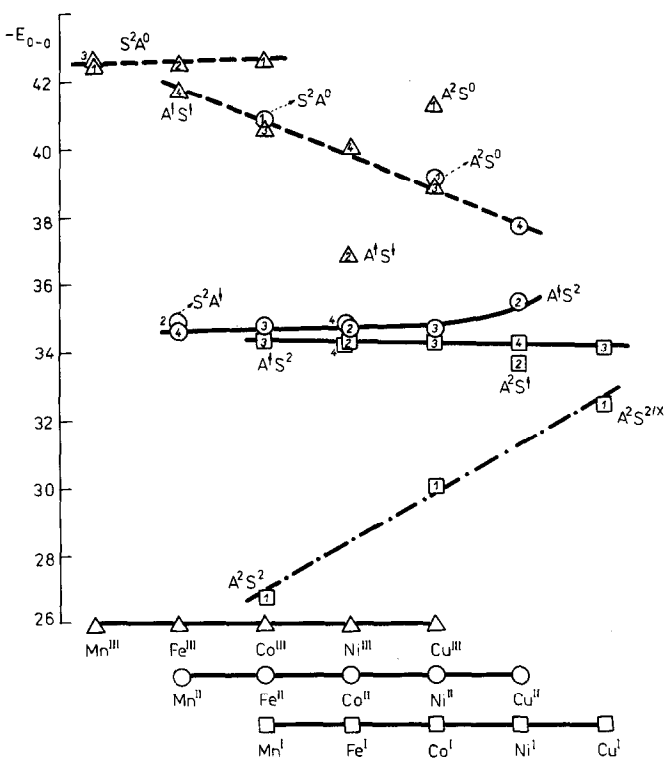

Fig. 14. Plot of the bicentric part of the total energy E_{O-O} (eV) vs. the number of valence electrons in $^{m}[MCl_4NH_3(O_2)]^{q}$ complexes.

bond. These quantities are plotted in Figs. 13 and 14 versus the number of electrons in a complex. The corresponding points in Figs. 13 and 14 have been connected with lines depending on the A^iS^j assignment. Remarkable parametric functions are obtained, so that the central atom effect on dioxygen activation becomes clearer. A more detailed analysis shows that weakening of the O–O bond is usually accompanied by strengthening of the M–O bond. Such a conclusion is based on the calculated values of W_{O-O} vs. W_{M-O} or E_{O-O} vs. E_{M-O}. This observation is similar to that previously reported on the basis of experimental interatomic distances $R_{O-O} = r_1$ and $R_{M-O} = r_2$ (see Section B and Fig. 2).

The dioxygen charge $Q(O_2)$ plotted versus the number of electrons in a complex exhibits a similar dependence (Fig. 15). Not only does the metal to dioxygen charge transfer contribute to the dioxygen effective charge but the opposite, dioxygen to metal, σ electron transfer also takes place. Therefore one-electron activated dioxygen has a value of $Q(O_2) \sim -0.5$(e) and the dioxygen effective charge in the case of two-electron activation does not exceed the value of $Q(O_2) \sim -1.0$. During the activation process the formal oxidation states of M and O_2 undergo a change. Therefore, re-formulation appears to be more convenient and new assignments for the oxidation states

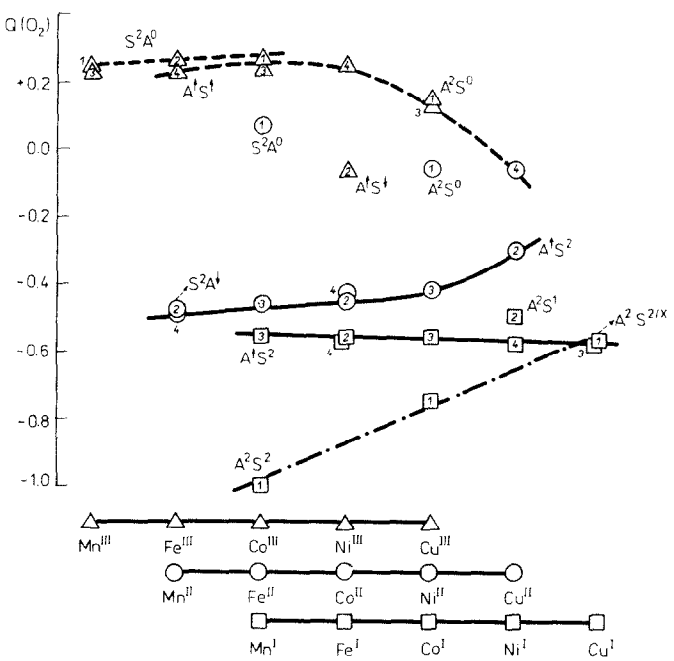

Fig. 15. Plot of the dioxygen charge $Q(O_2)$ (in units of e) vs. the number of valence electrons in $^m[MCl_4NH_3(O_2)]^q$ complexes.

are marked in Table 16 as a "condensed formulation". Here the unpaired electrons are marked by ↑ or ↓. Neither charge distributions, nor the electron populations d^x are superior for such a formulation (see, for comparison ref. 30). Judgement is made here mainly on the spin densities and electron configurations A^iS^j. In some cases an unambiguous assignment is possible only for the whole MO_2 unit. In several cases the other ligands also undergo one-electron oxidation or reduction.

Tables 17–19 summarize the principal results obtained for the complexes, $^m[M(H_2O)_5(O_2)]^q$, $^m[M(NH_3)_5(O_2)]^q$ and $^m[M(CN)_5(O_2)]^q$. The results are nearly the same when seen from the point of view of the central atom effect. Therefore only a plot of the bicentric part of the total energy versus the number of electrons is presented in Figs. 16–18. The anionic ligands CN^- again stabilize higher oxidation states (M^{III}, M^{II}) whereas the neutral

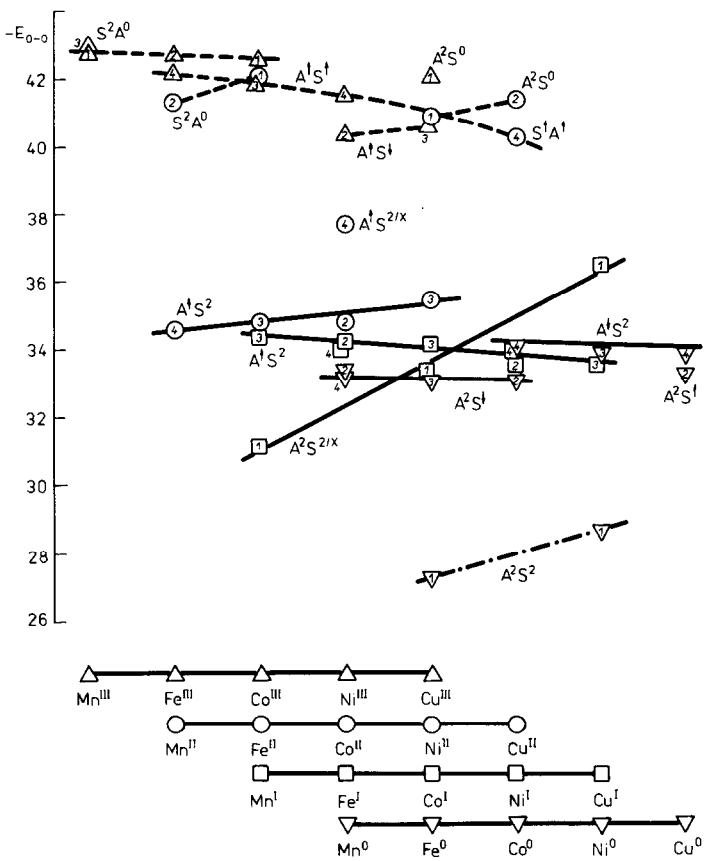

Fig. 16. Plot of the bicentric part of the total energy E_{O-O} (eV) vs. the number of valence electrons in $^m[M(H_2O)_5(O_2)]^q$ complexes.

TABLE 17

Calculated properties of $^{m}[M(H_2O)_5(O_2)]^{q}$ complexes [a]

M	q	m	Electron density			Spin density		Charge		Assignment
			A^iS^j	$X(\pi_A)$	d^x	$\rho(M)$	$\rho(O_2)$	$Q(M)$	$Q(O_2)$	
Mn	3	1	S^2A^0	0.00	4.46			1.19	0.33	$Mn^{III}(O_2)^0$
		3	S^2A^0	0.00	4.45	1.97	0.01	1.20	0.32	$^{\uparrow\uparrow}Mn^{III}(O_2)^0$
	2	2	S^2A^0	0.10	5.07	1.00	0.00	0.43	0.17	$^{\uparrow}Mn^{II}(O_2)^0$
		4	$A^{\uparrow}S^2$	1.03	4.59	1.93	1.04	1.02	−0.34	$^{\uparrow\uparrow}Mn^{III\uparrow}(O_2)^{-I}$
	1	1	A^2S^{2y}	1.98	5.06			0.39	−0.58	$(MnO_2)^I$
		3	$A^{\uparrow}S^2$	1.00	5.23	0.99	1.00	0.18	−0.46	$^{\uparrow}Mn^{II\uparrow}(O_2)^{-I}$
	0	2	$A^2S^{\downarrow}$	2.01	5.23	1.03	−0.96	0.08	−0.51	$^{\uparrow}Mn^{II\downarrow}(O_2)^{-I\uparrow}A^{-I}$
		4	$A^2S^{\downarrow}$	1.99	5.16	2.94	−0.95	0.15	−0.49	$^{\uparrow\uparrow\uparrow}Mn^{II\downarrow}(O_2)^{-I\uparrow}A^{-I}$
Fe	3	2	S^2A^0	0.00	5.48	0.98	0.01	1.03	0.35	$^{\uparrow}Fe^{III}(O_2)^0$
		4	$A^{\uparrow}S^{\uparrow}$	0.98	5.47	1.00	1.97	1.05	0.33	$^{\uparrow}Fe^{III\uparrow\uparrow}(O_2)^0$
	2	1	S^2A^0	0.10	6.14			0.20	0.27	$Fe^{II}(O_2)^0$
		3	$A^{\uparrow}S^2$	0.97	5.64	0.88	1.10	0.82	−0.28	$^{\uparrow}Fe^{III\uparrow}(O_2)^{-I}$
	1	2	$S^2A^{\uparrow}$	1.00	6.23	0.00	1.00	0.05	−0.45	$Fe^{II\uparrow}(O_2)^{-I}$
		4	$S^2A^{\uparrow}$	0.98	6.18	1.90	1.01	0.12	−0.44	$^{\uparrow\uparrow}Fe^{II\uparrow}(O_2)^{-I}$
	0	1	A^2S^2	1.90	6.35			−0.21	−0.83	$Fe^{II}(O_2)^{-II}$
		3	$S^{\downarrow}A^2$	1.99	6.17	1.97	−0.96	0.02	−0.48	$^{\uparrow\uparrow}Fe^{II\downarrow}(O_2)^{-I\uparrow}L_5^{-I}$
Co	3	1	S^2A^0	0.00	6.56			0.79	0.36	$Co^{III}(O_2)^0$
		3	$A^{\uparrow}S^{\uparrow}$	1.02	6.55	0.01	1.97	0.80	0.34	$Co^{III\uparrow\uparrow}(O_2)^0$

	2	2	$A^{\uparrow}S^{2}$	0.98	6.70	0.00	1.00	0.59	−0.27	$Co^{III\uparrow}(O_2)^{-I}$
		4	$A^{\uparrow}S^{2y}$	1.00	6.86	1.32	1.53	0.42	−0.01	$^{\uparrow\uparrow\uparrow}(CoO_2)^{II}$
	1	1	$A^{2}S^{2y}$	2.02	7.24			−0.10	−0.39	$(CoO_2)^{I}$
		3	$A^{\uparrow}S^{2}$	1.01	7.20	0.90	1.00	−0.04	−0.44	$^{\uparrow}Co^{II\uparrow}(O_2)^{-I}$
	0	2	$A^{2}S^{\downarrow}$	2.00	7.18	0.94	−0.97	−0.12	−0.48	$^{\uparrow}Co^{II\downarrow}(O_2)^{-I\uparrow}L_5^{-I}$
		4	$A^{\uparrow}S^{2}$	0.99	7.19	0.96	1.01	−0.12	−0.47	$^{\uparrow}Co^{II\uparrow}(O_2)^{-I\uparrow}L_5^{-I}$
Ni	3	2	$A^{\uparrow}S^{\downarrow}$	0.98	7.52	0.74	0.14	0.72	0.29	$^{\uparrow}Ni^{III\uparrow\downarrow}(O_2)^{0}$
		4	$A^{\uparrow}S^{\uparrow}$	0.97	7.52	0.79	1.98	0.71	0.36	$^{\uparrow}Ni^{III\uparrow\uparrow}(O_2)^{0}$
	2	1	$A^{2}S^{0}$	0.99	8.02			0.08	0.17	$Ni^{II}(O_2)^{0}$
		3	$A^{\uparrow}S^{2}$	0.98	7.73	0.95	0.90	0.44	−0.18	$^{\uparrow}Ni^{III\uparrow}(O_2)^{-I}$
	1	2	$A^{2}S^{\downarrow}$	1.96	8.12	1.72	−0.92	−0.06	−0.47	$^{\uparrow\uparrow}Ni^{II\downarrow}(O_2)^{-I}$
		4	$A^{\uparrow}S^{2}$	0.98	8.12	1.74	1.05	−0.06	−0.46	$^{\uparrow\uparrow}Ni^{II\uparrow}(O_2)^{-I}$
	0	1	$A^{2}S^{2}$	1.96	8.33			−0.39	−0.74	$Ni^{II}(O_2)^{-II}$
		3	$A^{\downarrow}S^{2}$	1.01	8.10	1.75	−0.97	−0.09	−0.50	$^{\uparrow\uparrow}Ni^{II\downarrow}(O_2)^{-I\uparrow}L_5^{-I}$
Cu	3	1	$A^{2}S^{0}$	1.97	8.42			0.76	0.27	$Cu^{III}(O_2)^{0}$
		3	$A^{\uparrow}S^{\downarrow}$	0.98	8.45	1.47	0.13	0.73	0.34	$^{\uparrow\uparrow}(CuL_5)^{III\uparrow\downarrow}(O_2)^{0}$
	2	2	$A^{2}S^{0}$	1.99	8.99	0.90	−0.01	0.05	0.24	$^{\uparrow}Cu^{II}(O_2)^{0}$
		4	$S^{\uparrow}A^{\uparrow}$	0.99	8.99	0.96	1.91	0.06	0.23	$^{\uparrow}Cu^{II\uparrow\uparrow}(O_2)^{0}$
	1	1	$A^{2}S^{2y}$	2.00	9.37			−0.44	−0.14	$(CuO_2)^{I}$
		3	$A^{\uparrow}S^{2}$	0.99	9.07	0.85	1.07	−0.08	−0.44	$^{\uparrow}Cu^{II\uparrow}(O_2)^{-I}$
	0	2	$A^{2}S^{\uparrow}$	1.99	9.56	−0.01	0.96	−0.72	−0.46	$Cu^{I\uparrow}(O_2)^{-I}$
		4	$A^{\uparrow}S^{2}$	0.98	9.05	0.89	1.04	−0.11	−0.50	$^{\uparrow}Cu^{II\uparrow}(O_2)^{-I\uparrow}A^{-I}$

[a] For footnotes see Table 16; L = H_2O.

TABLE 18

Calculated properties of $^{m}[M(NH_3)_5(O_2)]^{q}$ complexes [a]

M	q	m	Electron density			Spin density		Charge		Assignment
			A^iS^j	$X(\pi_A)$	d^x	$\rho(M)$	$\rho(O_2)$	$Q(M)$	$Q(O_2)$	
Mn	3	1	S^2A^0	0.00	4.77			0.51	0.30	$Mn^{III}(O_2)^0$
		3	S^2A^0	0.00	4.77	1.95	0.00	0.51	0.30	$^{\uparrow\uparrow}Mn^{III}(O_2)^0$
	2	2	S^2A^0	0.08	5.33	0.98	0.00	0.21	0.23	$^{\uparrow}Mn^{II}(O_2)^0$
		4	$A^{\uparrow}S^2$	1.01	4.88	1.79	1.17	0.37	−0.33	$^{\uparrow\uparrow}Mn^{III\uparrow}(O_2)^{-I}$
	1	1	S^2A^{2y}	0.86	5.46			−0.38	−0.40	$(MnO_2)^{I}$
		3	$A^{\uparrow}S^2$	1.00	5.38	0.97	1.01	−0.29	−0.50	$^{\uparrow}Mn^{II\uparrow}(O_2)^{-I}$
	0	2	$A^{\uparrow}S^2$	0.99	5.89	0.01	0.99	−0.98	−0.51	$Mn^{I\uparrow}(O_2)^{-I}$
		4	$A^{\uparrow}S^2$	1.00	5.73	1.54	1.00	−0.76	−0.51	$^{\uparrow\uparrow}Mn^{I\uparrow}(O_2)^{-I}$
Fe	3	2	S^2A^0	0.00	5.83	0.98	0.00	0.30	0.31	$^{\uparrow}Fe^{III}(O_2)^0$
		4	$A^{\uparrow}S^{\uparrow}$	1.00	5.83	0.98	1.98	0.29	0.30	$^{\uparrow}Fe^{III\uparrow\uparrow}(O_2)^0$
	2	1	S^2A^0	0.05	6.37			−0.39	0.27	$Fe^{II}(O_2)^0$
		3	$A^{\uparrow}S^{\uparrow}$	0.98	6.27	0.16	1.81	0.26	0.15	$Fe^{II\uparrow\uparrow}(O_2)^0$
	1	2	$A^{\uparrow}S^2$	1.00	6.40	0.00	1.00	−0.44	−0.49	$Fe^{II\uparrow}(O_2)^{-I}$
		4	$S^2A^{\uparrow}$	1.00	6.32	1.81	1.08	−0.34	−0.53	$^{\uparrow\uparrow}Fe^{II\uparrow}(O_2)^{-I}$
	0	1	A^2S^2	1.96	6.55			−0.70	−0.95	$Fe^{II}(O_2)^{-II}$
		3	$A^{\uparrow}S^2$	1.00	6.40	0.03	1.00	−0.48	−0.54	$Fe^{II\uparrow}(O_2)^{-I\uparrow}A^{-I}$
Co	3	1	S^2A^0	0.00	6.91			0.08	0.32	$Co^{III}(O_2)^0$
		3	$A^{\uparrow}S^{\uparrow}$	0.98	6.91	0.00	1.98	0.07	0.31	$Co^{III\uparrow\uparrow}(O_2)^0$

	2	2	$A^{\uparrow}S^{2}$	0.98	6.99	0.00	1.00	−0.04	−0.31	$Co^{III\uparrow}(O_2)^{-I}$
		4	$S^{\uparrow}A^{\uparrow}$	1.00	7.34	0.89	2.01	−0.47	0.25	$^{\uparrow}Co^{II\uparrow\uparrow}(O_2)^{0}$
	1	1	$A^{2}S^{2y}$	2.00	7.49			−0.68	−0.39	$(CoO_2)^{I}$
		3	$A^{\uparrow}S^{2}$	1.00	7.34	0.82	1.07	−0.48	−0.53	$^{\uparrow}Co^{II\uparrow}(O_2)^{-I}$
	0	2	$A^{2}S^{\downarrow}$	2.00	7.32	0.79	−0.90	−0.49	−0.59	$^{\uparrow}Co^{II\downarrow}(O_2)^{-I\uparrow}A^{-I}$
		4	$A^{\uparrow}S^{2}$	1.00	7.36	0.88	0.99	−0.53	−0.53	$^{\uparrow}Co^{II\uparrow}(O_2)^{-I\uparrow}A^{-I}$
Ni	3	2	$A^{\uparrow}S^{\downarrow}$	0.98	7.85	0.66	0.15	0.05	0.24	$^{\uparrow}Ni^{III\uparrow\downarrow}(O_2)^{0}$
		4	$S^{\uparrow}A^{\uparrow}$	0.98	7.86	0.72	2.05	0.04	0.27	$^{\uparrow}Ni^{III\uparrow\uparrow}(O_2)^{0}$
	2	1	$A^{2}S^{0}$	1.96	8.21			−0.40	0.12	$Ni^{II}(O_2)^{0}$
		3	$S^{\uparrow}A^{\uparrow}$	0.98	8.19	0.11	1.83	−0.37	0.09	$Ni^{II\uparrow\uparrow}(O_2)^{0}$
	1	2	$A^{2}S^{\uparrow}$	1.97	8.26	0.10	0.89	−0.46	−0.54	$Ni^{II\uparrow}(O_2)^{-I}$
		4	$A^{\uparrow}S^{2}$	0.98	8.27	1.64	1.09	−0.47	−0.52	$^{\uparrow\uparrow}Ni^{II\uparrow}(O_2)^{-I}$
	0	1	$A^{2}S^{2}$	1.97	8.24			−0.49	−0.91	$Ni^{II}(O_2)^{-II}$
		3	$S^{\uparrow}A^{2}$	1.99	8.77	0.88	0.94	−0.13	−0.59	$^{\uparrow}Ni^{I\uparrow}(O_2)^{-I}$
Cu	3	1	$A^{2}S^{0}$	1.97	8.78			0.05	0.21	$Cu^{III}(O_2)^{0}$
		3	$A^{\uparrow}S^{\downarrow}$	1.00	8.79	1.13	0.11	0.04	0.29	$^{\uparrow}Cu^{II\uparrow\downarrow}(O_2)^{0\uparrow}L_S^{-I}$
	2	2	$A^{2}S^{0}$	1.96	9.12	0.79	−0.02	−0.37	0.17	$^{\uparrow}Cu^{II}(O_2)^{0}$
		4	$S^{\uparrow}A^{\uparrow}$	0.98	9.12	0.82	1.91	−0.37	0.16	$^{\uparrow}Cu^{II\uparrow\uparrow}(O_2)^{0}$
	1	1	$A^{2}S^{2y}$	1.97	9.56			−0.92	−0.11	$(CuO_2)^{I}$
		3	$A^{2}S^{\uparrow}$	1.98	9.13	0.81	0.99	−0.38	−0.61	$^{\uparrow}Cu^{II\uparrow}(O_2)^{-I}$
	0	2	$S^{\uparrow}A^{2}$	1.99	9.81	0.01	0.97	−1.23	−0.55	$Cu^{I\uparrow}(O_2)^{-I}$
		4	$A^{\uparrow}S^{2}$	0.99	9.15	0.82	1.08	−0.40	−0.55	$^{\uparrow}Cu^{II\uparrow}(O_2)^{-I\uparrow}A^{-I}$

[a] For footnotes see Table 16; L = NH_3.

ligands, H_2O and NH_3, tend to stabilize low oxidation states (M^I, M^0) in metal–dioxygen complexes.

(vi) The equatorial–axial influence

In square-bipyramidal complexes $[M(\epsilon)A'A'']^q$ the collective, integral influence of the equatorial ligand plane ϵ on the properties of axial ligands A′ and A″ was recently described as the equatorial–axial (shortly equ–ax) influence [216]. In the present study the equatorial plane was simulated by four monodentate ligands, $\epsilon = 4\ L_e$, and their influence on the electronic structure and properties of the coordinated dioxygen $A' = O_2$ is under consideration (the second axial ligand $A'' = L_a = NH_3$, H_2O and CN^- is rather rigid, insensitive to the equ-ax influence). Study of the equ–ax

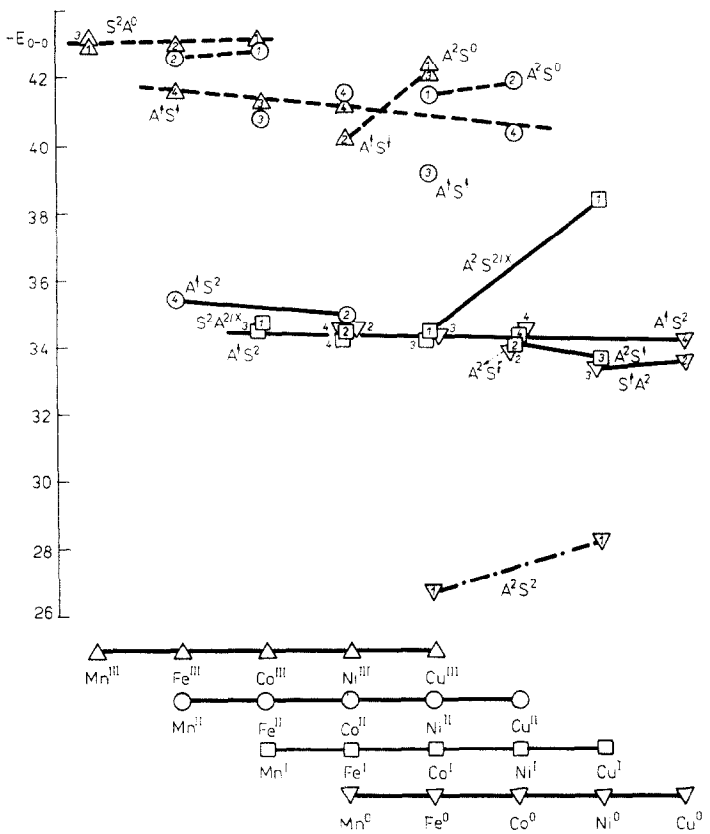

Fig. 17. Plot of the bicentric part of the total energy E_{O-O} (eV) vs. the number of valence electrons in $^m[M(NH_3)_5(O_2)]^q$ complexes.

influence is made difficult by the fact that it takes place side by side with the central atom effect.

From the results in Tables 16–19 it is concluded that the d^x populations increase, as a rule, in the series $L_e = Cl^-$, H_2O, NH_3 and CN^- for fixed ${}^mM^q$ values. One quantity which increases in this order is the ligand field strength. Table 20 presents classification of 140 dioxygen complexes by the local electron configurations A^iS^j. However, 15 complexes maintain their A^iS^j configurations within the series of equatorial ligands investigated. In the remaining cases the equ–ax influence is indicated in a discrete change of A^iS^j configurations. To the complexes insensitive to the equ–ax influence, belong: ${}^3Mn^{III}$, ${}^{2,4}Fe^{III}$, ${}^{1,3}Co^{III}$, ${}^4Ni^{III}$, ${}^1Cu^{III}$, ${}^4Mn^{II}$, ${}^1Fe^{II}$, ${}^2Co^{II}$, ${}^3Mn^{I}$, ${}^{2,4}Fe^{I}$, ${}^3Co^{I}$ and ${}^4Ni^{I}$. In addition, of the ${}^mM^0$ type complexes investigated six keep their local electron configuration, with $L_e = H_2O$ and NH_3, namely: ${}^1Fe^0$, ${}^{2,4}Co^0$, ${}^1Ni^0$ and ${}^{2,4}Cu^0$. It is interesting to point out that two-electron activated dioxygen occurs in ${}^1Mn^I$ and ${}^1Co^I$ complexes for anionic equatorial ligands ($L_e = Cl^-$, CN^-) and in ${}^1Fe^0$ and ${}^1Ni^0$ complexes for neutral equatorial ligands ($L_e = H_2O$, NH_3).

Finally, the local electron configurations A^iS^j are listed in Table 21 so that

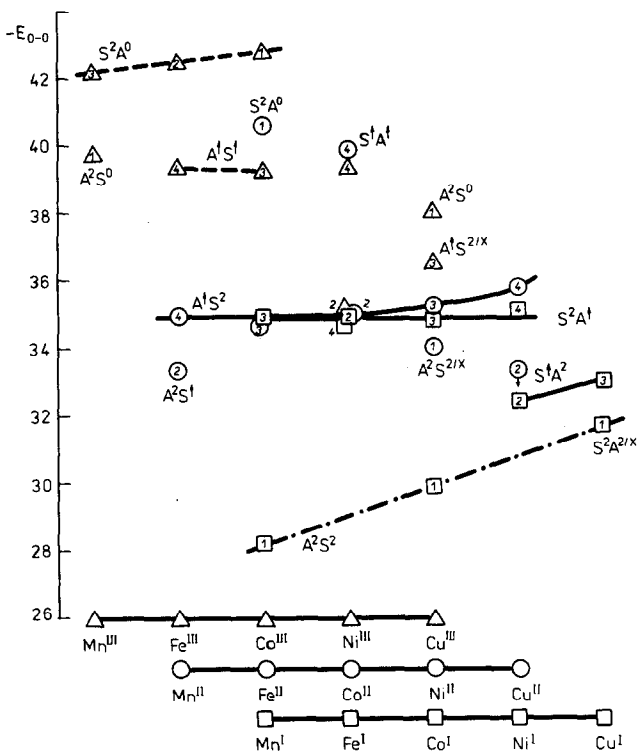

Fig. 18. Plot of the bicentric part of the total energy E_{O-O} (eV) vs. the number of valence electrons in ${}^m[M(CN)_5(O_2)]^q$ complexes.

TABLE 19 Calculated properties of $^{m}[M(CN)_5(O_2)]^{q}$ complexes [a]

M	q	m	Electron density			Spin density		Charge		Assignment
			A^iS^j	$X(\pi_A)$	d^x	$\rho(M)$	$\rho(O_2)$	$Q(M)$	$Q(O_2)$	
Mn	−2	1	A^2S^0	1.89	5.20			−0.60	0.11	$Mn^{III}(O_2)^0$
		3	S^2A^0	0.11	5.26	1.90	−0.02	−0.68	0.19	$^{\uparrow\uparrow}Mn^{III}(O_2)^0$
	−3	2	$A^2S^{\uparrow}$	2.00	5.26	0.02	0.96	−0.65	−0.47	$Mn^{III\uparrow}(O_2)^{-1}$
		4	$A^{\uparrow}S^2$	0.97	5.25	1.87	1.01	−0.64	−0.47	$^{\uparrow\uparrow}Mn^{III\uparrow}(O_2)^{-1}$
	−4	1	A^2S^2	1.94	5.42			−0.91	−0.88	$Mn^{III}(O_2)^{-II}$
		3	$A^{\uparrow}S^2$	0.98	5.62	0.93	1.00	−1.19	−0.54	$^{\uparrow}Mn^{II\uparrow}(O_2)^{-I}$
Fe	−2	2	S^2A^0	0.06	6.35	0.95	0.00	−0.93	0.23	$^{\uparrow}Fe^{III}(O_2)^0$
		4	$A^{\uparrow}S^{\uparrow}$	1.05	6.37	0.97	1.91	−0.93	0.22	$^{\uparrow}Fe^{III\uparrow\uparrow}(O_2)^0$
	−3	1	S^2A^0	0.27	6.61			−1.30	0.03	$Fe^{II}(O_2)^0$
		3	$A^{\uparrow}S^2$	1.02	6.33	0.94	1.01	−0.88	−0.45	$^{\uparrow}Fe^{III\uparrow}(O_2)^{-I}$
	−4	2	$A^{\uparrow}S^2$	1.02	6.66	0.00	0.99	−1.35	0.54	$Fe^{II\uparrow}(O_2)^{-I}$
		4	$S^2A^{\uparrow}$	1.05	6.58	1.65	1.14	−1.25	−0.60	$^{\uparrow\uparrow}Fe^{II\uparrow}(O_2)^{-I}$
Co	−2	1	S^2A^0	0.06	7.43			−1.13	0.25	$Co^{III}(O_2)^0$
		3	$A^{\uparrow}S^{\uparrow}$	1.06	7.43	0.02	1.92	−1.13	0.24	$Co^{III\uparrow\uparrow}(O_2)^0$
	−3	2	$A^{\uparrow}S^2$	1.01	7.42	0.00	0.99	−1.09	−0.43	$Co^{III\uparrow}(O_2)^{-I}$
		4	$S^{\uparrow}A^{\uparrow}$	1.08	7.65	0.90	1.93	−1.49	0.10	$^{\uparrow}Co^{II\uparrow\uparrow}(O_2)^0$
	−4	1	A^2S^2	1.94	7.61			−1.41	−0.75	$Co^{III}(O_2)^{-II}$
		3	$S^2A^{\uparrow}$	1.03	7.63	0.71	1.14	−1.40	−0.60	$^{\uparrow}Co^{II\uparrow}(O_2)^{-I}$
Ni	−2	2	$A^{\uparrow}S^2$	0.99	8.28	0.00	0.99	−0.99	−0.26	$Ni^{IV\uparrow}(O_2)^{-I}$
		4	$S^{\uparrow}A^{\uparrow}$	1.04	8.44	0.63	2.04	−1.23	0.20	$^{\uparrow}Ni^{III\uparrow\uparrow}(O_2)^0$
	−3	1	$A^2S^{2\cdot}$	1.95	8.49			−1.32	−0.43	$(NiO_2)^{II}$
		3	$S^2A^{\uparrow}$	0.98	8.42	0.47	1.29	−1.19	−0.47	$^{\uparrow}Ni^{III\uparrow}(O_2)^{-I}$
	−4	2	$S^{\uparrow}A^2$	1.98	8.55	0.03	0.92	−1.36	−0.79	$Ni^{II\uparrow}(O_2)^{-I}$
		4	$S^2A^{\uparrow}$	1.00	8.41	0.59	1.21	−1.19	−0.55	$^{\uparrow}Ni^{III\uparrow}(O_2)^{-I\uparrow}L_5^{-VI}$
Cu	−2	1	A^2S^0	2.00	9.24			−1.06	−0.15	$Cu^{III}(O_2)^0$
		3	$A^{\uparrow}S^{2\cdot}$	1.03	9.22	0.13	1.60	−1.02	−0.17	$Cu^{III\uparrow\uparrow}(O_2)^0$
	−3	2	$S^{\uparrow}A^2$	1.96	9.23	0.01	0.97	−0.99	−0.72	$Cu^{III\uparrow}(O_2)^{-I}$
		4	$A^{\uparrow}S^2$	0.99	9.28	0.51	1.42	−1.05	−0.34	$^{\uparrow}Cu^{IV\uparrow}(O_2)^{-I\uparrow}L_5^{-VI}$
	−4	1	$S^2A^{2\cdot}$	1.09	9.43			−1.24	−0.80	$(CuO_2)^{I}$
		3	$S^{\uparrow}A^2$	1.94	9.27	0.03	0.96	−1.05	−0.76	$Cu^{III\uparrow}(O_2)^{-I\uparrow}L_5^{-VI}$

[a] For footnotes see Table 16; L = CN^-.

the equ–ax influence, is more readily illustrated side by side with the central atom effect. We regard the activation process a consequence of the mutual influence of ligands (MIL concept [217]), mediated via the central atom. The last statement is based on the observation that the actual consequence of the equatorial–axial influence depends on the central atom characteristics ${}^{m}M^{q}$.

D. REACTIVITY OF ACTIVATED DIOXYGEN

Dioxygen activated through coordination to cobalt(II) complexes is a strong oxidant. Polarographic investigation shows [218] that paramagnetic cobalt–dioxygen complexes are faster one-electron oxidants than free dioxygen or non-oxygenated cobalt(II) complexes. The most important catalytic oxidation reactions on cobalt–dioxygen complexes cover the oxidation of methyl aromatics, such as *p*-xylene to terephthalic acid. The autooxidation of hydrocarbons, in general, exhibits some radical process characteristics. The formation of R$^{\cdot}$ from an RH substrate was accepted as the rate determining step of oxidation. An outer sphere hydrogen migration from RH to the dioxygen ligand is expected as the initiation step of the oxidation. Kinetic investigation of some alcohol oxidation reactions suggests the formation of a labile pre-reaction complex of the catalyst with dioxygen and alcohol [219].

Cobalt(II) complexes formed in acetic acid by reacting $CoBr_2$ with nitrogen-containing bases display a high catalytic activity and selectivity during the oxidation of hydrocarbons [220,221]. In the theoretical study below the reliability of the catalytic cycle is questioned. The catalyst was simulated simply by the $[CoX_4]^{2-}$ ion (X = Cl or Br) and toluene was chosen as the oxidized RH substrate. Here, step (i) represents the formation of the cobalt–dioxygen complex; step (ii) represents hydrogen migration to the dioxygen ligand and step (iii) indicates regeneration of the catalyst by splitting of the Co–O bond.

Coordinates descriptive of hydrogen migration from toluene to the coordinated dioxygen are shown in Fig. 19. The experimental geometry of toluene was used [210]. The carbon atom of the toluene methyl group was fixed at 3.0 (in units of 10^{-10} m) from the terminal oxygen. The total energy of the complex $[CoCl_4(O_2)HR]^{2-}$ was then calculated for four hydrogen positions moving towards the dioxygen. Fig. 20 indicates that not only the proton but also an electron is transferred so that the radical R$^{\cdot}$ is formed. Although such hydrogen migration is an energetically unfavorable process ($\Delta E = 3.3$ eV), the reaction barrier decreases approximately three-fold in comparison with the uncatalyzed abstraction

$$RH \rightarrow R^{\cdot} + H^{\cdot} \qquad (4)$$

where $\Delta E = 8.9$ eV. Both these values are probably overestimated but their ratio seems acceptable.

TABLE 20

Classification of 140 $^{m}[M(L_e)_4L_a(O_2)]^{q}$ type complexes by the local electron configuration of dioxygen π^* orbitals

A^iS^j	W_{O-O}	$-E_{O-O}$	n	$n+1$	$n+2$	$n+3$	$n+4$	$n+5$	$n+6$	$n+7$
(1) $L_e = Cl^-$, $L_a = NH_3$										
S^2A^0	1.88–1.91	42.6–42.7	$^{1,3}Mn^{III}$	$^{2}Fe^{III}$	$^{1}Co^{III}$					
	1.73	40.9			$^{1}Fe^{II}$					
A^2S^0	1.77	41.4					$^{1}Cu^{III}$			
	1.57	39.2					$^{1}Ni^{II}$			
$A^{\uparrow}S^{\uparrow}$, $S^{\uparrow}A^{\uparrow}$	1.26–1.39	39.0–41.8		$^{4}Fe^{III}$	$^{3}Co^{III}$	$^{4}Ni^{III}$	$^{3}Cu^{III}$			
	1.22	37.8						$^{4}Cu^{II}$		
$A^{\uparrow}S^{\downarrow}$	1.19	37.0				$^{2}Ni^{III}$				
$A^{\uparrow}S^2$, $S^2A^{\uparrow}$	1.17–1.18	34.7–35.5		$^{4}Mn^{II}$	$^{3}Fe^{II}$	$^{2,4}Co^{II}$	$^{3}Ni^{II}$	$^{2}Cu^{II}$		
	1.18–1.20	34.2–34.4			$^{3}Mn^{I}$	$^{2,4}Fe^{I}$	$^{3}Co^{I}$	$^{4}Ni^{I}$	$^{3}Cu^{I}$	
$S^2A^{\downarrow}$	1.19	34.8		$^{2}Mn^{II}$						
$A^2S^{\uparrow}$	1.16	33.7						$^{2}Ni^{I}$		
A^2S^{2y}	1.15	32.5							$^{1}Cu^{I}$	
A^2S^2	0.97–1.06	26.8–30.1			$^{1}Mn^{I}$		$^{1}Co^{I}$			
(2) $L_e = L_a = H_2O$										
S^2A^0	1.90	42.6–42.8	$^{1,3}Mn^{III}$	$^{2}Fe^{III}$	$^{1}Co^{III}$					
	1.77–1.86	41.3–42.1		$^{2}Mn^{II}$	$^{1}Fe^{II}$					
A^2S^0	1.84	42.1					$^{1}Cu^{III}$			
	1.73–1.79	40.9–41.4					$^{1}Ni^{II}$	$^{2}Cu^{II}$		
$A^{\uparrow}S^{\uparrow}$, $S^{\uparrow}A^{\uparrow}$	1.39–1.40	41.6–42.2		$^{4}Fe^{III}$	$^{3}Co^{III}$	$^{4}Ni^{III}$				
	1.32	40.3						$^{4}Cu^{II}$		
$A^{\uparrow}S^{\downarrow}$	1.33–1.35	40.4–40.7				$^{2}Ni^{III}$	$^{3}Cu^{III}$			
$A^{\uparrow}S^{2y}$	1.20	37.8				$^{4}Co^{II}$				
$A^{\uparrow}S^2$, $S^2A^{\uparrow}$	1.15	34.7–35.5		$^{4}Mn^{II}$	$^{3}Fe^{II}$	$^{2}Co^{II}$	$^{3}Ni^{II}$			
	1.17–1.18	33.6–34.4			$^{3}Mn^{I}$	$^{2,4}Fe^{I}$	$^{3}Co^{I}$	$^{4}Ni^{I}$	$^{3}Cu^{I}$	
	1.18	33.9–34.1						$^{4}Co^{0}$		$^{4}Cu^{0}$
$A^{\downarrow}S^2$	1.18	33.9							$^{3}Ni^{0}$	
$A^2S^{\uparrow}$	1.13	33.3								$^{2}Cu^{0}$
$A^2S^{\downarrow}$, $S^{\uparrow}A^2$	1.15	33.6						$^{2}Ni^{I}$		
	1.13–1.14	33.1–33.4				$^{2,4}Mn^{0}$	$^{3}Fe^{0}$	$^{2}Co^{0}$		

A^2S^{2y}	1.09–1.38	31.2–36.5			$^1Mn^I$		$^1Co^I$		$^1Cu^I$	
A^2S^2	0.98–1.01	27.3–28.7					$^1Fe^0$		$^1Ni^0$	
(3) $L_e = L_a = NH_3$										
S^2A^0	1.92–1.93	42.9–43.0	$^{1,3}Mn^{III}$	$^2Fe^{III}$	$^1Co^{III}$					
	1.89–1.92	42.6–42.8		$^2Mn^{II}$	$^2Fe^{II}$					
A^2S^0	1.85	42.4					$^1Cu^{III}$			
	1.76–1.80	41.4–41.8					$^1Ni^{II}$	$^2Cu^{II}$		
$A^\uparrow S^\uparrow$, $S^\uparrow A^\uparrow$	1.36–1.38	41.2–41.6		$^4Fe^{III}$	$^3Co^{III}$	$^4Ni^{III}$				
	1.26–1.37	39.1–41.5			$^3Fe^{II}$	$^4Co^{II}$	$^3Ni^{II}$	$^4Cu^{II}$		
$A^\uparrow S^\downarrow$	1.31–1.41	40.2–42.2				$^2Ni^{III}$	$^3Cu^{III}$			
$A^\uparrow S^2$, $S^2A^\uparrow$	1.16–1.17	34.9–35.4		$^4Mn^{II}$		$^2Co^{II}$				
	1.19	34.3–34.5			$^3Mn^I$	$^{2,4}Fe^I$	$^3Co^I$	$^4Ni^I$		
	1.19–1.20	34.1–34.5				$^{2,4}Mn^0$	$^3Fe^0$	$^4Co^0$		$^4Cu^0$
$A^2S^\uparrow$, $S^\uparrow A^2$	1.16–1.17	33.6–34.0						$^2Ni^I$	$^3Cu^I$	
	1.14–1.15	33.3–33.5							$^3Ni^0$	$^2Cu^0$
$A^2S^\downarrow$	1.17	33.8						$^2Co^0$		
S^2A^{2y}	1.28	34.7			$^1Mn^I$					
A^2S^{2y}	1.25–1.50	34.4–38.2					$^1Co^I$		$^1Cu^I$	
A^2S^2	0.98–1.02	26.7–28.2					$^1Fe^0$		$^1Ni^0$	
(4) $L_e = L_a = CN^-$										
S^2A^0	1.88–1.91	42.2–42.8	$^3Mn^{III}$	$^2Fe^{III}$	$^1Co^{III}$					
	1.69	40.6			$^1Fe^{II}$					
A^2S^0	1.48–1.64	38.1–39.8	$^1Mn^{III}$				$^1Cu^{III}$			
$A^\uparrow S^\uparrow$, $S^\uparrow A^\uparrow$	1.28	39.3–39.4		$^4Fe^{III}$	$^3Co^{III}$	$^4Ni^{III}$				
	1.29	39.9				$^4Co^{II}$				
$A^\uparrow S^{2y}$	1.19	36.6					$^3Cu^{III}$			
$A^\uparrow S^2$, $S^2A^\uparrow$	1.17	35.1				$^2Ni^{III}$				
	1.19–1.20	34.9–35.8		$^4Mn^{II}$	$^3Fe^{II}$	$^2Co^{II}$	$^3Ni^{II}$	$^4Cu^{II}$		
	1.21–1.22	34.7–35.1			$^3Mn^I$	$^{2,4}Fe^I$	$^3Co^I$	$^4Ni^I$		
$A^2S^\uparrow$, $S^\uparrow A^2$	1.14–1.16	33.4		$^2Mn^{II}$				$^2Cu^{II}$		
	1.12–1.15	32.4–33.0						$^2Ni^I$	$^3Cu^I$	
S^2A^{2y}	1.17	31.7							$^1Cu^I$	
A^2S^{2y}	1.21	34.1					$^1Ni^{II}$			
A^2S^2	0.99–1.04	28.2–29.9			$^1Mn^I$		$^1Co^I$			

[a] W_{O-O}, range of the Wiberg index; E_{O-O} (eV), range of the bicentric part of total energy; n, number of valence electrons.

TABLE 21

Equ–ax influence and central atom effect on the local electron configuration of dioxygen π^* orbitals in $^m[M(L_e)_4L_a(O_2)]^q$ complexes

M	Low-spin complexes ($m = 1, 2$)					High-spin complexes ($m = 3, 4$)				
	Mn	Fe	Co	Ni	Cu	Mn	Fe	Co	Ni	Cu
(1) $L_e = Cl^-$, $L_a = NH_3$										
M^{III}	S^2A^0	S^2A^0	S^2A^0	$A^\uparrow S^\downarrow$	A^2S^0	S^2A^0	$A^\uparrow S^\uparrow$	$A^\uparrow S^\uparrow$	$A^\uparrow S^\uparrow$	$S^\uparrow A^\uparrow$
M^{II}	$S^2A^\downarrow$	S^2A^0	$A^\uparrow S^2$	A^2S^0	$A^\uparrow S^2$	$A^\uparrow S^2$	$A^\uparrow S^2$	$A^\uparrow S^2$	$A^\uparrow S^2$	$S^\uparrow A^\uparrow$
M^{I}	A^2S^2	$A^\uparrow S^2$	A^2S^2	$A^2S^\uparrow$	A^2S^{2y}	$A^\uparrow S^2$	$A^\uparrow S^2$	$S^2A^\uparrow$	$S^2A^\uparrow$	$A^\uparrow S^2$
(2) $L_e = L_a = H_2O$										
M^{III}	S^2A^0	S^2A^0	S^2A^0	$A^\uparrow S^\downarrow$	A^2S^0	S^2A^0	$A^\uparrow S^\uparrow$	$A^\uparrow S^\uparrow$	$A^\uparrow S^\uparrow$	$A^\uparrow S^\downarrow$
M^{II}	S^2A^0	S^2A^0	$A^\uparrow S^2$	A^2S^0	A^2S^0	$A^\uparrow S^2$	$A^\uparrow S^2$	$A^\uparrow S^{2y}$	$A^\uparrow S^2$	$S^\uparrow A^\uparrow$
M^{I}	A^2S^{2y}	$S^2A^\uparrow$	A^2S^{2y}	$A^2S^\downarrow$	A^2S^{2y}	$A^\uparrow S^2$	$S^2A^\uparrow$	$A^\uparrow S^2$	$A^\uparrow S^2$	$A^\uparrow S^2$
M^{0}	$A^2S^\downarrow$	A^2S^2	$A^2S^\downarrow$	A^2S^2	$A^2S^\uparrow$	$A^2S^\downarrow$	$S^\downarrow A^2$	$A^\uparrow S^2$	$A^\downarrow S^2$	$A^\uparrow S^2$
(3) $L_e = L_a = NH_3$										
M^{III}	S^2A^0	S^2A^0	S^2A^0	$A^\uparrow S^\downarrow$	A^2S^0	S^2A^0	$A^\uparrow S^\uparrow$	$A^\uparrow S^\uparrow$	$S^\uparrow A^\uparrow$	$A^\uparrow S^\downarrow$
M^{II}	S^2A^0	S^2A^0	$A^\uparrow S^2$	A^2S^0	A^2S^0	$A^\uparrow S^2$	$A^\uparrow S^\uparrow$	$S^\uparrow A^\uparrow$	$S^\uparrow A^\uparrow$	$S^\uparrow A^\uparrow$
M^{I}	S^2A^{2y}	$A^\uparrow S^2$	A^2S^{2y}	$A^2S^\uparrow$	A^2S^{2y}	$A^\uparrow S^2$	$S^2A^\uparrow$	$A^\uparrow S^2$	$A^\uparrow S^2$	$A^2S^\uparrow$
M^{0}	$A^\uparrow S^2$	A^2S^2	$A^2S^\downarrow$	A^2S^2	$S^\uparrow A^2$	$A^\uparrow S^2$	$A^\uparrow S^2$	$A^\uparrow S^2$	$S^\uparrow A^2$	$A^\uparrow S^2$
(4) $L_e = L_a = CN^-$										
M^{III}	A^2S^0	S^2A^0	S^2A^0	$A^\uparrow S^2$	A^2S^0	S^2A^0	$A^\uparrow S^\uparrow$	$A^\uparrow S^\uparrow$	$S^\uparrow A^\uparrow$	$A^\uparrow S^{2y}$
M^{II}	$A^2S^\uparrow$	S^2A^0	$A^\uparrow S^2$	A^2S^{2y}	$S^\uparrow A^2$	$A^\uparrow S^2$	$A^\uparrow S^2$	$S^\uparrow A^\uparrow$	$S^2A^\uparrow$	$A^\uparrow S^2$
M^{I}	A^2S^2	$A^\uparrow S^2$	A^2S^2	$S^\uparrow A^2$	S^2A^{2y}	$A^\uparrow S^2$	$S^2A^\uparrow$	$S^2A^\uparrow$	$S^2A^\uparrow$	$S^\uparrow A^2$

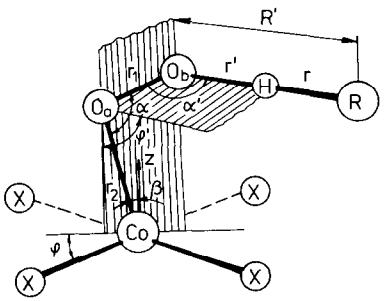

Fig. 19. Coordinates descriptive of a $[CoX_4(O_2)\cdots tol]$ complex model: $R_{Co-Cl} = 2.24$, $R_{Co-Br} = 2.40$, $r_1 = 1.19$, $r_2 = 1.85$, $r' = 1.05$, $R' = 3.0$ (in units of 10^{-10} m), $\alpha = 100°$, $\beta = 10°$, $\phi = 45°$, $\alpha' = 109°$, $\phi' = 90°$.

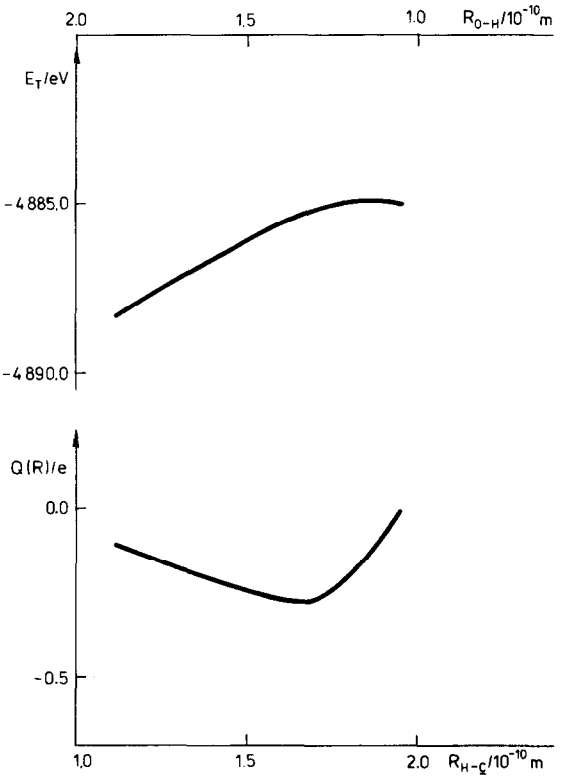

Fig. 20. Total molecular energy E_T and group charge of $C_6H_5CH_2$, $Q(R)$, vs. the hydrogen migration coordinate R_{H-C} or R_{O-H}.

The decomposition of $[CoCl_4(OOH)]^{2-}$ can occur in two ways:
(1) homolytic splitting of the Co–O bond through a triplet state (T) dissociation pathway yields $[CoCl_4]^{2-}$ and $OOH^{\cdot}$ products;
(2) heterolytic splitting of the Co–O bond through a singlet state (S) dissociation pathway gives $[CoCl_4]^{-}$ and OOH^{-} products. The results show (Fig.

21) that the singlet state of $[CoCl_4(OOH)]^{2-}$ is more stable around the energy minimum ($R_{Co-O} \approx 1.85$) but at the dissociation limit the triplet state is energetically favourable. The low-spin–high-spin crossover occurs at $R_{Co-O} \approx 2.3$; the dissociation starts heterolytically (S) but ends homolytically (T). These results justify regeneration of the catalyst $[CoCl_4]^{2-}$ and is the necessary condition for acceptance of the above mentioned catalytic cycle.

Similar results were obtained using $[CoBr_4]^{2-}$ in the role of catalyst. The calculated total molecular energies of some species allow a construction of the energy diagram (Fig. 22). It may be concluded that the substitution of Br for a Cl atom in the catalyst does not significantly affect the hydrogen migration from toluene to the coordinated dioxygen: the same barrier ($\Delta E = 3.3$ eV) was obtained in both cases. Since the step (iii), i.e. regenera-

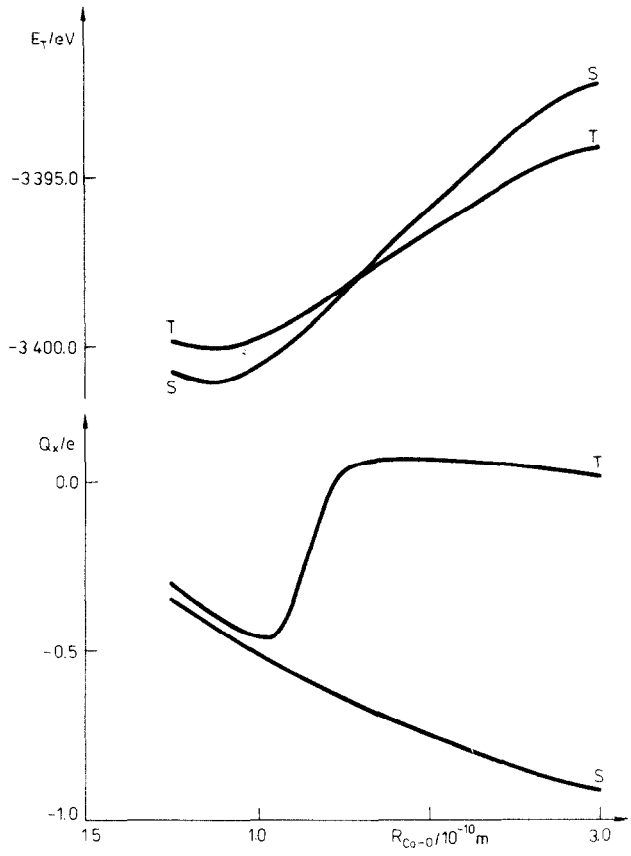

Fig. 21. Total molecular energy E_T and group charge of OOH, Q_X, on dissociation of the Co–O bond in the $[CoCl_4(OOH)]^{2-}$ complex. S, singlet spin state; T, triplet spin state.

tion of the catalyst, exhibits a much higher reaction barrier (8.0 or 6.2 eV for X = Cl and X = Br, respectively), this is the rate determining step. Splitting of the Co–O bond in $[CoBr_4(OOH)]^{2-}$ is easier than in $[CoCl_4(OOH)]^{2-}$ probably due to the higher lability of the Co–O_2 bond in $[CoBr_4(O_2)]^{2-}$ compared with $[CoCl_4(O_2)]^{2-}$. Scheme **XVII** leads to construction of simple

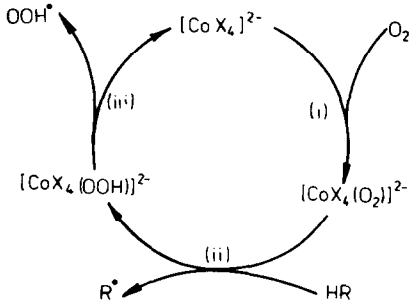

kinetic equations similar to those suggested by Tsuchida et al. [222] for the enzyme-type catalysis. Their solution yields a rough estimate for production of R· [183]

$$v(X = Br)/v(X = Cl) \sim \exp[2(eV)/RT] \quad (5)$$

so that $[CoBr_4]^{2-}$ appears to be a much more effective catalyst than $[CoCl_4]^{2-}$.

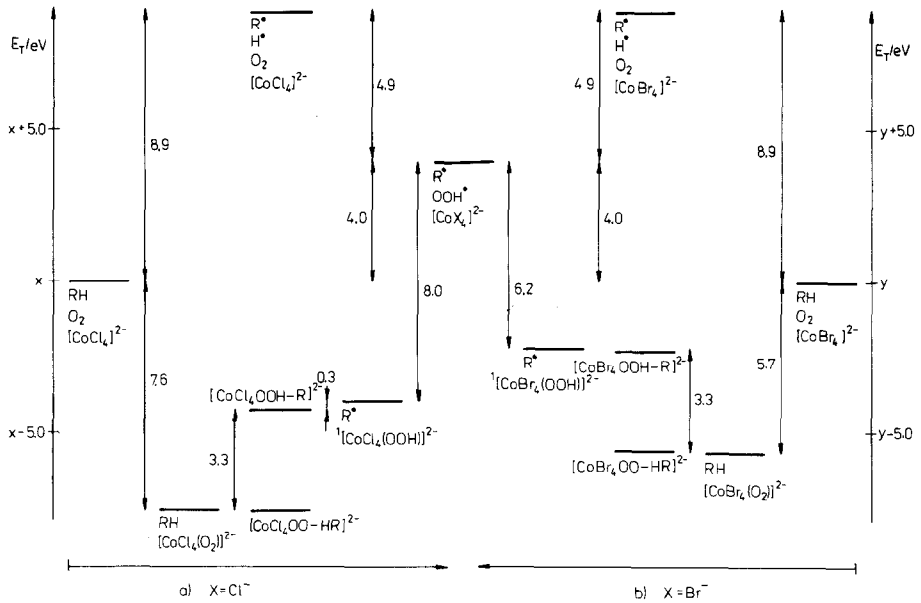

Fig. 22. Energy diagram of toluene oxidation on the $[CoCl_4]^{2-}$ and $[CoBr_4]^{2-}$ catalyst.

Finally, the low-spin–high-spin crossover during the dissociation of $[CoX_4(OOH)]^{2-}$ has a certain probability, $P_{S,T} << 1$, which according to the Landau–Zener theory [223–225] is given by

$$P_{S,T} = 2\,e^{-\gamma}(1 - e^{-\gamma}) \approx 2\gamma \tag{6}$$

where $\gamma \sim |E_{S,T}|^2$. In the interaction energy at the crossing point $E_{S,T} = \langle \psi_S | \hat{H}_{so} | \psi_T \rangle$ both the LCAO coefficients and the spin-orbit coupling constants contribute ($\hat{H}_{so}$ is the spin-orbit operator, ψ_S and ψ_T are the singlet and triplet wavefunctions of the complex, respectively). As the spin-orbit coupling constant for Br is much higher than that for Cl, the integral $E_{S,T}$ becomes higher in the case of $[CoBr_4(OOH)]^{2-}$ in comparison with $[CoCl_4(OOH)]^{2-}$. Therefore the low-spin–high-spin crossover is accelerated in the first case. This effect supports the conclusion presented above that the complex $[CoBr_4]^{2-}$ is a better catalyst than $[CoCl_4]^{2-}$ in the oxidation of methyl aromatics (toluene).

E. CONCLUDING REMARKS

The ability of dioxygen to bind to transition metal centres is illustrated in a great number of stable complexes; many of which have been prepared in the form of a monocrystal suitable for X-ray structure analysis. According to experimental data the type of dioxygen coordination covers a great number of different structural types. Among cobalt(II) complexes certain correlations between structural parameters were found. These systematic structural changes are mutually controlled by certain electronic factors which follow from the composition of the ligand sphere. Thus the MIL concept seems to be operative in studying dioxygen activation. The O–O bond length represents only one quantity suitable for measuring the degree of dioxygen activation. Because the dioxygen ligand behaves as a good π acceptor, its coordination is usually accompanied by filling of its π^* orbitals, so that the molecule is softened.

Quantum chemical calculations appear to be suitable for study of individual electronic factors operative in dioxygen activation. In the light of molecular orbital calculations: (1) electron localization in dioxygen π^* orbitals is the crucial factor for dioxygen activation; (2) dioxygen complexes can be classified into three groups, namely a group with non-activated (such as free O_2), one-electron activated (e.g. O_2^-) and two-electron activated (e.g. O_2^{2-}) dioxygen; (3) as a rule, the higher oxidation states (M^{III} or M^{II}) lead to dioxygen deactivation; lower oxidation states (M^{II}, M^{I} and M^{0}) support one-electron activation; two-electron activation occurs only in some closed-shell ($m = 1$) low-oxidation state complexes ($^1Mn^I$, $^1Fe^0$, $^1Co^I$, $^1Ni^0$ and $^1Cu^I$); (4) a negligible axial base influence was found in low-spin cobalt(II)

and iron(II) dioxygen complexes (the axial base was an N-donor ligand); (5) a strong central atom effect (the influence of atomic number, oxidation and spin state) was found by variation of ${}^{m}M^{q}$, considering the local electron configurations (A^iS^j) of dioxygen π^* orbitals; (6) considerable equatorial–axial influence is shown in a discrete change of A^iS^j configurations and consequently in the degree of dioxygen activation; (7) the ability of one-electron activated dioxygen to oxidize organic substrates in a catalytic cycle has been proven (at least toluene is oxidized on $Co-O_2$ complexes), a result which is in full agreement with experiment.

ACKNOWLEDGEMENTS

The author wishes to thank Professor J. Gažo and Dr. P. Pelikán for their interest and helpful discussion. Many thanks also to Mrs. M. Danková for technical assistance.

NOTE ADDED IN PROOF

Additional experimental and theoretical information may be cited in connection with the subject under study. Namely:

(1) one extensive review article [226] on cobalt–dioxygen complexes;

(2) X-ray structure determination of 1 : 1 iron–dioxygen complexes of the bent end-on type (Table 22), namely oxy-myoglobin [227] and oxy-erythrocruorin [228];

(3) X-ray structure determination of unusual $[Co(salmdpt)] \cdot [Co(salmdpt)(O_2)] \cdot 2ben$, where salmdpt = *N*,*N*′-(3,3′-dipropylmethylamine)bis(salicylideneaminato) dianion, with bent end-on mode of dioxygen coordination in the oxygenated molecule [229] (Table 22);

(4) X-ray structure determination of 1 : 1 peroxo-like (side-on type) complexes, namely the refinements of $Na_2[NbF_5(O_2)] \cdot 2H_2O$ [230] and $Na_3[HF_2][NbF_5(O_2)]$ [231]; the reports on $K_3[HF_2][TaF_5(O_2)]$ [232,233] and the unusual $K_6[TaF_5(O_2)] \cdot [O(TaF_4(O_2))_2] \cdot H_2O$ [234] (Table 22);

(5) X-ray structure determination of 2 : 1 monobridging complexes (Table 22), namely $[O_2(Co(tren)NH_3)_2] \cdot (SCN)_4 \cdot 2H_2O$ [235] and $[O_2(Co(papd))_2](S_2O_6)(NO_3)_2 \cdot 4H_2O$ [236], where tren = tris(2-amineethyl) amin and papd = 1,5,8,11,15-pentaazapentadecane;

(6) X-ray structure determination of 2 : 1 dibridging complexes (Table 22), namely $[(O_2)(tren)(Co(tren))_2] \cdot (ClO_4)_2 \cdot 2H_2O$ [237], $[(O_2)(OH)(Co(tren))_2](ClO_4)_3 \cdot 3H_2O$ [238], $[(O_2)(OH)(Co(dmtad))_2](ClO_4)_3 \cdot 2H_2O$ [239], $[(O_2)(OH)(Co(en)_2)_2](ClO_4)_3 \cdot H_2O$ [240], $[(O_2)(OH)(Co(en)_2)_2](NO_3)(S_2O_6) \cdot 2H_2O$ [241] and $[(O_2)(OH)(Co(en)_2)_2](NO_3)_4 \cdot H_2O$ [241], where dmtad = 4,7-dimethyl-1,4,7,10-tetraazadecane;

TABLE 22

Structural parameters of metal–dioxygen complexes [a]

No.	Compound [b]	Distance (10^{-10} m)			Angle (deg)	R (%)	Ref.
		O–O	M–O	M–O	M–O–O Φ		
1	[Fe(TpivPP)(2-MeIm)(O_2)]·EtOH	1.205 (16)	1.898 (7)		129.0 (12)		
		1.232 (22)			128.5 (18)	8	227
2	oxy-erythrocruorin	1.25 (20)	1.8 (2)		170 (30)	10	228, 229
3	oxy-myoglobin	1.21 (10)	2.02 (7)		111	20	230, 231
4	oxy-cobaltomyoglobin	1.26 (8)	1.89 (8)		131		232
5	[Co(salmdpt)(O_2)] [Co(salmdpt)]·2ben	1.06 (5)	1.88 (2)		137 (4)		
					133 (4)	9	233
6	[Co(salpeen)(O_2)]·MeCN	1.06 (3)	1.90 (3)		134 (4)	9	234
7	Ti(OEP)(O_2)	1.445 (5)	1.822 (4)	1.827 (4)		6	235
8	Ti(dipic)(H_2O)$_2$(O_2)	1.458 (2)	1.833 (2)	1.833 (2)		3	236
9	Na_4[O(Ti($C_6H_6O_6N$)(O_2))$_2$]·11 H_2O	1.469 (2)	1.889 (2)	1.892 (2)		3	237
10	($C_{12}H_{10}N_2$)[$NbF_5(O_2)$]	1.483 (8)	1.884 (5)	1.872 (6)			
		1.440 (16)	1.883 (8)	1.924 (10)		3	238
11	Na_3[HF_2][$NbF_5(O_2)$]	1.481 (4)	1.924 (2)	1.940 (2)		2	239
12	Na_2[$NbF_5(O_2)$]·2H_2O	1.411 (31)	1.962 (14)	1.962 (14)			
		1.506 (26)	1.933 (12)	1.933 (12)		3	240
13	K_3[HF_2][$TaF_5(O_2)$], 190 K	1.389 (24)	1.925 (10)	1.925 (10)		5	241, 242
	170 K	1.443 (22)	1.936 (10)	1.936 (10)		7	242
14	K_6[$TaF_5(O_2)$] [O($TaF_4(O_2)$)$_2$]·H_2O	1.39	1.93	1.93			
		1.64	1.99	1.99			
		1.75	1.95	1.95		3	243
15	(NEt_4)[TaF_4(C_6H_7NO)(O_2)]	1.67 (5)	1.98 (3)	1.99 (3)			
		1.43 (8)	1.84 (6)	1.85 (6)		6	244
16	NH_4[MoO(F)(pydca)(O_2)]	1.46 (1)	1.914 (6)	1.930 (7)		5	245
17	(NEt_4)[F(MoO(pydca)(O_2))$_2$]	1.43 (1)	1.919 (4)	1.927 (4)		4	246

TABLE 22 (continued)

No.	Compound [b]	Distance (10^{-10} m)			Angle (deg)		R (%)	Ref.
		O–O	M–O	M–O	M–O–O	Φ		
18	$[MoO(C_5H_3N(CO_2)_2)(H_2O)(O_2)]$	1.447 (8)	1.907 (5)	1.912 (6)			3	247
19	$H[MoO(C_5H_4NCO_2)] \cdot 2C_5H_4NCO_2H \cdot H_2O$	1.467 (3)	1.914 (2)	1.954 (2)				
		1.462 (3)	1.923 (2)	1.948 (2)			5	247
20	$[Co(As_4C_{24}H_{38})(O_2)]ClO_4$	1.424 (11)	1.862 (6)	1.867 (7)			5	249
21	$[Rh(Ph_3P)_3Cl(O_2)] \cdot 2CH_2Cl_2$	1.413 (9)	2.005 (8)	2.081 (8)			5	250
22	$[Ir(dppm)_2(O_2)]PF_6$	1.453 (17)	2.002 (12)	2.007 (12)			6	251
23	$[Ir(dppm)_2(O_2)]ClO_4$	1.486 (11)	2.048 (9)	2.057 (9)			6	251
24	$[Ir(PMe_2Ph)_4(O_2)]BPh_4$	1.485 (17)	2.037 (9)	2.050 (10)			5	252
25	$Ni(t\text{-}BuNC)_2(O_2)$	1.45 (1)	1.808 (8)	1.808 (8)			10	253
26	$[Pd(Ph(t\text{-}Bu)_2P)_2(O_2)] \cdot tol$	1.372	2.051	2.057				254
27	$[Pt(Ph(t\text{-}Bu)_2P)_2(O_2)] \cdot tol$	1.432	2.018	2.021				254
28	$[O_2(Co(tren)NH_3)_2](SCN)_4 \cdot 2H_2O$	1.511 (9)	1.889 (3)		111.5 (3)	180	7	255
29	$[O_2(Co(papd))_2](S_2O_6)(NO_3)_2 \cdot 4H_2O$	1.486 (7)	1.924 (5)		111.9 (4)	180	7	256
30	$[(O_2)Rh(Ph_3P)_2Cl]_2 \cdot 2CH_2Cl_2$	1.44 (1)	1.980 (7)	2.198 (7)	78.4 (3)			
			2.069 (7)	2.778 (7)	103.4 (5)		4	257
31	$[(O_2)(tren)(Co(tren))_2](ClO_4)_4 \cdot 2H_2O$	1.485 (25)	1.877 (16)		116.5 (12)	19.8		
			1.914 (17)		115.1 (13)		12	258
32	$[(O_2)(OH)(Co(tren))_2](ClO_4)_3 \cdot 3H_2O$	1.462 (26)	1.857 (18)		112.1 (12)	60.7		
			1.869 (20)		109.4 (14)		14	259
33	$[(O_2)(OH)(Co(dmtad))_2](ClO_4)_3 \cdot 2H_2O$	1.429 (20)	1.843 (15)		107.3 (10)	68.0		
			1.946 (14)		109.9 (10)		9	260
34	$[(O_2)(OH)(Co(en)_2)_2](ClO_4)_3 \cdot H_2O$	1.460 (13)	1.880 (8)		108.3 (6)	64.5		
			1.866 (10)		110.2 (6)		6	261
35	$[(O_2)(OH)(Co(en)_2)_2](NO_3)(S_2O_6) \cdot 2H_2O$	1.465	1.860		110.0	60.7		
			1.865		110.6		9	262
36	$[(O_2)(OH)(Co(en)_2)_2](NO_3)_4 \cdot H_2O$	1.339	1.872		119.7	22.0		
			1.875		120.0		8	262

TABLE 22 (continued)

No.	Compound [b]	Distance (10^{-10} m)			Angle (deg)	R (%)	Ref.
		O–O	M–O	M–O	M–O–O Φ		
37	$K_3[VO(C_2O_4)(O_2)_2]\cdot H_2O$	1.460	1.866	1.934			
		(6)	(4)	(4)			
		1.451	1.856	1.911		6	263
		(6)	(4)	(4)			
38	$[Cr(NH_3)_3(O_2)_2]$	1.42	1.88	1.89			
		(3)	(2)	(2)			
		1.42	1.87	1.86			
		(3)	(2)	(2)			
		1.45	1.87	1.91			264
		(3)	(2)	(2)			
39	$[Cr(en)(H_2O)(O_2)_2]\cdot H_2O$	1.46	1.87	1.95			
		(2)	(2)	(2)			
		1.48	1.84	1.87			265
		(2)	(2)	(2)			
40	$[MoO(MeCH(OH)CONMe_2)(O_2)_2]$	1.459	1.915	1.935			
		(6)	(5)	(5)			
		1.451	1.901	1.930		5	266
		(7)	(5)	(5)			
41	$(NH_4)_4[Mo_8O_{24}(O_2)_2(H_2O)_2]\cdot 4H_2O$	1.43	1.95	1.95		4	267
42	$(NH_4)_4[Mo_3O_7(O_2)_4]\cdot 2H_2O$	1.47 –1.49	1.94 –2.01			4	267
43	$K_5[Mo_7O_{21}(O_2)_2(OH)]\cdot 6H_2O$	1.40 –1.43	1.92 –1.95			6	267

[a] For footnotes see Table 2. [b] salmdpt = *N,N'*-(3,3'-dipropylmethylamine)bis(salicylideneaminato) dianion; salpeen = *N,N'*-(2-(2'-pyridyl)ethyl)-ethylenebis(salicylideneiminato) dianion; pydca = pyridine-2,6-dicarboxylate; tren = tris(2-amineethyl)amin; papd = 1,5,8,11,15-pentaazapentadecane; dmtad = 4,7-dimethyl-1,4,7,10-tetraazadecane.

(7) a preliminary report on the structure of $(NH_4)_4[Mo_3O_7(O_2)_4]\cdot 2H_2O$, $K_5[Mo_7O_{21}(O_2)_2(OH)]\cdot 6H_2O$ and $(NH_4)_4[Mo_8O_{24}(O_2)_2(H_2O)_2]\cdot 4H_2O$ [242] (Table 22);

(8) semiempirical MINDO-type calculations on the $Fe(O_2)$ model system [243,244]; and

(9) semiempirical INDO-type and ab initio MO-LCAO-SCF calculations on the complex $Fe(por)(SCH_3)(O_2)$ as a model of oxy-cytochrome P450 [245].

REFERENCES

1 L.H. Vogt, Jr., H.M. Faigenbaum and S.E. Wiberly, Chem. Rev., 63 (1963) 269.
2 J.A. O'Connor and E.A.V. Ebsworth, Adv. Inorg. Chem. Radiochem., 6 (1964) 279.

3 E. Bayer and P. Schretzmann, Struct. Bonding, 2 (1967) 181.
4 S. Fallab, Angew. Chem., 79 (1967) 500.
5 J.P. Franck, C. Bocard, I. Sérée de Roch and L. Sajus, Rev. Inst. Fr. Pét., 24 (1969) 710.
6 A.G. Stykes and J.A. Weill, Prog. Inorg. Chem., 13 (1970) 1.
7 R.G. Wilkins, Adv. Chem. Ser., 100 (1971) 111.
8 J.A. MacGinetty, in Sharp (Ed.), International Review of Sciences, Inorganic Chemistry, Vol. 15, Butterworth Univ., 1972, p. 229.
9 V.J. Choy and C.J. O'Connor, Coord. Chem. Rev., 9 (1972–73) 145.
10 L. Klevan, J. Peone and S.K. Madan, J. Chem. Educ., 50 (1973) 670.
11 J.S. Valentine, Chem. Rev., 73 (1973) 235.
12 A.E. Martell and M.M. Taqui Khan, in G.L. Eichhorn (Ed.), Inorganic Biochemistry, Vol. 2, Elsevier, Amsterdam, 1973, p. 654.
13 C. Bocard and I. Sérée de Roch, Rev. Inst. Fr. Pét., 28 (1973) 891.
14 F. Basolo, J. Indian Chem. Soc., 51 (1974) 1.
15 G. Henrici-Olivé and S. Olivé, Angew. Chem., 86 (1974) 1.
16 E. Ochiai, J. Inorg. Nucl. Chem., 37 (1975) 1503.
17 F. Basolo, B.M. Hoffman and J.A. Ibers, Accounts Chem. Res., 8 (1975) 384.
18 J.I. Bratushko and K.B. Yatzimirskii, in K.B. Yatzimirskii (Ed.), Uspekhi Khimiyi Koordinatsionnykh Soedinenii, Naukova Dumka, Kiyev, 1975, p. 7.
19 A.V. Savitskij and V.I. Nelyubin, Usp. Khim., 44 (1975) 214; Russ. Chem. Rev. (Engl. Transl.), 44 (1975) 110.
20 G. McLendon and A.E. Martell, Coord. Chem. Rev., 19 (1976) 1.
21 R.W. Erskine and B.O. Field, Struct. Bonding, 28 (1976) 1.
22 L. Vaska, Accounts Chem. Res., 9 (1976) 175.
23 J.P. Collman, Accounts Chem. Res., 10 (1977) 265.
24 G. Henrici-Olivé and S. Olivé, Coordination and Catalysis, Verlag Chemie, Weinheim, 1977.
25 J.E. Lyons, in M. Tsutsui and R. Ugo (Eds.), Fundamental Research in Homogeneous Catalysis, Plenum Press, New York, 1977, p. 1.
26 J.E. Lyons, in R. Ugo (Ed.), Aspects of Homogeneous Catalysis, Vol. 3, Reidel, Dordrecht, 1977, p. 1.
27 H. Mimoun, Rev. Inst. Fr. Pét., 33 (1978) 259.
28 A.B.P. Lever and H.B. Gray, Accounts Chem. Res., 11 (1978) 348.
29 R.D. Jones, D.A. Summerville and F. Basolo, Chem. Rev., 79 (1979) 139.
30 D.A. Summerville, R.D. Jones, B.M. Hoffman and F. Basolo, J. Chem. Educ., 56 (1979) 157.
31 R.S. Drago, Coord. Chem. Rev., 32 (1980) 97.
32 J.P. Collman, R.R. Gagne, C.A. Reed, W.T. Robinson and G.A. Rodley, Proc. Natl. Acad. Sci. U.S.A., 71 (1974) 1326.
33 J.P. Collman, R.R. Gagne, C.A. Reed, T.R. Halbert, G. Lang and W.T. Robinson, J. Am. Chem. Soc., 97 (1975) 1427.
34 G.B. Jameson, G.A. Rodley, W.T. Robinson, R.R. Gagne, C.A. Reed and J.P. Collman, Inorg. Chem., 17 (1978) 850.
35 G.B. Jameson, F.S. Molinaro, J.A. Ibers, J.P. Collman, J.I. Brauman, E. Rose and K.S. Suslick, J. Am. Chem. Soc., 100 (1978) 6769.
36 M. Calligaris, G. Nardin, L. Randaccio and G. Tauzher, Inorg. Nucl. Chem. Lett., 9 (1973) 419.
37 As cited in ref. 32.
38 G.A. Rodley and W.T. Robinson, Nature (London), 235 (1972) 438.

39 W.P. Schaefer, B.T. Huie, M.G. Kurilla and S.E. Ealick, Inorg. Chem., 19 (1980) 340.
40 A. Avdeef and W.P. Schaefer, J. Am. Chem. Soc., 98 (1976) 5153.
41 R.S. Gall and W.P. Schaefer, Inorg. Chem., 15 (1976) 2758.
42 R.S. Gall, J.F. Rogers, W.P. Schaefer and G.G. Christoph, J. Am. Chem. Soc., 98 (1976) 5135.
43 B.T. Huie, R.M. Leyden and W.P. Schaefer, Inorg. Chem., 18 (1979) 125.
44 L.D. Brown and K.N. Raymond, J. Chem. Soc. Chem. Commun., (1974) 470.
45 L.D. Brown and K.N. Raymond, Inorg. Chem., 14 (1975) 2595.
46 R. Guilard, M. Fontesse, P. Fournari, C. Lecomte and J. Protas, J. Chem. Soc. Chem. Commun., (1976) 161.
47 D. Schwarzenbach, Helv. Chim. Acta, 55 (1972) 2990.
48 D. Schwarzenbach, Inorg. Chem., 9 (1970) 2391.
49 R. Drew and F. Einstein, Inorg. Chem., 12 (1973) 829.
50 R. Stomberg, Acta Chem. Scand. Part A, 34 (1980) 193.
51 R. Stomberg, I.B. Svensson and L. Trysberg, cited in ref. 50.
52 Ž. Ružič-Toroš, B. Kojič-Prodič, F. Gabela and M. Šljukič, Acta Crystallogr., Sect. B, 33 (1977) 692.
53 D. Grandjean and R. Weiss, Bull. Soc. Chim. Fr., 8 (1967) 3044.
54 I. Larking and R. Stomberg, Acta Chem. Scand., 24 (1970) 2043.
55 N.W. Terry, E.L. Amma and L. Vaska, J. Am. Chem. Soc., 94 (1972) 653.
56 J. Halpern, B.L. Goodall, G.P. Khare, H.S. Lim and J.J. Pluth, J. Am. Chem. Soc., 97 (1975) 2301.
57 J. McGinnety, N. Payne and J. Ibers, J. Am. Chem. Soc., 91 (1969) 6301.
58 M.J. Nolte and E. Singleton, Acta Crystallogr., Sect. B, 32 (1976) 1410.
59 M. Laing, M.J. Nolte and E. Singleton, J. Chem. Soc. Chem. Commun., (1975) 660.
60 M.J. Nolte and E. Singleton, Acta Crystallogr., Sect. B, 31 (1975) 2223.
61 M.J. Nolte, E. Singleton and M. Laing, J. Am. Chem. Soc., 97 (1975) 6396.
62 J. McGinnety and J. Ibers, J. Chem. Soc. Chem. Commun., (1968) 235.
63 M. Weininger, I. Taylor and E. Amma, J. Chem. Soc. Chem. Commun., (1971) 1172.
64 J. Ibers and S. LaPlaca, Science, 145 (1964) 920.
65 S. LaPlaca and J. Ibers, J. Am. Chem. Soc., 87 (1965) 2581.
66 W.A. Spofford III and E.L. Amma, as cited in refs. 22 and 55.
67 J. McGinnety, R. Doedens and J. Ibers, Inorg. Chem., 6 (1967) 2243.
68 J. McGinnety, R. Doedens and J. Ibers, Science, 155 (1967) 709.
69 P. Cheng, C. Cook, S. Nyburg and K. Wan, Can. J. Chem., 49 (1971) 3772.
70 T. Kashiwagi, N. Yasuoka, N. Kasai, M. Kakudo, S. Takahashi and N. Hagihara, J. Chem. Soc. Chem. Commun., (1969) 743.
71 G. Cook, P. Cheng and S. Nyburg, J. Am. Chem. Soc., 91 (1969) 2123.
72 F.R. Fronczek, W.P. Schaefer and R.E. Marsch, Inorg. Chem., 14 (1975) 611.
73 W.P. Schaefer and R.E. Marsch, J. Am. Chem. Soc., 88 (1966) 178.
74 W.P. Schaefer and R.E. Marsch, Acta Crystallogr., 21 (1966) 735.
75 N.G. Vannerberg and C. Brosset, Acta Crystallogr., 16 (1963) 247.
76 R.E. Marsch and W.P. Schaefer, Acta Crystallogr., Sect. B, 24 (1968) 246.
77 F.R. Fronczek and W.P. Schaefer, Inorg. Chim. Acta, 9 (1974) 143.
78 W.P. Schaefer, Inorg. Chem., 7 (1968) 725.
79 N.G. Vannerberg, Acta Crystallogr., 18 (1965) 449.
80 F.R. Fronczek, W.P. Schaefer and R.E. Marsch, Acta Crystallogr., Sect. B, 30 (1974) 117.
81 J. Fritch, G. Christoph and W.P. Schaefer, Inorg. Chem., 12 (1973) 2170.
82 T. Shibahara, S. Koda and M. Mori, Bull. Chem. Soc. Jpn., 46 (1973) 2070.

83 B.C. Wang and W.P. Schaefer, Science, 166 (1969) 1404.
84 M. Calligaris, G. Nardin and L. Randaccio, J. Chem. Soc. Chem. Commun., (1969) 763.
85 M. Calligaris, G. Nardin, L. Randaccio and A. Ripamonti, J. Chem. Soc. A, (1970) 1069.
86 A. Avdeef and W.P. Schaefer, Inorg. Chem., 15 (1976) 1432.
87 L. Lindblom, W. Schaefer and R. Marsch, Acta Crystallogr., Sect. B, 27 (1971) 1461.
88 J.H. Timmons, A. Clearfield, A.E. Martell and R.H. Niswander, Inorg. Chem., 18 (1979) 1042.
89 J.H. Timmons, R.H. Niswander, A. Clearfield and A.E. Martell, Inorg. Chem., 18 (1979) 2977.
90 G.G. Christoph, R.E. Marsch and W.P. Schaefer, Inorg. Chem., 8 (1969) 291.
91 U. Thewalt and R.E. Marsch, J. Am. Chem. Soc., 89 (1967) 6364.
92 U. Thewalt and R.E. Marsch, Inorg. Chem., 11 (1972) 351.
93 U. Thewalt, Z. Anorg. Allg. Chem., 393 (1972) 1.
94 M. Bennett and R. Donaldson, J. Am. Chem. Soc., 93 (1971) 3307.
95 R.E. Drew and F.W.B. Einstein, Inorg. Chem., 11 (1972) 1079.
96 I.B. Svensson and R. Stomberg, Acta Chem. Scand., 25 (1971) 898.
97 G. Mathern and R. Weiss, Acta Crystallogr., Sect. B, 27 (1971) 1572.
98 G. Mathern and R. Weiss, Acta Crystallogr., Sect. B, 27 (1971) 1582.
99 G. Mathern and R. Weiss, Acta Crystallogr., Sect. B, 27 (1971) 1598.
100 R. Stomberg, Ark. Kemi, 24 (1965) 111.
101 R. Stomberg and I.-B. Ainalem, Acta Chem. Scand., 22 (1968) 1439.
102 B.F. Pedersen and B. Pedersen, Acta Chem. Scand., 17 (1963) 557.
103 R. Stomberg, Ark. Kemi, 22 (1964) 29.
104 R. Stomberg, Nature (London), 196 (1962) 570.
105 E.H. McLaren and L. Helmholtz, J. Phys. Chem., 63 (1959) 1279.
106 R. Stomberg and C. Brosset, Acta Chem. Scand., 14 (1960) 441.
107 R. Stomberg, Acta Chem. Scand., 17 (1963) 1563.
108 B. Chevrier, Th. Diebolt and R. Weiss, Inorg. Chim. Acta, 19 (1976) L57.
109 J.-M. Le Carpentier, R. Schlupp and R. Weiss, Acta Crystallogr., Sect. B, 28 (1972) 1278.
110 R. Stomberg, Acta Chem. Scand., 24 (1970) 2024.
111 R. Stomberg, L. Trysberg and I. Larking, Acta Chem. Scand., 24 (1970) 2678.
112 I. Larking and R. Stomberg, Acta Chem. Scand., 26 (1972) 3708.
113 R. Stomberg, Acta Chem. Scand., 23 (1969) 2755.
114 A. Mitschler, J.M. Le Carpentier and R. Weiss, J. Chem. Soc. Chem. Commun., (1968) 1260.
115 J.-M. Le Carpentier, A. Mitschler and R. Weiss, Acta Crystallogr., Sect. B, 28 (1972) 1288.
116 R. Stomberg, Acta Chem. Scand., 22 (1968) 1076.
117 F.W.B. Einstein and B.R. Penfold, Acta Crystallogr., 17 (1964) 1127.
118 N.W. Alcock, J. Chem. Soc. Chem. Commun., (1966) 536.
119 N.W. Alcock, J. Chem. Soc. A, (1968) 1588.
120 L. Pauling and C.D. Coryell, Proc. Natl. Acad. Sci. U.S.A., 22 (1936) 210.
121 L. Pauling, Haemoglobin, Butterworths, London, 1949.
122 L. Pauling, Nature (London), 203 (1964) 182.
123 J.J. Weiss, Nature (London), 202 (1964) 83.
124 J.J. Weiss, Nature (London), 203 (1964) 183.
125 J.S. Griffith, Proc. R. Soc. London, Ser. A, 235 (1956) 23.
126 J. Chatt and L.A. Duncanson, J. Chem. Soc., (1953) 2939.
127 A.A. Vlček, Trans. Faraday Soc., 56 (1960) 1137.

128 J.D. Dunitz and L.E. Orgel, J. Chem. Soc., (1953) 2594.
129 T. Shibahara, M. Mori, K. Matsumoto and S. Ooi, Bull. Chem. Soc. Jpn., 54 (1981) 433.
130 E.-I. Ochiai, Inorg. Nucl. Chem. Lett., 10 (1974) 453.
131 Y. Ellinger, J.M. Latour, J.C. Marchon and R. Subra, Inorg. Chem., 17 (1978) 2024.
132 C. Bachmann, J. Demuynck and A. Veillard, J. Am. Chem. Soc., 100 (1978) 2366.
133 I.B. Bersuker and S.S. Stavrov, Chem. Phys., 54 (1980) 331.
134 A.B.P. Lever, J. Mol. Struct., 59 (1980) 123.
135 G. McLendon, S.R. Pickens and A.E. Martell, Inorg. Chem., 16 (1977) 1551.
136 B.B. Wayland, J.V. Minkiewicz and M.E. Abd-Elmageed, J. Am. Chem. Soc., 96 (1974) 2795.
137 R.S. Drago, T. Beugelsdijk, J.A. Breese and J.P. Cannady, J. Am. Chem. Soc., 100 (1978) 5374.
138 B.S. Tovrog, D.J. Kitko and R.S. Drago, J. Am. Chem. Soc., 98 (1976) 5144.
139 B.M. Hoffman, C.J. Weschler and F. Basolo, J. Am. Chem. Soc., 98 (1976) 5473.
140 Y. Seno, J. Otsuka, O. Matsuoka and N. Fuckikami, J. Phys. Soc. Jpn., 33 (1972) 1645.
141 J. Otsuka, O. Matsuoka, N. Fuckikami and Y. Seno, J. Phys. Soc. Jpn., 35 (1973) 854.
142 J. Otsuka, Y. Seno, N. Fuckikami and O. Matsuoka, in B. Pullman and N. Goldblum (Eds.), Metal–Ligand Interactions in Organic Chemistry and Biochemistry, Jerusalem Symp. Quantum Chem. Biochem., Vol. 9, Part 2, Reidel, Dordrecht, 1977, p. 59.
143 W.A. Goddard III. and B.D. Olafson, Proc. Nat. Acad. Sci. U.S.A., 72 (1975) 2335.
144 M.P. Halton, Theor. Chim. Acta, 24 (1972) 89.
145 M.P. Halton, Inorg. Chim. Acta, 8 (1974) 131.
146 M. Zerner, M. Gouterman and H. Kobayashi, Theor. Chim. Acta, 6 (1966) 363.
147 F. Adar, M. Gouterman and S. Aronowitz, J. Phys. Chem., 80 (1976) 2184.
148 S. Aronowitz, M. Gouterman and J.C.W. Chien, cited in M. Gouterman, in D. Dolphin (Ed.), The Porphyrins, Vol. III, Physical Chemistry, Part A, Academic Press, New York, 1978, p. 112.
149 G.H. Loew and R.F. Kirchner, J. Am. Chem. Soc., 97 (1975) 7388.
150 W.A. Eaton, L.K. Hanson, P.J. Stephens, J.C. Sutherland and J.B.R. Dunn, J. Am. Chem. Soc., 100 (1978) 4991.
151 R.F. Kirchner and G.H. Loew, J. Am. Chem. Soc., 99 (1977) 4639.
152 G.H. Loew and R.F. Kirchner, Int. J. Quantum Chem., Quantum Biol. Symp., 5 (1978) 403.
153 B.H. Huynh, D.A. Case and M. Karplus, J. Am. Chem. Soc., 99 (1977) 6103.
154 A. Dedieu, M.-M. Rohmer, M. Benard and A. Veillard, J. Am. Chem. Soc., 98 (1976) 3717.
155 A. Dedieu, M.-M. Rohmer and A. Veillard, in B. Pullman and N. Goldblum (Eds.), Metal–Ligand Interactions in Organic Chemistry and Biochemistry, Jerusalem Symp. Quantum Chem. Biochem., Vol. 9, Part 2, Reidel, Dordrecht, 1977, p. 101.
156 Z.S. Herman and G.H. Loew, J. Am. Chem. Soc., 102 (1980) 1815.
157 G.H. Loew, Z.S. Herman and M.C. Zerner, Int. J. Quantum Chem., 18 (1980) 481.
158 R. Boča, J. Mol. Catal., 14 (1982) 307.
159 P. Fantucci and V. Valenti, J. Am. Chem. Soc., 98 (1976) 3832.
160 A. Dedieu, M.-M. Rohmer and A. Veillard, J. Am. Chem. Soc., 98 (1976) 5789.
161 A. Dedieu and A. Veillard, Theor. Chim. Acta, 36 (1975) 231.
162 M.-M. Rohmer, A. Dedieu and A. Veillard, Theor. Chim. Acta, 39 (1975) 189.
163 J.E. Linard, P.E. Ellis Jr., J.R. Budge, R.D. Jones and F. Basolo, J. Am. Chem. Soc., 102 (1980) 1896.
164 J.I. Bratushko and J.P. Nazarenko, Teor. Eksp. Khim., 10 (1974) 36.

165 I. Hyla-Kryspin, L. Natkaniec and B. Ježowska-Trzebiatowska, Chem. Phys. Lett., 35 (1975) 311.
166 I. Hyla-Kryspin, L. Natkaniec and B. Ježowska-Trzebiatowska, Bull. Acad. Pol. Sci., Ser. Sci. Chim., 25 (1977) 193.
167 I. Hyla-Kryspin, L. Natkaniec and B. Ježowska-Trzebiatowska, Proc. 8th Conf. Coord. Chem., Smolenice-Bratislava, 1980, p. 131.
168 B.K. Teo and W.K. Li, Inorg. Chem., 15 (1976) 2005.
169 R. Boča, P. Pelikán and J. Gažo, Proc. 1st Summer School and 4th Symp., Metal Complex Catalysis, S-2, Wroclaw-Karpacz, Poland 1979, p. 54.
170 R. Boča, J. Mol. Struct., 65 (1980) 173.
171 R. Boča and P. Pelikán, Inorg. Chim. Acta, 44 (1980) L65.
172 A. Andreev and N. Neshev, React. Kinet. Catal. Lett., 1 (1974) 297.
173 J.G. Norman Jr., J. Am. Chem. Soc., 96 (1974) 3327.
174 M.-M. Rohmer, M. Barry, A. Dedieu and A. Veillard, Proc. Int. Symp. At. Mol. Solid-State Theory, Collision Phenom. Comput. Methods, 1977.
175 A. Dedieu and M.-M. Rohmer, J. Am. Chem. Soc., 99 (1977) 8050.
176 A. Dedieu, M.-M. Rohmer, H. Veillard and A. Veillard, Nouv. J. Chim., 3 (1979) 653.
177 L.K. Hanson and B.M. Hoffman, J. Am. Chem. Soc., 102 (1980) 4602.
178 S. Sakaki, K. Hori and A. Ohyoshi, Inorg. Chem., 17 (1978) 3183.
179 R. Boča, J. Mol. Catal., 9 (1980) 275.
180 R. Boča, J. Mol. Catal., 10 (1981) 187.
181 R. Boča, J. Mol. Catal., 14 (1982) 313.
182 R. Boča, J. Mol. Catal., 18 (1983) 41.
183 R. Boča, J. Mol. Catal., 12 (1981) 351.
184 R. Boča, to be published.
185 M. Čeppan, L. Lapčík, M. Liška and P. Pelikán, Eur. Polym. J., 16 (1980) 607.
186 S. Beran, P. Jírů, B. Wichterlová and R. Zahradník, Proc. 6th Int. Congr. Catal., London, 1976, p. A23.
187 S. Beran, P. Jírů, B. Wichterlová and R. Zahradník, React. Kin. Catal. Lett., 5 (1976) 131.
188 J.P. Collman, R.R. Gagne, H.B. Gray and J.W. Hare, J. Am. Chem. Soc., 96 (1974) 6522.
189 B.M. Hoffman, C.J. Weschler and F. Basolo, J. Am. Chem. Soc., 98 (1976) 5473.
190 B.M. Hoffman, T. Szymanski, T.G. Brown and F. Basolo, J. Am. Chem. Soc., 100 (1978) 7253.
191 W.M. Coleman and L.T. Taylor, Coord. Chem. Rev., 32 (1980) 1.
192 C. Daul, C.W. Schläpter and A. von Zelewski, Struct. Bonding, 36 (1979) 129.
193 R. Boča and M. Liška, Program MOSEMI, unpublished work.
194 R. Boča, Program MOSEM2, unpublished work.
195 J.A. Pople and D.L. Beveridge, Approximate Molecular Orbital Theory, McGraw-Hill, New York, 1970.
196 D.W. Clack, N.S. Hush and J.R. Yandle, J. Chem. Phys., 57 (1972) 3503.
197 H.L. Hase and A. Schweig, Theor. Chim. Acta, 31 (1973) 215.
198 J.C. Slater, Phys. Rev., 36 (1930) 57.
199 M. Zerner and M. Gouterman, Theor. Chim. Acta, 4 (1965) 44.
200 P. Pelikán and M. Liška, private communication.
201 M. Liška, P. Pelikán and J. Gažo, Koord. Khim., 5 (1979) 978.
202 K.B. Wiberg, Tetrahedron, 24 (1968) 1083.
203 R. Boča, P. Pelikán and M. Haring, J. Mol. Catal., 11 (1981) 41.
204 A.T. Amos and G.G. Hall, Proc. R. Soc., London, Ser. A, 263 (1961) 483.

205 R. Boča, Program PCILO3, Q.C.P.E., to be published.
206 P.E. Stevenson and D.L. Burkey, J. Am. Chem. Soc., 96 (1974) 3061.
207 D.W. Clack, Mol. Phys., 27 (1974) 1513.
208 T. Anno and H. Teruya, J. Chem. Phys., 52 (1970) 2840.
209 P. Pelikán, M. Liška, R. Boča and L. Turi Nagy, Chem. Zvesti, 32 (1978) 607.
210 L.E. Sutton (Ed.), Interatomic Distances, Spec. Publ. Nos. 11 (1958) and 18 (1965), Chem. Soc., London.
211 E. Melamud, B.L. Silver and Z. Dori, J. Am. Chem. Soc., 96 (1974) 4689.
212 D. Getz, E. Melamud, B.L. Silver and Z. Dori, J. Am. Chem. Soc., 97 (1975) 3846.
213 D.V. Stynes, H.C. Stynes, B.R. James and J.A. Ibers, J. Am. Chem. Soc., 95 (1973) 1796.
214 C.K. Chang and T.G. Traylor, J. Am. Chem. Soc., 95 (1973) 8477.
215 F.A. Walker, J. Am. Chem. Soc., 95 (1973) 1154.
216 J. Gažo, R. Boča, E. Jóna, M. Kabešová, Ľ. Macášková, J. Šíma, P. Pelikán and F. Valach, Coord. Chem. Rev., 43 (1982) 87.
217 J. Gažo, Zh. Neorg. Khim., 22 (1977) 2936.
218 J. Costa, A. Puxeddu and L.B. Stefani, Inorg. Nucl. Chem. Lett., 6 (1970) 191.
219 A. Savitskii, Zh. Obsch. Khim., 44 (1974) 1548.
220 M. Hronec, R. Přikryl and V. Veselý, Chem. Zvesti, 29 (1975) 440.
221 M. Hronec and V. Veselý, Collect. Czech. Chem. Commun., 42 (1977) 3392.
222 E. Tsuchida, M. Kaneko and H. Nishide, Makromol. Chem., 151 (1972) 235.
223 L. Landau, Phys. Z. Sowjetunion, 2 (1932) 46.
224 C. Zener, Proc. R. Soc. London Ser. A, 137 (1932) 696.
225 C. Zener, Proc. R. Soc. London Ser. A, 140 (1933) 660.
226 T.D. Smith and J.R. Pilbrow, Coord. Chem. Rev., 39 (1981) 295.
227 S.E.V. Philips, Nature, 273 (1978) 247.
228 E. Weber, W. Steigemann, T.A. Jones and R. Huber, J. Mol. Biol., 120 (1978) 327.
229 R. Cini and P. Orioli, J. Chem. Soc., Chem. Commun., (1981) 196.
230 R. Stomberg, Acta Chem. Scand. Ser. A, 35 (1981) 489.
231 R. Stomberg, Acta Chem. Scand. Ser. A, 35 (1981) 389.
232 Z. Ružič-Toroš, B. Kojič-Prodič and M. Sljukič, Acta Crystallogr. Sect. B, 32 (1976) 1096.
233 R. Stomberg, Acta Chem. Scand. Ser. A, 36 (1982) 423.
234 W. Massa and G. Pausewang, Z. Anorg. Allg. Chem., 456 (1979) 169.
235 U. Thewalt, M. Zehnder and S. Fallab, Helv. Chim. Acta, 60 (1977) 867.
236 M. Zehnder und U. Thewalt, Z. Anorg. Allg. Chem., 461 (1980) 53.
237 M. Zehnder, U. Thewalt and S. Fallab, Helv. Chim. Acta, 62 (1979) 2099.
238 M. Zehnder, U. Thewalt and S. Fallab, Helv. Chim. Acta, 59 (1976) 2290.
239 H. Mäcke, M. Zehnder, U. Thewalt and S. Fallab, Helv. Chim. Acta, 62 (1979) 1804.
240 S. Fallab, M. Zehnder and U. Thewalt, Helv. Chim. Acta, 63 (1980) 1491.
241 U. Thewalt and G. Struckmeier, Z. Anorg. Allg. Chem., 419 (1976) 163.
242 L. Trysberg and R. Stomberg, Acta Chem. Scand. Ser. A, 35 (1981) 823.
243 G. Blyholder, J. Head and F. Ruette, Theor. Chim. Acta, 60 (1982) 429.
244 G. Blyholder, J. Head and F. Ruette, Inorg. Chem., 21 (1982) 1539.
245 M.-M. Rohmer and G.H. Loew, Int. J. Quantum Chem., Quantum Biol. Symp., 6 (1979) 93.